The Dissertation Committee for Sanghee Ki Certifies that this is the approved version of the following dissertation :

THYMOCYTES REQUIRE STROMAL-DERIVED SIGNALS, INCLUDING ACTIVATION OF CHEMOKINE RECEPTORS EBI2 AND GPR146, FOR PROPER DIFFERENTIATION AND SELECTION

Committee:

Lauren I. R. Ehrlich, Supervisor

Edward M. Marcotte

Haley Tucker

Steven Vokes

Vishwanath R. Iyer

THYMOCYTES REQUIRE STROMAL-DERIVED SIGNALS, INCLUDING ACTIVATION OF CHEMOKINE RECEPTORS EBI2 AND GPR146, FOR PROPER DIFFERENTIATION AND SELECTION

by

Sanghee Ki, BS; MSEd

Dissertation

Presented to the Faculty of the Graduate School of

The University of Texas at Austin

in Partial Fulfillment

of the Requirements

for the Degree of

Doctor of Philosophy

The University of Texas at Austin

August 2016

Dedication

I dedicate this work

to family who always love and support me

to my husband, Daechan, who is the reason I live.

Acknowledgements

I would like to thank my advisor, Lauren Ehrlich for her support and guidance through my PhD. Thanks to her patience and mentorship, I have learned a lot and was able to grow up as a scientist.

I would also like to thank my committee members for good insights and opinions which helped to polish my research. I want to give special thanks to Qiang and Steven Vokes who taught me how to do southern blots and generously offered to let me use their lab space. I especially thank our mouse facility staff for keeping our cages clean everyday.

I really appreciate all the members of the Ehrlich Lab. Thanks to Hilary for supporting all of our mouse work and giving vigor to daily life, Todd for giving valuable advice, Jessica for lots of help with imaging and for comfort, Zicheng for guidance on experimental techniques and being a good companion throughout the whole period, Hiran for being a good friend to me, and Aram and Yu for being good companions.

I thank my parents and brother who always give their love and support and my parents-in-law whose understanding sustains me. My last and largest thanks goes to my husband, Daechan, who has always been with me when times are tough or good, and supports me with love, and my son Onyu, who teaches me the joy of life.

THYMOCYTES REQUIRE STROMAL-DERIVED SIGNALS, INCLUDING ACTIVATION OF CHEMOKINE RECEPTORS EBI2 AND GPR146, FOR PROPER DIFFERENTIATION AND SELECTION

Sanghee Ki, Ph.D.

The University of Texas at Austin, 2016

Supervisor: Lauren I. R. Ehrlich

The thymus is the primary lymphoid organ where immature thymocytes differentiate and mature to become functional T cells that are self-MHC restricted and self-tolerant. In addition to developing T cells, the thymus is comprised of stromal cells, subdivided into cortical and medullary regions, which form a component of the microenvironment for thymocyte development. Throughout their development, thymocytes undergo bidirectional crosstalk with the thymic epithelial cells, which is essential for proper development of both the thymocyte and epithelial subsets.

Thymic involution is a detrimental process of aging which results in degeneration of the thymic microenvironment, reduction in T cell output, and contraction of the naïve T cell pool, thus contributing to impaired immune responses in aging individuals. Molecular and cellular changes that drive thymic atrophy during aging are not well understood. To address this gap in knowledge, I analyzed transcriptional changes in purified thymic stromal subsets early in the process of age-associated thymic involution (Chapter 2). These

studies revealed that there is gradual down-regulation of cell cycle genes and E2F3 transcriptional targets in thymic epithelial cell subsets as the thymus begins to involute. This suggests that diminished proliferative activity in a subset of thymic epithelial cells is a major contributing factor to age-associated involution. I also identified an increasingly proinflmamatory signature in thymic dendritic cells early in the involution process. These results have provided novel insights into the mechanisms behind thymic atrophy and identify cellular targets for thymic rebound strategies.

Chemokine receptors, a subset of G protein coupled receptors (GPCRs), have been implicated in guiding thymocytes between different thymic regions, thus enabling interactions with local stromal subsets that support T cell differentiation. For example, chemokine receptors play an essential role in driving thymocyte migration into the medulla, where thymocytes scan numerous self-antigens to establish central tolerance. Importantly, failure of thymocytes to enter the thymic medulla results in impaired self-tolerance, leading to autoimmunity. We have identified EBI2 and GPR146 as candidate GPCRs that could contribute to thymocyte accumulation in the medulla, interactions with antigen presenting cells therein, and thus the induction of tolerance. In chapter 3, I report that EBI2 is essential for negative selection toward some self-antigens and restrains regulatory T cell generation in the thymus. Through two-photon imaging, I identified reduced motility and medullary accumulation as mechanisms by which EBI2 deficiency could impair negative selection. In chapter 4, I describe generation of a GPR146 deficient mouse strain, and initial studies indicating GPR146 is involved in thymocyte differentiation and selection. Through these studies we have revealed novel functions for GPCRs in promoting thymocyte migration and the induction of self-tolerance.

Table of Contents

List of Figures

Chapter 1: Introduction

1.1 THYMOCYTE DEVELOPMENT

A healthy immune system must be able to protect hosts from infection and malignant outgrowth by initiating a powerful immune response. However, this same powerful system also has the capability to cause collateral damage to healthy, non-infected tissue when eliminating pathogens, or in extreme cases, develop immune responses activated by self-tissue in the absence of infections (autoimmunity). Thus the immune system requires multiple layers of control mechanisms to keep the immune system well-balanced. Besides having innate immune system in our body, adaptive immune system is important for having pathogen specificity and immunological memory. One of the major lymphocyte subsets in the adaptive immune system are T cells, which are so named because they differentiate in the thymus from immature precursors called thymocytes. The thymus is a primary lymphoid organ that provides a specialized environment for differentiation of T cells from hematopoietic progenitors. The thymus consists of not only developing T cells, or thymocytes, but also of heterogeneous thymic stormal cells. The thymus is broadly organized into two main areas, the outer cortex and inner medulla. Both compartments contain unique stromal subsets such as medullary thymic epithelial cells (mTECs), cortical thymic epithelial cells (cTECs), and dendritic cells (DCs) that provide essential signals required for proper T cell development (1).

Early thymocyte progenitors, derived from precursors in the bone marrow, enter the thymus through blood vessels at the cortico-medullary junction (CMJ) (2). T cells differentiate through several discrete stages as they mature. Double negative cells (DNs), so named because they do not express either CD4 and CD8 on their surface, are the earliest thymocyte progenitors. When hematopoietic progenitors enter the thymus at the CMJ, they are not yet committed to the T cell lineage. Through interactions with stromal cells in the cortex, DN cells commit to the T cell lineage (3). Once they committed to the T cell lineage, T cells go through multiple steps to express unique and functional T cell receptors (TCR) on their surface. The TCR is essential for recognizing foreign antigen presented by host-antigen presenting cells. When an infection has occurred, short forms of the peptides that are derived from the pathogen proteome is presented on self-MHC molecules on antigen presenting cells. Unique TCRs expressed on thymocytes must be able to recognize peptide-self-MHCII complexes. Since rearrangement is mostly random, it is important that thymocytes express a wide range of TCRs by gene rearrangement and form polyclonal TCR repertoire during the developmental process to have the potential to recognize an array of potential foreign antigens presented by self-MHC (4, 5).

More mature DN cells then migrate towards the middle of the cortex where they begin to rearrange their T cell receptor beta chain (TCRβ) genes, through a process known as VDJ recombination (6). Those cells that do not make an in-frame TCRβ rearrangement fail to express TCRβ protein, and they undergo apoptosis. The process which check successful generation of TCRβ chain is called β-selection. If a functional TCRβ chain is produced, it is pared with pre-TCR-α chain, which is a fixed, non-rearranged generated

alpha gene, to form a complex called the pre-TCR. They signal through the pre-TCR, survive, proliferate, and differentiate into double positive (DP) thymocytes that express both CD4 and CD8 co-receptors. DP cells are localized throughout the cortex, where they undergo TCRα chain gene rearrangements, giving them the opportunity to express a functional TCRαβ heterodimer on their surface. DP cells that successfully express TCRαβ are subject to positive selection, which ensures survival of only those thymocytes that express TCRs that are self-major histocompatibility complex (MHC)-restricted. Positive selection ensures that only thymocytes with potentially functional TCRs mature (Figure1.1) (6-9).

Positive selection occurs in the cortex where cTECs present self-peptide:MHC complexes on their surfaces (Figure1.1). Low avidity interactions between the TCRs on DP thymocytes and self-peptide:MHC complexes on cTECs lead to survival of DP cells and up-regulation of chemokine receptors (such as CCR4(10)), enabling post-positive selection cells to migrate toward the medulla, where they undergo further maturation. If a DP cell undergoes positive selection following a TCR interaction with peptide presented on MHC-I it differentiates into a $CD8^+$ single positive (SP) cell, while positive selection in response to MHC-II complexes drives differentiation into the $CD4^+$ SP lineage. $CD4^+$ T cells are helper T cells which promote immune response by secreting cytokines. $CD8^+$ T cells are called cytotoxic T cells, which abolish pathogen-infected cells.

Once SP cells enter the medulla, they are subject to negative selection, the process by which cells bearing TCRs with high affinity for self-antigens are eliminated, thus preventing export of autoreactive T cells that induce autoimmunity. SP cells scan self-

peptide:MHC complexes presented by mTECs and DCs in the medulla. Recently, several studies have shown that negative selection occurs not only in medulla, but also in cortex. (11-13) Using *Bim*$^{-/-}$; Nur77^{GFP} mice in which TCR signaling can be monitored by GFP level and negatively selected thymocytes are rescued by blocking apoptosis, it is shown that there are DP thymocytes undergoing negative selection in cortex. (12, 13) This suggests that antigen presenting cells in cortex may contribute to eliminating autoreactive thymocytes.

SP cells that interact with self-peptide:MHCs with intermediate affinity are more likely to differentiate into regulatory T cells (Tregs), whose role in the periphery is to actively suppress immune responses against self-antigens (7, 8). There are several mechanisms proposed as to how Treg suppress immune responses(14, 15). It has been proposed that Treg cells can suppress immune response by repression of activated thymocyte proliferation in a cell contact dependent manner (16, 17). Additionally, there are other studies which show that suppressive cytokines, IL-10 and TGFβ, also induce reduction of thymocyte activation to inhibit immune response (18-20).

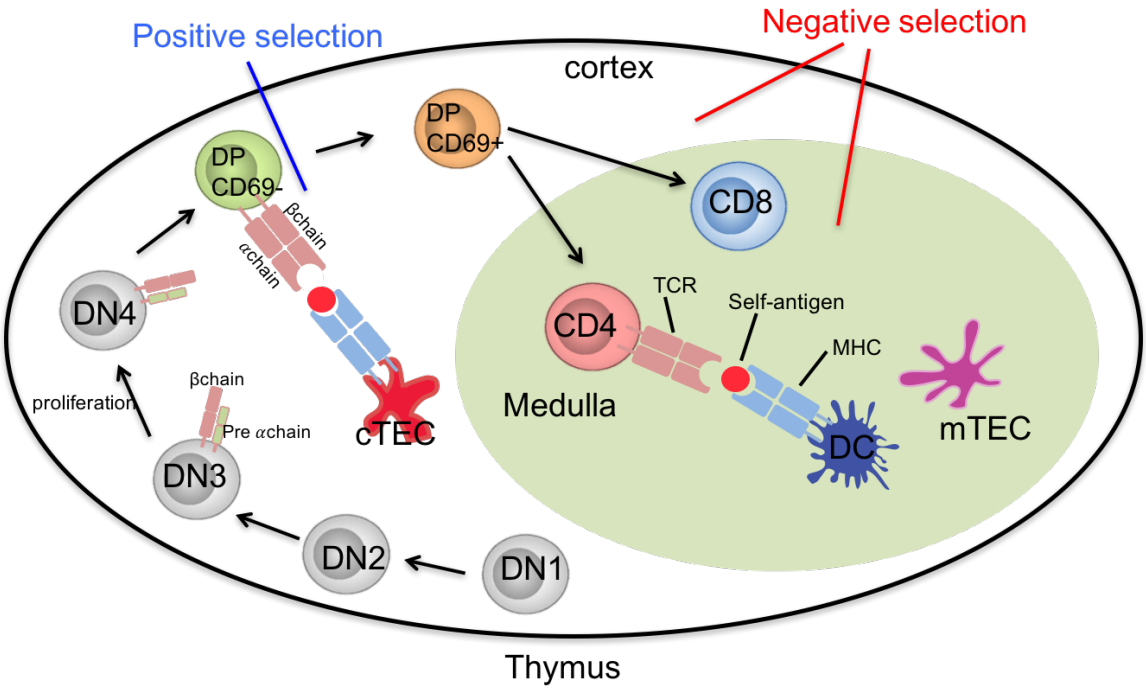

Figure1.1 An overview of thymocyte differentiation

Thymocyte development occurs in successive differentiation stages in which thymocytes localize to distinct thymic regions. The thymus is composed of cortical and medullary regions. Immature thymocytes (DN1-DN4) commit to the T cell lineage and initiate TCR gene rearrangements as they traverse the cortex. DP cells undergo positive selection in the cortex, signaling a transition to the SP stage. SP cells translocate to the medulla where they are subject to negative selection against numerous self-antigens, and then emigrate from the thymus to join the peripheral naïve T cell pool.

At both the DP and SP stages, thymocyte fate is dictated largely by signal strength of the TCR as it engages peptide:MHC complexes on surrounding stromal cells. DP thymocytes expressing TCRs with very weak to no affinity for self-peptide:MHC complexes undergoes "death by neglect". This is because the level of TCR signaling is not sufficient to upregulate expression of pro-survival genes. High affinity TCR interactions at the DP and SP stages causes apoptosis, thus eliminating potentially auto-reactive cells before they have the opportunity to enter the periphery and cause autoimmunity (9). SP cells that encounter self-peptide:MHC complexes of intermediate affinities can undergo further maturation, or differentiation into the regulatory T cell lineage. However, the TCR affinity threshold that determines which cell fate is adopted, as well as other molecular signals that modulate this decision have not been clearly elucidated. Once thymocytes have matured completely in the medulla, they are exported from the thymus as naïve T cells and migrate into secondary lymphoid organs, where they may join the peripheral T cell pool and contribute to adaptive immune responses against pathogens and tumors.

Each stage of thymocyte development is governed by signals delivered by thymic stromal cells. Thymic stromal cells reciprocally depend on signals from thymocytes for their maturation and maintenance. Thus, understanding the cellular and molecular signals that govern this bi-directional crosstalk is essential to our understanding of differentiation of a healthy, diverse, and self-tolerant T cell compartment.

1.2 THYMIC STROMAL CONTRIBUTION TO THYMOCYTE DEVELOPMENT

1.2.1 Cortical Thymic Epithelial Cells

cTECs are thymic epithelial cells localized within the cortical region of the thymus. They are phenotypically and transcriptionally distinct from thymic epithelial cells in the medulla and have a unique role in promoting thymocyte differentiation. cTECs are defined by the expression of cytokeratin–8/18, Ly51, MHCII, and Epcam (21, 22). Key roles played by cTECs include provision of signals that promote T-lineage commitment (23, 24) and positive selection (25).

Thymocyte progenitors that enter blood vessels at the CMJ encounter a cTEC population expressing DLL4 to activate Notch signaling, which is required for T-lineage commitment. Thus, in the absence of Notch signals, thymocyte progenitors differentiate into NK cells or B cells (26). This has been shown in *in-vitro* culture assays using DLL1 expressing OP9-DL1 cells, where hematopoietic cells develop into T cells and hematopoietic cells with no signal develop into B cells (26, 27). Furthermore, it has been demonstrated that cTECs provide DLL4, which is essential for commitment of pre-cursors to the T cell lineage (28). cTEC also express IL-7, and signaling through the IL-7R is required for survival and proliferation of thymocytes at DN3 and DN4 (6, 24, 29).

In addition to providing survival and differentiation signals to DN thymocytes, cTECs have the unique capability of positively selecting DP thymocytes that express self-MHC restricted TCRs. cTECs present peptides on both MHC-I and MHC-II molecules. There are several unique aspects of the proteolytic machinery that alters presentation of

self-peptides so as to promote thymocyte positive selection. Peptides presented by the MHC-I molecules are generated in the cytosol by the proteasome. Interestingly, cTECs express a unique catalytic proteosomal subunit β5t, that distinctly cleaves self-proteins to generate peptides for positive selection. (30, 31). In the absence of β5t, positive selection of CD8SP is impaired (31-33). In addition, replacing expression of β5t in cTECs with other proteasomal subunits that are not expressed by mTECs did not restore positive selection of CD8SP thymocytes (34). Together, these studies demonstrate that a unique pool of peptides generated by β5t is required for efficient positive selection of CD8SP thymocytes, although it is not understood why or how this peptide pool is specialized for this function. MHC-II peptide presentation is also uniquely regulated in cTECs, which express high levels of the serine protease TSSP and the lysosomal protease cathepsin L, which generate peptides required for efficient positive selection (35, 36). Thus, cTECs are required for positive selection of DP thymocytes with a diverse repertoire of TCRs that are both MHC-I and MHC-II restricted.

1.2.2 mTEC

mTECs are localized within the medulla region of the thymus and are responsible for presenting tissue restricted antigens to developing thymocytes, which is critical for negative selection. mTECs are defined as $CD80^{+}$, $EpCAM^{+}$, $MHC\text{-}II^{+}$, and $UEA\text{-}1^{+}$ through flow cytometry analysis and by $Cytokeratin\text{-}5^{+}$ and $Cytokeratin\text{-}14^{+}$ through immunohistochemistry (25). mTECs are subdivided into $mTEC^{lo}$ ($CD80^{lo}$ $MHC\text{-}II^{lo}$) and

mTEC^{hi} (CD80^{hi} MHC-II^{hi}) subsets which are functionally distinct in their capacity to select medullary thymocytes. Previously it was thought that all mTEC^{lo}s were the precursors of mTEC^{hi}s but recently it has been recently shown that the portion of mTEC^{lo} is 'post-aire mTEC' which indicate that mTEC^{lo}s are a heterogeneous cell population (37, 38).

Differentiation of mTECs in the medulla, which is essential for central tolerance, is regulated by crosstalk between thymocytes and mTEC progenitors. It has also been demonstrated that RANKL (Receptor activator of nuclear factor kappa-B ligand) on positively-selected thymocytes binds RANK on mTEC^{lo}s, promoting mTEC maturation (39). Therefore, RANKL-deficient mice show a significant reduction in their number of mTECs and fail to establish self-tolerance (39, 40) Along with RANKL, it has been demonstrated that other ligands of the tumor necrosis factor superfamily (TFNSF) cytokines also contribute to mTEC differentiation, such as CD40L (40) and lymphotoxin (LT)(41) (25). Furthermore, TCR-mediated interactions between CD4^{+} T cells and self-antigen-MHCII on mTECs play a pivotal role in promoting the expansion of mature mTECs in the medulla (42). This indicates that crosstalk between mTECs and T cells is necessary for mTEC maturation, and thus central tolerance.

The medulla is a specialized microenvironment for enforcing self-tolerance of maturing T cells, and thus, preventing autoimmune disorders. In order to educate thymocytes against auto-reactivity, mTECs have the unique ability to express a broad range of self-proteins otherwise expressed only in terminally-differentiated organs, such as the eye or pancreas. These tissue restricted antigens (TRAs), such as insulin and albumin (43) have no functional role in mTEC cellular biology, but when presented on the cell surface

in the context of MHC serve to delete auto-reactive SP cells. SP cells accumulate in the medulla, where they rapidly scan the antigenic library expressed on medullary APCs. SP cells with high affinity for self-antigens undergo apoptosis in a process referred to as negative selection. TRA expression on mTECs is promoted by the transcriptional regulator AIRE, which promotes low-level expression of genes that are epigenetically silenced in TECs (44, 45). Mutations in AIRE have been identified in APECED (autoimmune polyendocrinopathy-candidiasis-ectodermal dystrophy) patients, who suffer from multi-organ autoimmunity, as do AIRE-deficient mice, indicating that AIRE is essential for enforcing mTEC TRA expression and establishing self-tolerance (46, 47). However, over half of TRAs are AIRE independent, suggesting complementary mechanisms for inducing TRAs in mTECs (48-50). AIRE is expressed in the more differentiated $mTEC^{hi}$ subset, as opposed to $mTEC^{lo}$ cells. Recent studies using single cell RNA transcriptome analysis have identified that 95% of the reported TRA are expressed by mTECs (51). However, only 1-3% of $Aire^{+}$ $mTEC^{hi}$ cells are stochastically expressing each Aire dependent TRA at a given time (50, 52). Therefore, it is important that SP thymocytes must efficiently scan TRAs in the medulla to encounter the full range of auto-antigens to eliminate thymocytes expressing self-reactive TCRs.

1.2.3 Dendritic cells and their role in negative selection

In addition to TECs, dendritic cells are the other major antigen presenting cell subset in the thymus, (53). There are two types dendritic cells in the thymus, plasmacytoid

DCs (pDCs) and conventional DCs (cDCs). pDCs are defined by the expression of CD45RA^{+}, PDCA1^{+}, B220^{+}, and CD11c^{mid}. cDCs are defined by CD11c^{hi}, MHCII^{+}, and CD45RA^{-}. cDCs can be further divided into signal regulatory protein-α^{+}(Sirpα) DCs and Sirpα^{-}DCs, which are defined as Sirpα^{+} CD11b^{+} CD8^{-} and Sirpα^{-} CD11b^{+} CD8^{+} DCs, respectively (54).

All dendritic cells originate from hematopoietic progenitors in the bone marrow (55). Within the thymus, Sirpα^{-}DCs have been shown to develop from intrathymic hematopoietic progenitors (56-59). Additional studies using congenically marked parabiotic mice and cell transfer experiments have demonstrated that. the other two DC subtypes, pDCs and Sirpα^{+}DCs, are recruited to the thymus from the periphery (60). Accordingly, Sirpα^{-}DCs are known as resident DCs and Sirpα^{+}DCs are called migratory DCs (30).

Thymic DCs are critical for the induction of negative selection and Treg generation. Mice lacking MHC-II in bone marrow derived APCs have an accumulation in CD4SP cells in the thymus, reflecting impaired deletion of autoreactive cells (61, 62). CD11c depleted mice have comparably impaired negative selection, with severe autoimmune consequences (63). Previous studies have also shown that MHC-II deficient APCs result in impaired Treg induction (64-66). In addition, to presenting self-peptides derived from their own proteome to induce tolerance, DCs also present TRAs to thymocytes. DCs don't express AIRE; instead, they acquire TRAs from mTEC^{hi} cells, although the mechanisms of transfer are incompletely understood (67, 68) (64). Furthermore, antigens presented by dendritic cell

are also acquired from the blood and other peripheral tissues (58, 69-71). Sirpα^{+}DCs are able to sample antigens from the bloodstream and migrate into the thymus, which is mostly mediated by CCR2. (70, 71) By contrast, thymic Sirpα^{-}DCs present antigens from mTEC more efficiently than Sirpα^{+}DCs. Their localization in the medulla is guided by Xcr1 (66, 72). Given the distinct self-antigens displayed by multiple DC subsets, SP thymocytes also must scan many DCs, in addition to mTECs, during their residence in the medulla to encounter the full range of displayed auto-antigens.

1.3 CONTRIBUTION OF CHEMOKINE RECEPTORS TO CENTRAL TOLERANCE INDUCTION IN THE THYMUS

If T cells do not enter the medulla or interact with APCs, autoimmunity will ensue; therefore, it is important to elucidate the cellular and molecular mechanisms that influence SP medullary entry and scanning of APC subsets therein. The importance of medullary entry for central tolerance is exemplified by studies of CCR7-deficient mice. CCR7 is a G protein-coupled receptor that is upregulated after positive selection. CCL19 and CCL21, ligands for CCR7, are expressed by mTECs, and lead to accumulation of SP cells in the medulla (73). 2-photon imaging have revealed that CCR7 contributes to chemotaxis of SP cells towards the medulla as well as their rapid motility (74). Because many CCR7-deficient thymocytes are aberrantly localized to the cortex, they do not efficiently interact with medullary APCs in the medulla, resulting in failed central tolerance and eventual autoimmune diseases (75). These findings indicate that entering and accumulating with the

medulla and interacting efficiently with mTECs and DCs therein is vital for the formation of self-tolerance. Indeed, a previous study showed that thymocytes in *Mst1*$^{-/-}$ mice migrate slowly and have impaired interactions with mTECs in the context of CCR7 signaling, resulting in incomplete negative selection (76). While CCR7 is an essential mediator of medullary entry and central tolerance induction, our data indicates that additional GPCRs contribute to these processes. Pertussis Toxin (PTX) inhibits signaling through heterotrimeric G proteins, and treatment with PTX disrupts the migration of lymphocytes via GPCRs, including chemokine receptors. While PTX treatment abolished thymocyte medullary entry, CCR7-deficiency merely diminishes the accumulation of SP thymocytes within the medulla, indicating other GPCRs promote thymocyte medullary entry. Recently our lab demonstrated a role for CCR4 in DP CD69^{+} thymocyte migration, suggesting that CCR4 is vital for medulla entry of DP CD69^{+} thymocytes. However, CCR4 deficient cells do not completely block medulla entry. These findings indicate that cooperation of GPCRs acts synergistically to enforce efficient medullary entry, and thus central tolerance (74). It has also recently been shown that though *Ccr4*$^{-/-}$*Ccr7*$^{-/-}$ SP cells are defective in entering the medulla, some are able to migrate in, suggesting additional chemokine receptors contribute to their medullary migration (77).

Once thymoyctes enter the medullary region, they have to migrate rapidly to scan mTECs and DCs displaying the full spectrum of diverse TRAs. Two-photon imaging has revealed that medullary thymocytes migrate faster than those in the cortex and make frequent, transient contacts with DCs (67, 74, 78) While DP and CD4SP in the cortex migrate at 5μm/min and 14.3μm/min, respectively, CD4SP in the medulla migrate at a

speed of 16μm/min (76) and contact approximately 500 DCs in the medulla (79). It is likely that the rapid motility of SP cells in the medulla promotes efficient scanning all of the self-antigens presented within the medulla. Thus, it is also important to evaluate the contribution of candidate GPCRs to rapid motility, as well as medullary entry and accumulation of post-positive selection thymocytes.

1.4 THE CONTRIBUTION OF THYMIC STROMAL CELLS TO AGE-ASSOCIATED THYMIC INVOLUTION

Involution of the thymus with age is a well-established phenomenon, which contributes to a decline in immune responses in aged individuals. The thymus in mice begins to involute after 6weeks of age, when the thymus reaches its maximum size. The thymic atrophy causes the decease in naïve T cell output (80, 81). The turn-over rate and number of TECs decreases progressively with age during thymic involution (82). The expression of *Foxn1*, a transcription factor required for TEC differentiation, declines with age in mice (83-87), and is thought to be a major factor regulating thymic involution. Additionally, organismal senescence results in abnormal thymic stromal organization (86, 88, 89). Even though it has been shown that the proliferation rate of thymocytes in the thymus declines with age, it was unclear whether the dysfunctional phenotype of aged thymocytes is caused by intrinsic or extrinsic defects. One recent study has indicated that an aged thymic microenvironment contributes to the aging process, as transplantation of old bone marrow into young mice enables the generation of functional thymocytes (90).

Another study demonstrated that a reduction of androgen hormone helps regenerate aged thymus and enhances T cell function (81, 91). While castration results in larger thymuses in older mice, it does not completely halt thymic involution, suggesting that other mechanisms are at play (92). A recent study has also shown that transplantation of young colony-forming thymic epithelial cells into 9 to 12 month-old mice resulted in partially rejuvenating the thymus, ultimately leading to normal T cell production. However, the circulating components from young mice by heterochronic parabiosis is not sufficient to rescue aged thymus (93). Yet another study showed, transduction of cyclin D1 and inactivation of Rb family proteins restores thymic mass in aged mice (94, 95). Despite many studies producing a partial restoration of thymus function in aged mice, the mechanisms by which involution occurs in the aging thymus remain elusive.

1.5 DISSERTATION OBJECTIVE

Elucidation of age associated thymic stromal changes during thymic involution by global transcriptional analysis of thymic stromal subsets

Age associated thymic involution results in impaired thymic structure, reduction of thymocyte output, and lowered T cell function, which leads to decreased immune function and infections (5, 89, 96). Given that crosstalk between thymocytes and thymic stroma cells is critical for thymocyte development, these reduced immune functions may be partially due to changes in the thymic microenvironment. Elucidation of molecular

mechanisms underlying thymic involution may ultimately lead to therapies that could rejuvenate immune capabilities in older individuals.

To identify such molecular mechanism, we analyzed transcriptomes of thymic stromal subsets during early thymic involution. Interestingly, genes differentially expressed in older mice were mostly found in $mTEC^{lo}$, $Sirp\alpha^{-}DC$, and $Sirp\alpha^{+}DCS$, but not in cTEC, $mTEC^{hi}$ or fibroblast populations. Our data suggests that the expression of cell cycle related genes were decreased in $mTEC^{lo}$. Further analysis showed that E2F3, which controls cell cycle progression, target genes are downregulated in 6month of thymic epithelial cells especially in cTEC and $mTEC^{lo}$. Additionally, pro-inflammatory genes in DC and DCS were increased with age. One of those proinflammatory cytokine, IL-1 is known to promote thymic atrophy (97), which suggests that thymic dendritic cells contributes to thymic involution. Out data expands the knowledge on the etiology of age associated thymic involution

Understanding the role of EBI2 and GPR146 in thymocyte development

Throughout thymocyte development, thymocyte progenitors undergo bidirectional crosstalk with the thymic epithelial cells, which is important for proper development of both the thymocyte and epithelial subsets. Chemokine receptors, a subset of G protein coupled receptors (GPCRs), have been implicated in guiding thymocytes into the different thymic regions, thus enabling the required interactions with different stromal subsets. Notably, failure of thymocytes to enter the thymic medulla resulted in deformation of

medullary thymic epithelial cells, which are important for presenting TRAs and eliminating self-reactive thymocytes through negative selection. To identify GPCRs that contribute to thymocyte medullary entry and are important for central tolerance, we performed transcriptome analysis. Based on expression profiling, we identified EBI2 and GPR146 as candidate GPCRs that could contribute to thymocyte medullary entry and/or negative selection.

Our study has found that EBI2 is required for negative selection in response to low level of endogenous antigens. Additionally, EBI2 deficiency alters the cell fate decision in favor of Treg generation over negative selection in response to higher affinity antigens. Along with this, we found that *Ebi2*$^{-/-}$ mice showed altered TCR repertoire. Further analysis showed that EBI2 contributes to rapid motility and accumulation of CD4SP in medulla, which are important for efficient negative selection of thymocytes.

In order to determine the role of GPR146 in thymocyte development, we successfully generated *Gpr146*$^{-/-}$ mice. Furthermore, analysis on *Gpr146*$^{-/-}$ mice revealed that *Gpr146*$^{-/-}$ cells showed high cellularity than *Gpr146*$^{+/+}$, when bone marrow cells were transferred to reconstitute the thymus in a competitive condition. This suggests new and potential roles of GPR146 in thymocyte development.

Chapter 2: Global transcriptional profiling reveals distinct functions of thymic stromal subsets and age-related changes during thymic involution

The contents of the chapter are modified from *Cell reports*, 9(1), pp.402–415. Sanghee Ki, Daechan Park, Hilary J. Selden, Jun Seita, Haewon Chung, Jonghwan Kim, Vishwanath R. Iyer, Lauren I. R. Ehrlich, 2014. Global transcriptional profiling reveals distinct functions of thymic stromal subsets and age-related changes during thymic involution.[1,2]

2.1 ABSTRACT

Age-associated thymic involution results in diminished T cell output and function in aged individuals. However, molecular mediators contributing to the decline in thymic function during early thymic involution remain largely unknown. Here we present transcriptional profiling of purified thymic stromal subsets from mice 1, 3, and 6 months of age, spanning early thymic involution. The data implicate novel biological functions for a subset of thymic epithelial cells. The predominant transcriptional signature of early thymic involution is decreased expression of cell cycle associated genes and E2F3

[1] Acknowledgments: We thank Ellen Richie and Nancy Manley for helpful discussions and Elizabeth Zuo for microarray hybridization. This work was supported by the Cancer Prevention and Research Institute of Texas (R1003; to L.I.R.E.) and the NIH/NIAID (R01AI104870-01A1; to L.I.R.E.).

[2] Authorship contributions: SK and DP performed bioinformatics analyses, with advice from VI and LE, and wrote the manuscript with LE. SK and HC generated fluidigm data with guidance from JK. HS and LE generated primary data. JS provided advice on GExC.

transcriptional targets in thymic epithelial subsets. Also, expression of pro-inflammatory genes increases with age in thymic dendritic cells. Many genes previously implicated in late involution are already deregulated by 3 to 6 months of age. We provide these thymic stromal datasets, along with thymocyte datasets, in a readily searchable web-based platform, as a resource for investigations into thymocyte: stromal interactions and mechanisms of thymic involution.

2.2 INTRODUCTION

The thymus is spatially organized into cortical and medullary regions, containing heterogeneous stromal cells, including thymic epithelial cells (TECs), dendritic cells, macrophages, fibroblasts, and endothelial cells (98). As thymocytes mature, they migrate through distinct thymic microenvironments, where they undergo bi-directional crosstalk with local stromal cells, essential for the generation of a diverse, and self-tolerant T cell pool (6). Signals provided by developing thymocytes are also required for differentiation and maintenance of thymic stromal cells (99). While some molecular signals responsible for this bidirectional signaling have been characterized, many remain to be identified.

Thymocyte:stromal cell crosstalk first occurs in the cortex where thymocyte progenitors encounter cortical TECs (cTECs) that express NOTCH1 ligands, SCF, and IL-7, which are essential for thymocyte survival, proliferation and commitment to the T cell lineage (6, 100). In addition, cTECs display self-peptide:MHC complexes that promote positive selection of self-MHC restricted thymocytes, and apoptosis of autoreactive cells

(101). Reciprocally, unidentified signals from early thymocyte progenitors are critical for cTEC differentiation (22).

Following positive selection, thymocytes migrate into the medulla where they interact with medullary thymic epithelial cells (mTECs). mTECs can be subdivided into $mTEC^{lo}$ and $mTEC^{hi}$ subsets, based on differential expression of CD80 and MHC class II. The $mTEC^{hi}$ subset expresses the chromatin modulator AIRE, which promotes expression of tissue-restricted antigens (TRAs), genes otherwise expressed in a limited number of differentiated tissues, such as the pancreas or retina (44, 102) . When medullary thymocytes engage TRAs on mTECs, they undergo apoptosis or differentiate into regulatory T cells, thus establishing central tolerance to peripheral self-antigens. Conversely, $mTEC^{lo}$ cells must engage thymocytes entering the medulla, via tumor necrosis factor superfamily members, to drive differentiation to the $mTEC^{hi}$ stage (99). Thus, bi-directional signaling in the medulla between TECs and maturing thymocytes is critical for thymocyte tolerance and medullary stromal organization.

Thymic dendritic cells also play a critical role in central tolerance. Conventional thymic dendritic cells can be subdivided into $Sirp\alpha^{-}CD8^{+}CD11b^{-}$ (DC) and $Sirp\alpha^{+}CD8^{-}CD11b^{+}$ (DCS) subsets (60). Thymic dendritic cells can acquire TRAs from mTECs to mediate deletion of autoreactive thymocytes (102). In addition, DCS traffic peripheral antigens into the thymus to mediate negative selection or induction of regulatory T cells (57, 65). Thymic dendritic cells require chemotactic signals from mTECs to accumulate in the medulla and function properly (72), underscoring the complex interplay between

thymocytes and various stromal subsets required to ensure production of a self-tolerant T cell repertoire.

The thymus involutes in an age-dependent manner, resulting in diminished TEC cellularity and turn-over (82), disrupted thymic architecture, decreased thymic output, and reduced T cell function (5, 89, 96). Both hematopoietic age-related dysfunction and degeneration of the thymic stromal compartment likely contribute to thymic involution (96, 103). While reduced levels of the transcription factor Foxn1 contribute to TEC atrophy (86), and genetic manipulation of cell-cycle regulators can maintain thymic mass in aged mice (94, 95), specific molecular pathways driving degeneration of the thymic stroma early in the process of involution remain to be discerned. Furthermore, while manipulation of sex steroids or growth factor levels in aged individuals can transiently increase thymic size (91, 104), the resultant thymi are not functionally equivalent to young thymi, and may be incapable of maintaining central tolerance (92). Thus, identifying molecular pathways that regulate stromal changes associated with involution remains an important goal.

Here we present global transcriptional profiling of purified thymic stromal subsets from mice at 1, 3, and 6 months of age, enabling the community to query stromal subset-specific gene expression before and during early thymic involution. Griffith et al. previously reported transcriptional profiles of non-sorted thymic stroma from the cortex, medulla and cortico-medullary junction, enabling evaluation of regionalized gene expression in young and aged thymi (92, 105). The current resource provides complementary information about gene expression in specific stromal cell types during early thymic involution. Our data reveal predicted, as well as unexpected expression of

genes in different thymic stromal subsets that suggest novel stromal cell functions. Interestingly, decreased expression of cell-cycle genes and downregulation of E2F3 activity are major hallmarks of early thymic involution in the TEC compartment. Upregulation of proinflammatory genes in thymic dendritic cell subsets also occurs over this time course. Analysis of genes previously implicated in late thymic involution reveals some of these factors may contribute to early involution, while others are likely sequelae of the aging process. To facilitate use of this resource, we provide our thymic stromal gene expression data, along with our previous thymocyte transcriptional profiling data, as an in silico model in the readily searchable web-based platform Gene Expression Commons (GExC) (106) (https://gexc.stanford.edu/model/475). Exploration of our datasets on this user-friendly interface will enhance elucidation of the molecular pathways mediating thymocyte-stromal cell crosstalk and age-associated thymic stromal changes.

2.3 Experimental Procedures

Mice

C57BL/6J mice were housed at the UT Austin animal facility, under conditions approved by the Institutional Animal Care and Use Committee.

FACS isolation of thymic stromal subsets and transcriptional profiling

Thymi from 1, 3, and 6-month-old male C57Bl/6J mice were digested with Collagenase D (Roche, Switzerland), followed by Collagenase/Dispase (Roche) in the presence of DNase I, as described previously(107). Cells were immunostained with FITC-conjugated *Ulex europaeus* agglutinin I (UEA-1) (Vector Laboratories) and the following fluorochrome-conjugated antibodies (eBioscience or BioLegend, unless indicated): EpCAM (G8.8), TER-119 (TER- 119), CD11c (N418), CD31 (390), Sirpα (P84), B220 (RA3-6B2), I-A/I-E (M5/114.15.2), CD80 (16-10A1), CD45 (30-F11, BD Biosciences), and biotinyated Ly-51 (6C3). Stromal subsets were FACS purified by double sorting to >95% purity on a FACSAria (BD Biosciences); data were analyzed with FlowJo (Treestar).

Sample preparation and transcriptional profiling

Stromal subsets were collected directly in 1ml of TRIzol (Life Technologies), and RNA was purified. 1μg of high-quality total RNA was amplified, converted to cDNA using the two-cycle cDNA synthesis protocol, labeled, and hybridized onto Mouse Genome 430 2.0 arrays (Affymetrix) at the Stanford PAN facility core according to Affymetrix's specifications. CEL files were uploaded to GExC(106, 108), where the data were normalized using the RMA algorithm (108) for normalization. An in-silico model of gene expression data from thymic stromal subsets and previous thymocyte subsets (GSE34723) (106, 108) is available (https://gexc.stanford.edu/model/detail/475). Thymic stromal expression data have been deposited in GEO (GSE56928).

Bioinformatics analysis

R (version 2.15.2) was used for hierarchical clustering (function "hclust") and DEG identification (package "limma" version 3.14.4) (109). p-values were adjusted using the Benjamini–Hochberg procedure to correct for multiple comparisons, and an adjusted p-value of 0.01 and a fold change of 2 were used as cut-offs for DEG. Subtype-specific DEGs were defined as genes differentially expressed in all pairwise comparisons with other subsets of the same age. Age-associated DEGs were defined as the union of differentially expressed genes from pairwise comparisons of single stromal subsets compared at different ages. To identify Aire-regulated genes in $mTEC^{hi}$ cells, we analyzed Aire deficient and wild-type $mTEC^{hi}$ expression data from the following datasets using R (package "affy" version 1.36.1): GSM49731, GSM49732, GSM49735, GSM49736 (48, 110). We defined the top 400 DEGs, ranked according to fold change, as Aire-regulated genes. Probe IDs were annotated using version 33 of these array platforms, and gene symbols were then compared to our $mTEC^{hi}$ DEG list to identify the extent of overlap. TRAs identified on the basis of unique tissue expression (92) were also compared to our $mTEC^{hi}$ DEG list for overlap.

PCA was performed with the "princomp" function in MATLAB R2012b, and Cluster 3.0 was used for K-means clustering. For Gene Ontology analysis, DAVID version 6.7 was used with probe Ids (111). GSEA was carried out by searching Molecular Signature Database (MSigDB) version 4.0 provided by the Broad Institute (http://www.broad.mit.edu/gsea/) (112). When multiple probe IDs mapped to a gene symbol, the maximum probe value was used for GSEA. For identification of aging associate gene sets, 1:3:6 was used for phenotype labels of ages 1, 3, and 6 months to

calculate Pearson correlations, and then the immunologic signatures (C7) and the curated gene sets (C2) of the MSigDB gene sets were queried. A nominal (NOM) p-value cut-off was applied to the results from C7. Boxplots were generated after converting human genes into mouse orthologs using the mouse annotation from Mouse Genome Informatics (MGI) released April 4, 2012. Statistical significance was determined using paired Student's t-tests.

To generate heat maps, log2-transformed expression intensities were centered on the mean (defined as zero) for each probe to compare relative expression across subtypes and ages.

RT-PCR on the Fluidigm platform

For each FACS sorted stromal subset, cDNA was synthesized from 300ng RNA using qScriptTM cDNA SuperMix (Quanta). cDNAs were diluted and preamplified with 2X Taqman preamp Master Mix (Applied BioSystems), using a pool of custom primers for transcripts of interest. qPCRs were carried out on cDNA distributed on 48.48 Dynamic Arrays, using primers for genes of interest on a BioMark System according to manufacturer's instructions (Fluidigm).

2.4 RESULTS

2.4.1 Transcriptional profiling of thymic stromal subsets at 1, 3, and 6 months of age

We FACS purified thymocyte stromal subsets from mice over the course of early thymic involution to identify subtype specific and age-regulated transcriptional profiles. Thymic cTEC, mTEC^{lo}, mTEC^{hi}, DC, DCS, and fibroblast populations were FACS purified from C57BL/6J male mice at 1, 3 and 6 months of age as follows: cTEC (Epcam^{+}CD11c^{-} UEA1^{-}MHCII^{+}Ly51^{+}), mTEC^{lo}(Epcam^{+}CD11c^{-}UEA1^{+} MHCII^{lo} CD80^{lo}), mTEC^{hi} (Epcam^{+}CD11c^{-}UEA1^{+}MHCII^{hi}CD80^{hi}), DC (MHCII^{+}Epcam^{-}CD11c^{+}Sirpα^{-}CD80^{+}), DCS (MHCII^{+}Epcam^{-}CD11c^{+}Sirpα^{+}CD80^{+}), and fibroblasts (MHCII^{-}CD45^{-}Ter119^{-}CD31^{-}) (Figure 2.1A). During the sort setup, we ensured that all Epcam^{+} TECs were included in the initial MHCII^{+} gate (Figure 2.1B). Purified mRNA from biological duplicates of each subset at each age was analyzed on Affymetrix Mouse 430 2.0 microarrays. Resultant data were uploaded to the GExC platform for normalization (106), and resultant normalized signal intensity values were used for all subsequent bioinformatics analyses herein.

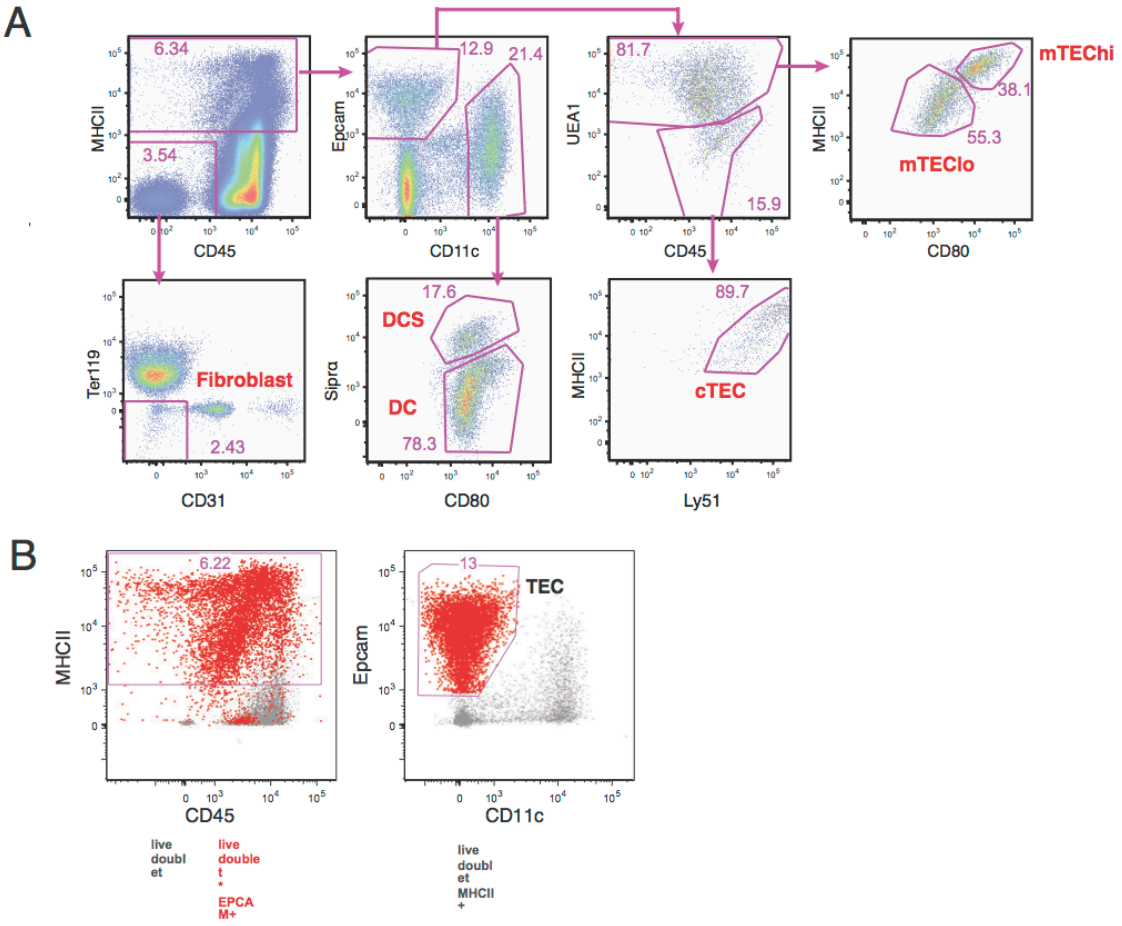

Figure 2.1 Gating schemes for FACS sorted thymic stromal subsets

(A) Strategy for sorting thymic stromal subsets (gated on live events; frequencies within gates displayed). **(B)** Backgating analysis of the EPCAM^{+}CD11c^{-} TEC population gated in the panel on the right demonstrates that the majority of TECs are within the MHCII^{+} gate in the left panel. Comparable backgating was used to adjust the MHCII^{+} gate during the initial sort setup to ensure MHCII^{lo} TECs were not excluded during cell sorting. Red events on the left panel represent cells gated as EPCAM^{+}CD11c^{-} in the absence of the MHCII^{+} gate displayed in the left panel.

To assess consistency between duplicate datasets and to globally compare transcriptional profiles between stromal subsets, we performed unsupervised hierarchical clustering and principal components analysis (PCA) on the 30% of genes most variable in expression across subsets (Figure 2.2A and 2.2B). Duplicate datasets clustered closely together, indicating reliability of the data. Stromal subtypes clustered together regardless of age (Figure 2.2A), demonstrating that each stromal subset maintains its transcriptional identity during thymic involution. Stromal subsets at 6 months of age were further from their 1 and 3 month counterparts, indicative of age-related transcriptional changes in the data. Interestingly, age-associated changes were implicated not only in TEC subsets, which have been suggested to be drivers of involution, but also in dendritic cells and fibroblasts. Overall, PCA was consistent with hierarchical clustering (Figure 2.2B), and showed that mTEC^{hi} were distal to other TEC subsets, likely due to expression of diverse TRAs. As expected, dendritic cell subtypes clustered together, while fibroblasts were distinct from other stromal subsets.

To validate our data, we queried genes previously reported to be differentially expressed in distinct stromal subsets (Figure 2.2C). TECs expressed cytokeratins and the transcription factor Foxn1, confirming their identity (22, 113). As expected, cTEC and mTEC^{lo} expressed high levels of Il7 (114, 115), while Ccl25, Cxcl12, Dll4, Enpep/Ly51, Ly75/CD205, and Psmb11/β5t were predominantly expressed by cTECs (31, 116, 117). Aire, Cldn3, and Cldn4 were expressed specifically in mTEC^{hi} cells, as expected (118). MHCII genes were expressed by dendritic cells and TECs, consistent with their roles in antigen presentation, while dendritic cells and mTEC^{hi} expressed high levels of Cd80 and

Cd86. ItgaX (CD11c) was expressed uniquely by dendritic cells, with Sirpα and Xcr1 (72) expressed uniquely in the DCS and DC subsets, respectively. Fibroblasts expressed Pdgfrα and Pdgfrβ, and the extracellular matrix (ECM) component Col6a3, as anticipated for mesenchymal cells (119).

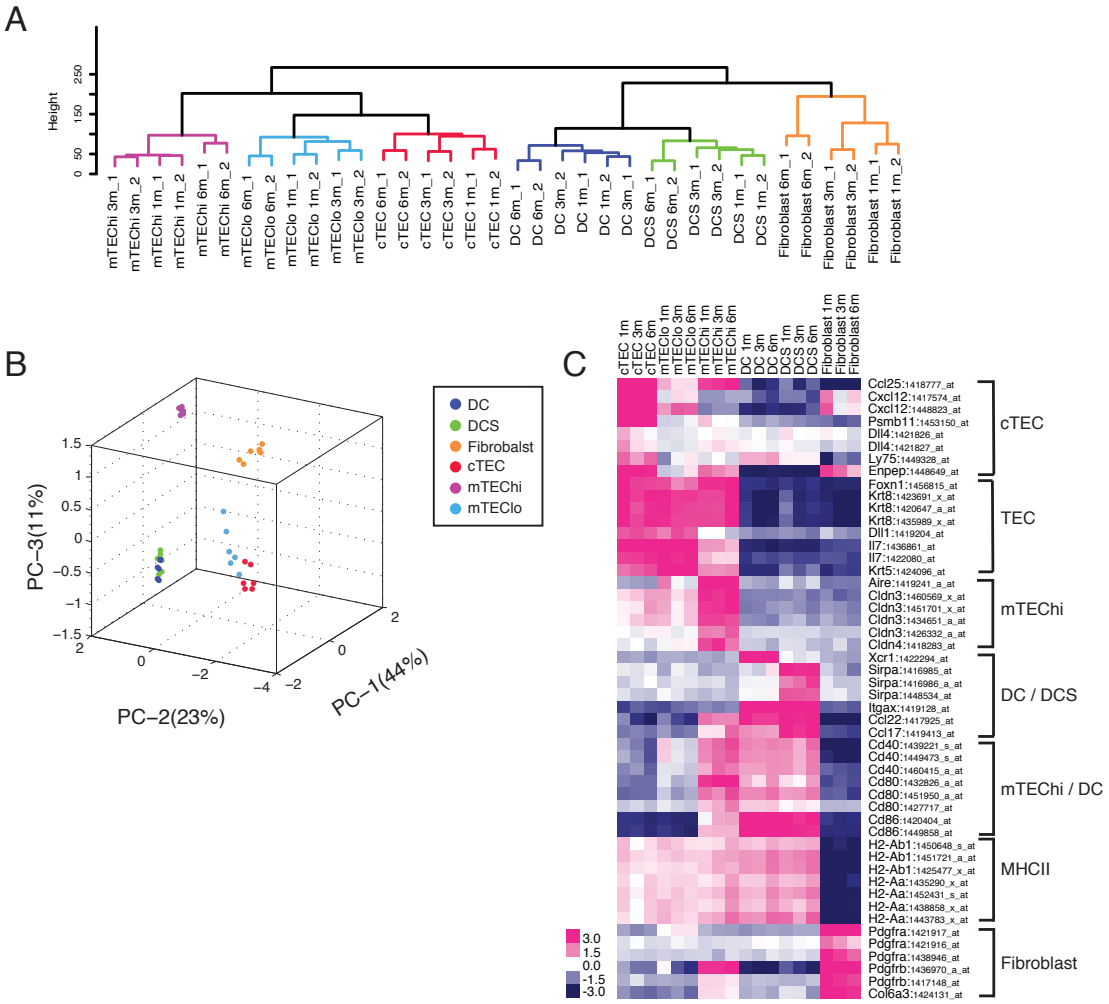

Figure 2.2 Expression profiling of thymic stromal subsets.

(A) Hierarchical clustering and (B) PCA were carried out on the top 30% of genes most variable in expression. Each symbol in the PCA represents a single array. (C) Expression of known thymic stromal subset-specific genes is presented as a heat map, using the average of biological duplicates for each subset. Probesets with a dynamic range ≥ 3 (in GExC) were displayed if multiple probesets were present for one gene.

To further validate our data, we sorted an additional biological replicate of thymic stromal subsets from mice 1 month of age, and confirmed subset-specific expression of 25 genes by qRT-PCR analysis on the Fluidigm platform (Figure 2.3). Together, these analyses validate the datasets, and demonstrate that thymic stromal subset identity is maintained during aging.

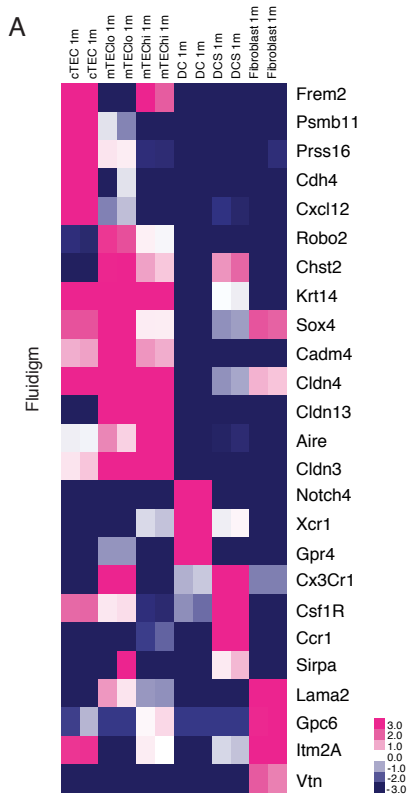

Figure 2.3 Confirmation of expression profiling data.

(A) To confirm the microarray expression profiling data, 3 - 4 genes identified as DEGs in each subset were chosen for validation by high throughput qRT-PCR (Fluidigm) on an additional biological replicate for each stromal subset.

2.4.2 Differentially expressed genes suggest distinct functions of thymic stromal subsets

We identified differentially expressed genes (DEGs) in each stromal subset as those genes uniquely up- or down-regulated by >2 fold relative to all other stromal subsets of the same age, with an adjusted p-value <0.01. As expected from PCA analysis, mTEC^{hi} and fibroblast subsets had the most unique DEGs at each age (Figure 2.4A). We next investigated common functional characteristics of unique DEGs in each subset. The top Gene Ontology (GO) term hit for DEGs from 1-month old fibroblasts was 'cell adhesion', with 'extracellular matrix' appearing as well, suggesting that although fibroblasts were sorted based on the absence of markers in other subsets, the population is greatly enriched in mesenchymal cells. A heat map of genes in the GO term 'cell adhesion' category, reveals ECM components and integrins that are likely relevant substrates for adhesion and migration in the thymus (Figure 2.4B).

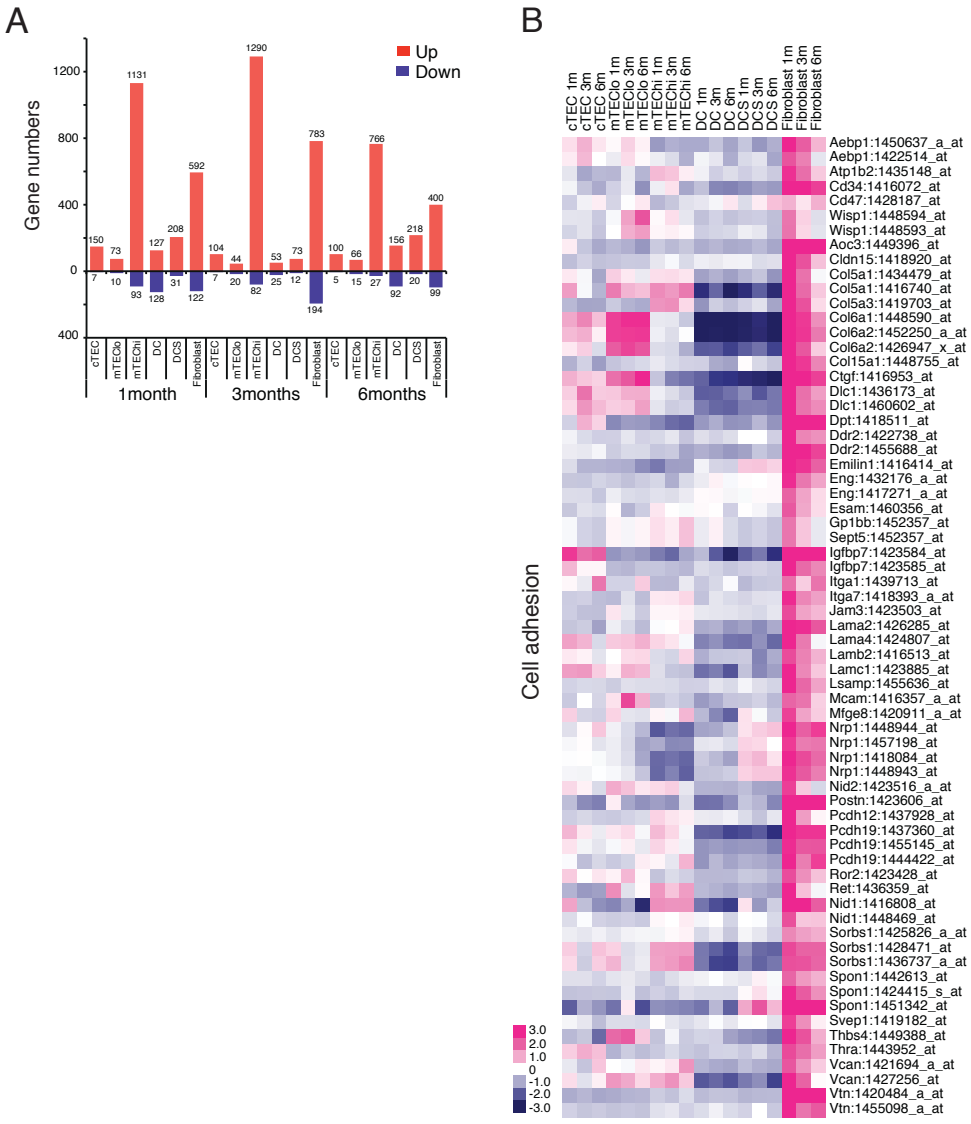

Figure 2.4 Mesenchymal signature of fibroblasts revealed by DEGs

(A) The number of stromal subset-specific DEGs, identified by pair-wise comparisons between stromal subsets of the same age, is displayed. (B) The heat map displays the relative expression of all up-regulated DEGs from 1-month fibroblasts that overlap with the "cell adhesion" GO term.

The large number of DEGs and dissimilarity in overall transcriptional relatedness of mTEC^{hi} relative to other stromal subsets (Figures 2.4A) may have been due to expression of diverse TRAs (43). To address this possibility, we identified Aire-regulated genes by analyzing published expression data from Aire deficient versus wild-type mTEC^{hi} cells (48). After excluding genes not shared between microarray platforms, we compared the list of Aire-regulated genes to mTEC^{hi} up-regulated DEGs. Of the 560 mTEC^{hi} up-regulated DEGs, only 150 (37%) were Aire-regulated (Figure 2.5A), suggesting many mTEC^{hi} DEGs are Aire-independent. Furthermore, comparison against a list of TRAs identified on the basis of limited tissue expression (92), revealed overlap with only 9% of mTEC^{hi} DEGs (Figure 2.5B). Thus, many mTEC^{hi} DEGs may have a biological function, rather than serving as TRAs. Interestingly, the top GO hit term for 1 month mTEC^{hi} DEGs was 'defense response' (p-value: 8x10-7), which included chemokines (Ccl20, Cxcl13, Cxcl3), defensins (Defb19, Defb3, Defb5, Defb6, Defb8, Defa21, Defa22), and cytokines (Il1f6, Il23a, Il5) (Figure 2.5C). Only 15 of 55 defense response genes were identified as TRAs (not shown). Thus, mTEC^{hi} cells may promote defense responses in the thymus. Consistent with a unique biological state of the mTEC^{hi} subset, AIRE has been shown to regulate differentiation of mTEC^{hi} cells (120).

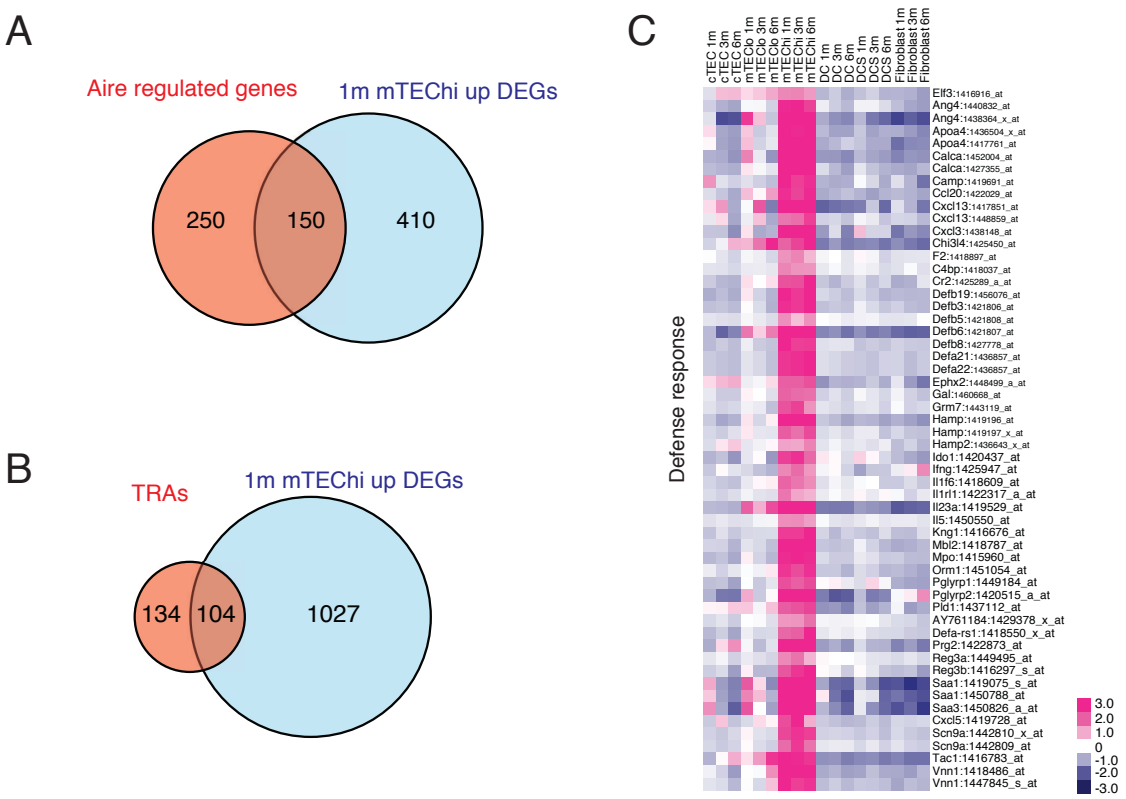

Figure 2.5 Defense response function of mTEC^{hi} revealed by DEGs.

(A) Overlap between Aire-regulated genes (48) and 1 month mTEChi up-regulated DEGs, shared between microarray platforms. (B) Overlap between TRAs (92) and 1 month mTEChi up-regulated DEGs. (C) A heat map displaying the relative expression of up-regulated mTEChi DEGs that overlap with the 'defense response' GO term hit.

Because of the transcriptional relatedness of cTEC to mTEC^{lo} and DC to DCS (Figure 2.2A-B), few DEGs were identified in these subsets (Figure 2.4A). Although these DEGs are likely important for the unique biology of these subsets (Figure 2.6A), the number of DEGs was too low to proceed with downstream bioinformatics analyses.

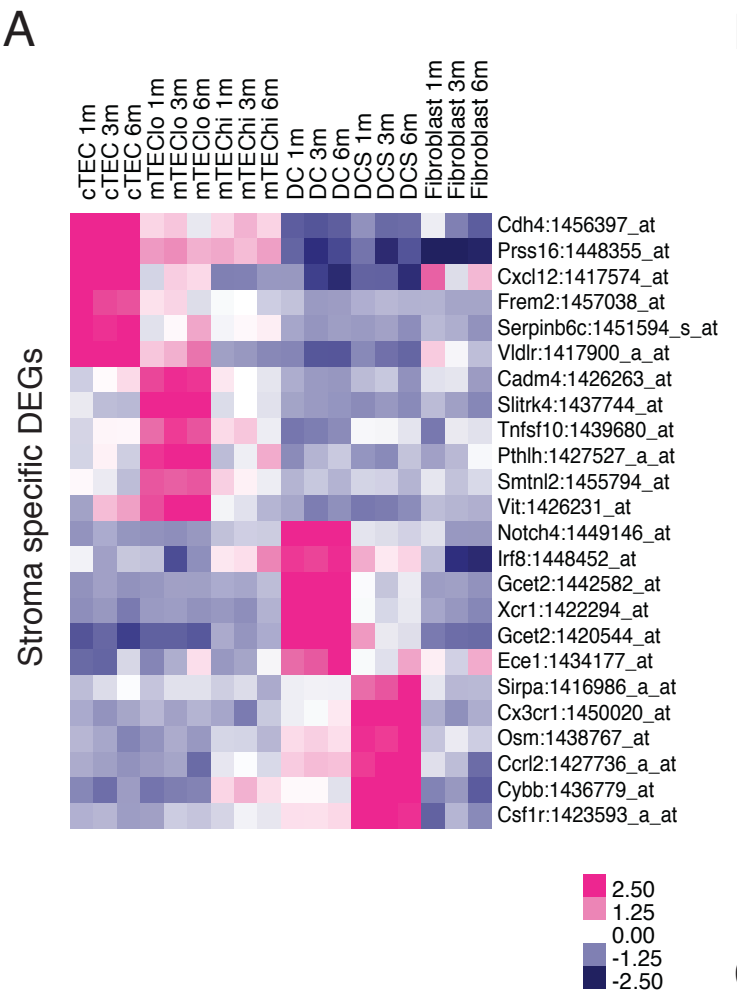

Figure 2.6 Unique DEGs in cTEC, mTEC^{lo}, DC and DCS subsets.

(A) The heat map displays the relative expression of select genes identified as unique DEGs in cTEC, mTEC^{lo}, DC and DCS subsets.

Therefore, we identified additional DEGs in cTEC after omitting mTEC^{lo}, and in DC after omitting DCS from the comparisons, and vice versa (Figure 2.7A-B). GO analyses of these DEGs confirmed epithelial characteristics of cTEC and mTEC^{lo} subsets (Figure 2.8). The "epithelium development" and "cell adhesion" terms contained previously known as well as unreported genes in cTEC and mTEC^{lo} subsets (Figures 2.9), including several genes involved in Wnt signaling, such as Wnt4 and the receptors Fzd2 and Fzd3 (consistent with Bredenkamp et al., 2014; Griffith et al., 2012). Fgfr2 likely regulates TEC cellularity, as its ligand KGF causes transient thymic regeneration in aged mice (104). Cldn8 was expressed in cTECs, while Cldn9 and Cldn12 were expressed in cTEC and mTEC^{lo} subsets, demonstrating TEC subset specificity of claudin family members, consistent with expression of Cldn3 and Cldn4 in mTEC^{hi} cells (118). The top hit from GO analyses of DC and DCS DEGs was 'immune response' (Figure 2.8), including Toll like receptors, cytokines, and chemokines (Figures 2.10), consistent with the central role for dendritic cells in eliciting and modulating immune responses.

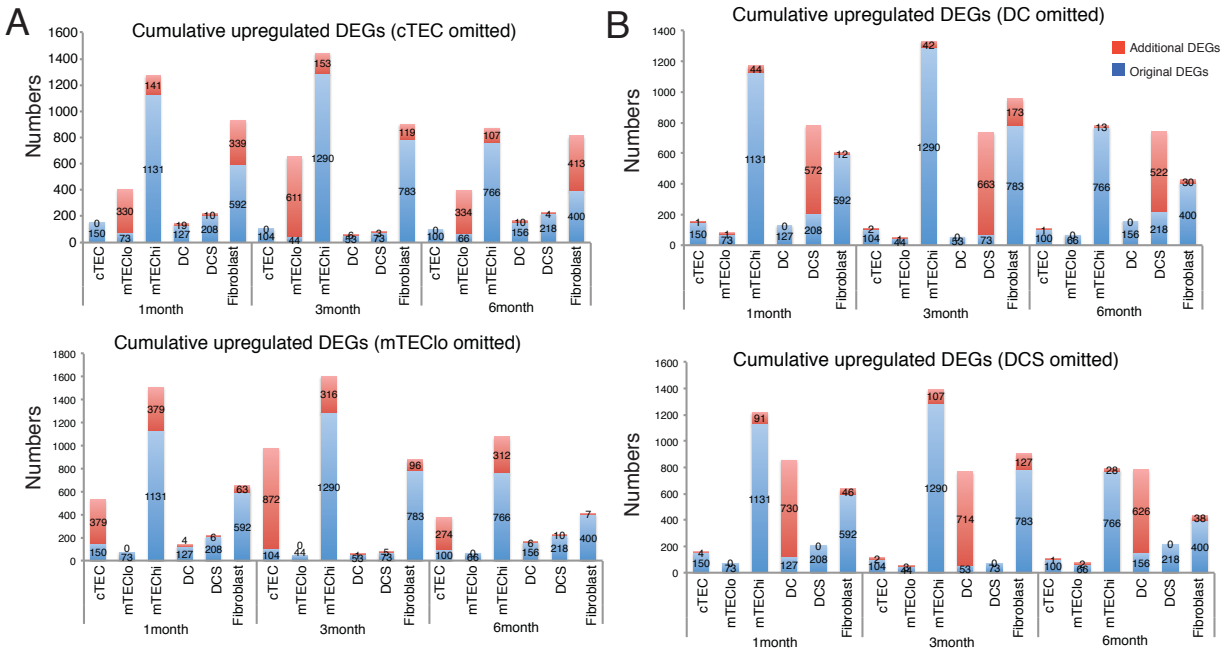

Figure 2.7 Additional DEGs of cTEC, mTEC^{lo}, DC, and DCS

(A) The graph depicts the number of cTEC and mTEClo DEGs identified before and after excluding each other during the analysis. The blue bars show the original number of DEGs when all subsets were compared in pairwise comparisons, while the red bar shows the number of additional DEGs newly identified after omitting the indicated subtype from the analysis. (B) The graph depicts the number of DC and DCS DEGs identified before and after excluding each other during the analysis, as in A.

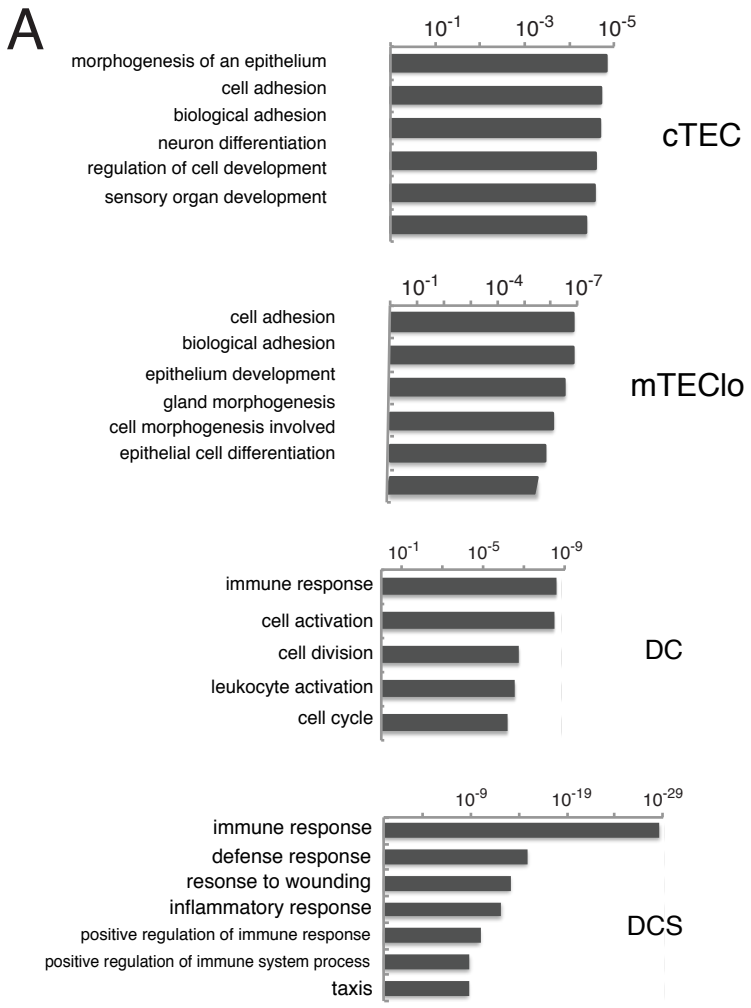

Figure 2.8 Epithelial identity of cTEC/mTEC^{lo} and immune response function of DC/DCS revealed by DEGs.

(A) GO term analyses of DEGs from cTEC/ mTEClo confirm the epithelial identity of these subsets. GO term analyses of DEGs from DC/ DCS confirm the immune response function of these subsets.

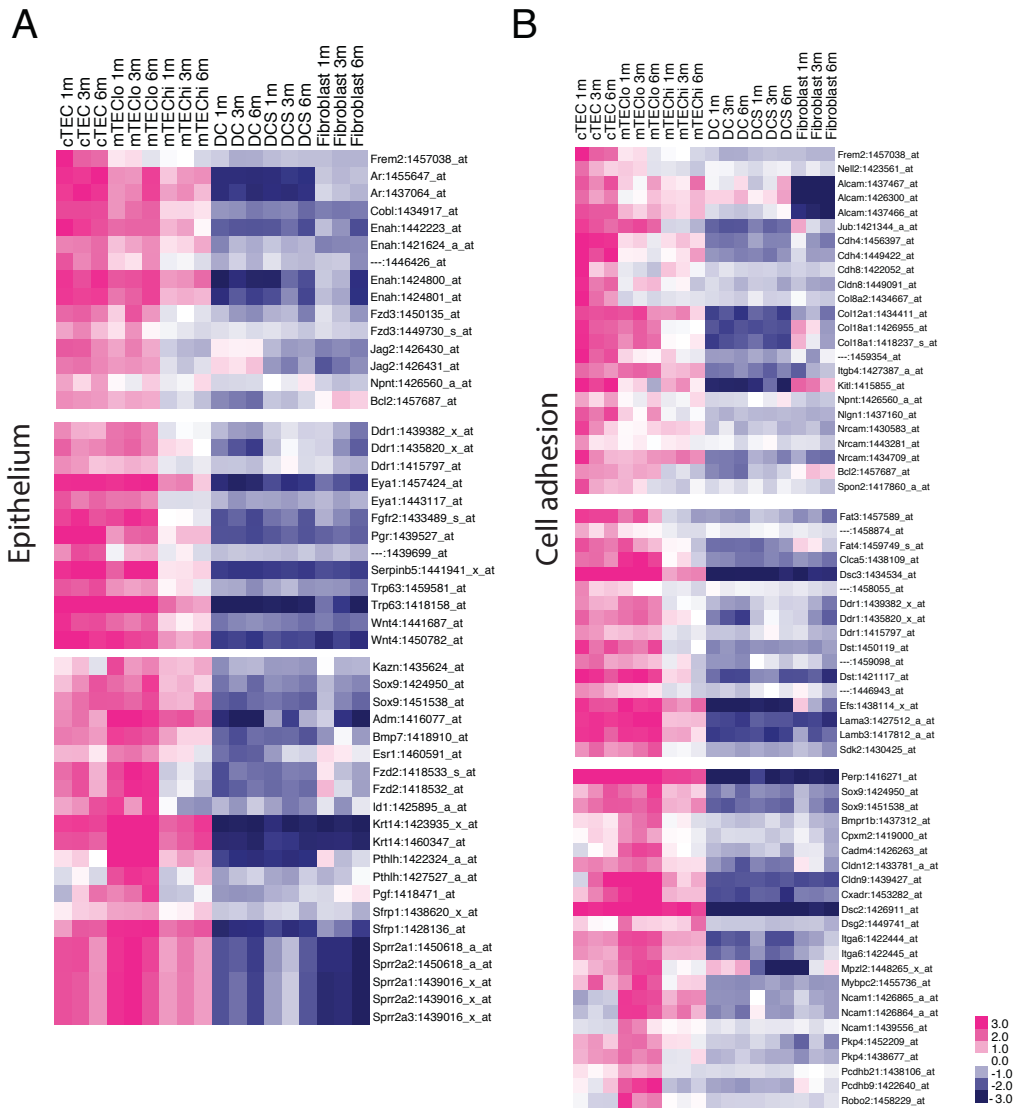

Figure 2.9 Epithelial identity of cTEC/mTEClo revealed by DEGs.

The heat maps display the relative expression of all genes in the (A) ‘epithelium’ and ‘epithelium development’ GO terms and (B) ‘cell adhesion’ GO term that overlapped with up-regulated DEGs identified in 1-month cTEC and mTEClo cells.

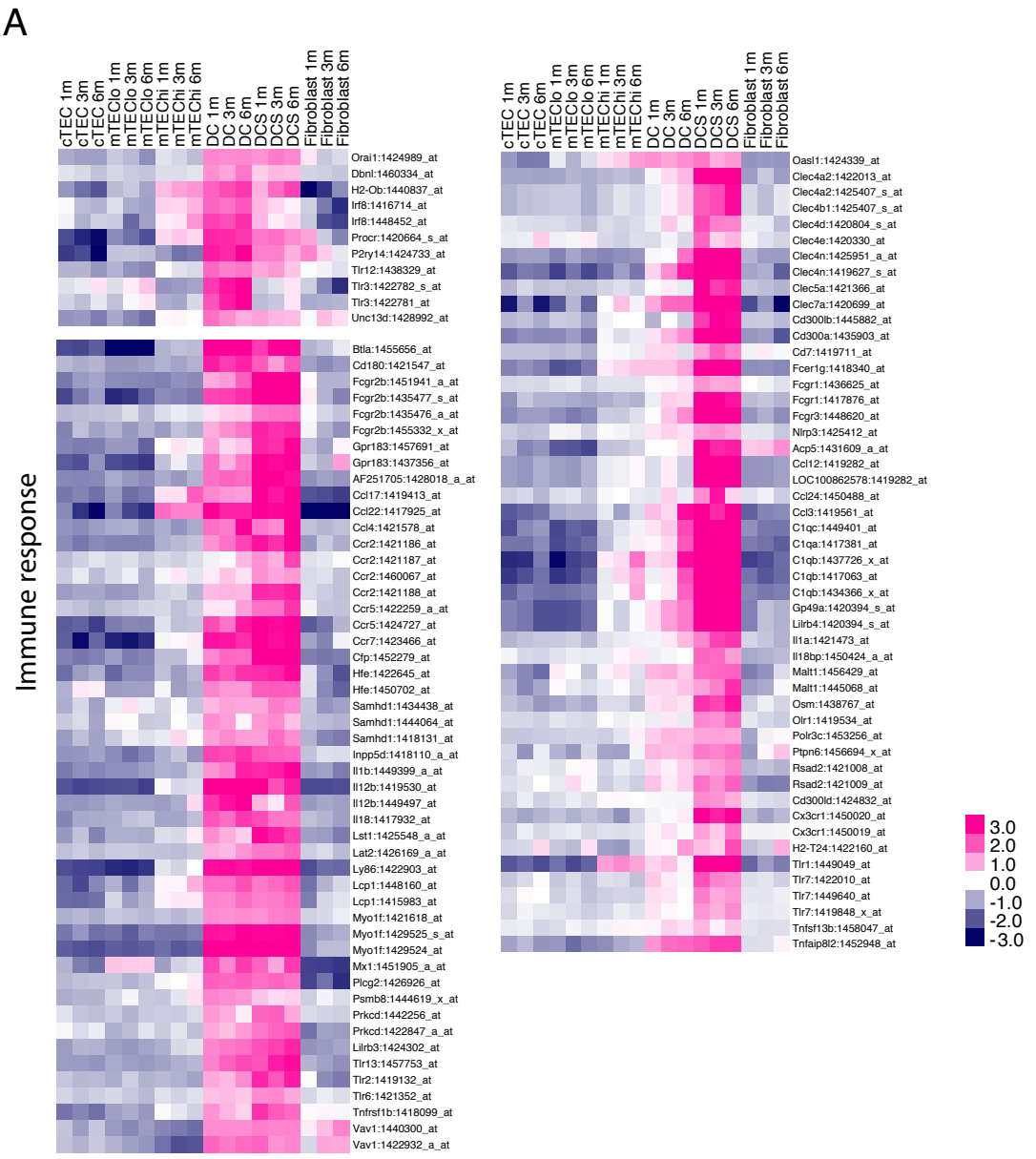

Figure 2.10 Immune response function of DC/DCS revealed by DEGs.

The heat maps display the relative expression of all genes in the ‘immune response’ GO term that overlapped with up-regulated DEGs identified in 1-month DC and DCS subsets.

2.4.3 Thymic involution is associated with down-regulation of cell cycle genes in the mTEC^{lo} subset and decreased activity of E2F3 in cTEC and mTEC^{lo} cells

Thymocyte and thymic stromal cellularity are greatest in mice around 1 month of age and subsequently decline as the thymus involutes (82). To evaluate transcriptional changes associated with early thymic involution, we compared gene expression in stromal subsets from mice at 1, 3, and 6 months of age. We identified aging-associated DEGs as those genes modulated by ≥ 2 fold, with an adjusted p-value ≤ 0.01 in pairwise comparisons of each subset at the three ages. Using these criteria, no aging-associated DEGs were identified in fibroblasts or cTECs, with only 1 DEG in mTEC^{hi} (*Igha*). In contrast, a significant number of DEGs were identified in DC, DCS, and mTEC^{lo} subsets (Figure 2.11A). Over 90% of the DEGs in DC and DCS were up-regulated with age, whereas DEGs in mTEC^{lo} were both up- and down-regulated with similar frequencies. We conducted K-means clustering on DEGs from each subset to identify groups of genes up- or down-regulated as aging progresses from 1 through 6 months of age. Cluster 3 from mTEC^{lo} contained genes progressively and significantly down-regulated with age (Figure 2.11B-C). We performed GO term analyses on each cluster to identify biological functions associated with age-related changes, and found significant hits only for mTEC^{lo} cluster 3. Genes in this cluster were associated with the cell cycle (Figure 2.11D), implicating a progressive decrease in expression of cell cycle regulators, such as *Aurkb, Cdc20, Cdc6*, and *Ccnb1*, in mTEC^{lo} during involution (Figure 2.11E).

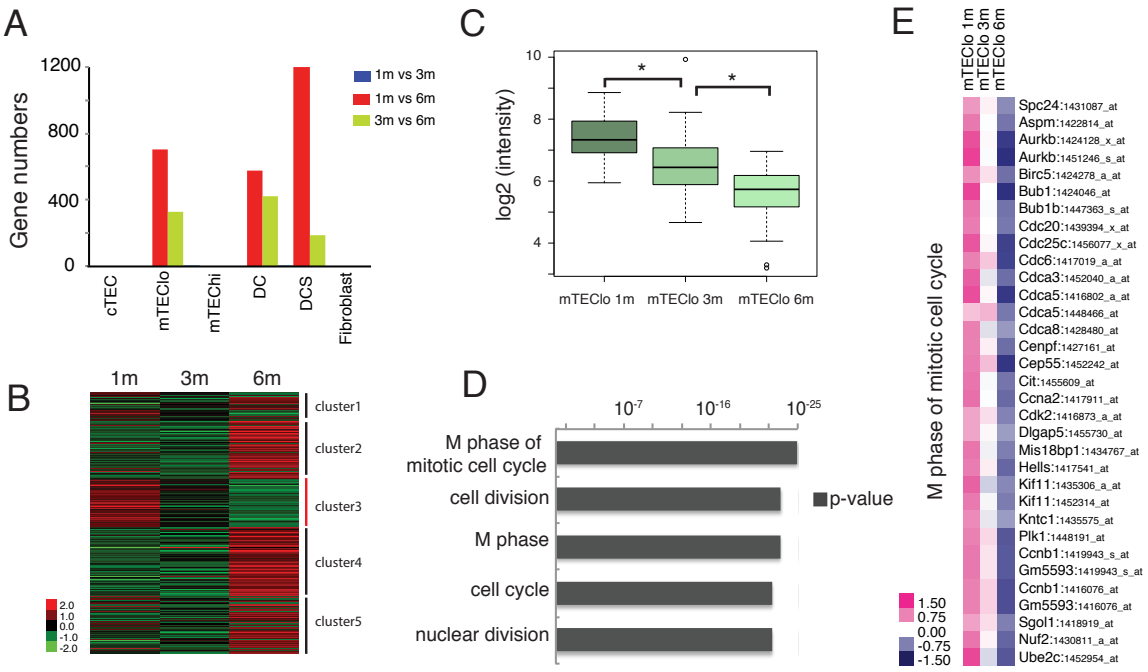

Figure 2.11 Cell cycle genes are significantly down-regulated in mTEC^{lo} subsets in early thymic involution.

(A) The number of up- or down-regulated DEGs identified from pairwise comparisons of stromal subsets at different ages is shown. (B) The heat map displays K-means clustering of all age-associated DEGs identified in the mTEC^{lo} subset. (C) The boxplot displays expression levels of mTEC^{lo} DEGs in cluster 3 from B, which are progressively down-regulated with age (p-value < 2.2 x 10^{-16}). (D) The top 5 GO term hits from cluster 3 of mTEC^{lo} DEGs reveal down-regulation of cell-cycle associated genes during aging. (E) The heat map displays the relative expression of down-regulated age-associated DEGs in mTEC^{lo} that overlap with the 'M phase of mitotic cell cycle' GO term.

We next utilized gene set enrichment analysis (GSEA) to identify aging-associated gene sets, without imposing an arbitrary fold-change cutoff. Strikingly, E2F3 target genes (121) were significantly down-regulated with age in both cTEC and mTEC^{lo} subsets (Figure 2.12A). This decline was gradual in mTEC^{lo} cells from 1 to 6 months, but precipitous in cTECs between 1 and 3 months (Figure 2.12B). E2F3 is a transcription factor critical for normal cellular proliferation (122), and many target genes are regulators of the cell cycle, such as *Cdc6*, *Ccna2*, *Aurka*, and *Cdc7* (Figure 2.12C). Together, these analyses suggest that a decline in E2F3 activity results in decreased cell-cycle progression in cTEC and mTEC^{lo} cells, likely contributing to the decline in TEC cellularity early in the process of thymic involution.

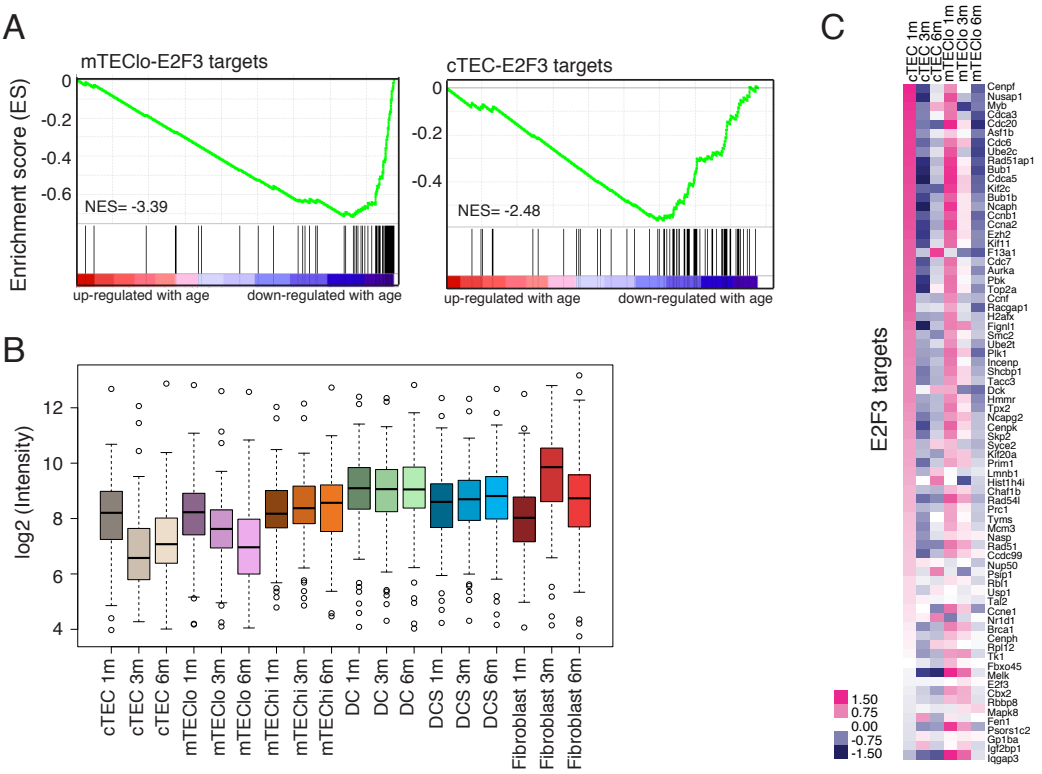

Figure 2.12 E2F3 target genes are significantly down-regulated in mTEC^{lo} and cTEC subsets in early thymic involution.

(F) GSEA reveals expression of E2F3 target genes is down-regulated with age in mTEC^{lo} and cTEC subsets. (cTEC NOM p-value < 10^{-3} NES=-2.48; mTEC^{lo} NOM p-value < $10^{-3,}$ NES=-3.39) (G) The boxplot shows expression levels of E2F3 target genes in stromal subsets at 1, 3, and 6 months of age. Decreased expression of E2F3 target genes is apparent in aging cTEC and mTEC^{lo} subsets. (H) Relative expression of E2F3 target genes in cTEC and mTEClo subsets at 1, 3, and 6 months of age.

2.4.4 DC and DCS have an increasingly pro-inflammatory signature with age

Although GO term analyses did not yield significant hits for aging-associated DEGs in DC and DCS subsets, GSEA revealed an increasingly pro-inflammatory signature with age. Genes induced after LPS simulation in human monocytes were up-regulated with age in thymic DC and DCS (Figure 2.13A) (123). Aging is associated with increased inflammation (124) and inflammatory cytokines become elevated in human thymi with age (125). Both previously described and unreported pro-inflammatory molecules, including Il1a, Il1b, Cxcl2, Il-6, Il12b, Il18, and Tnf were upregulated in thymic dendritic cells at 6 months of age (Figure 2.13B), suggesting that an increasingly inflammatory environment generated by aging dendritic cells contributes to early thymic involution.

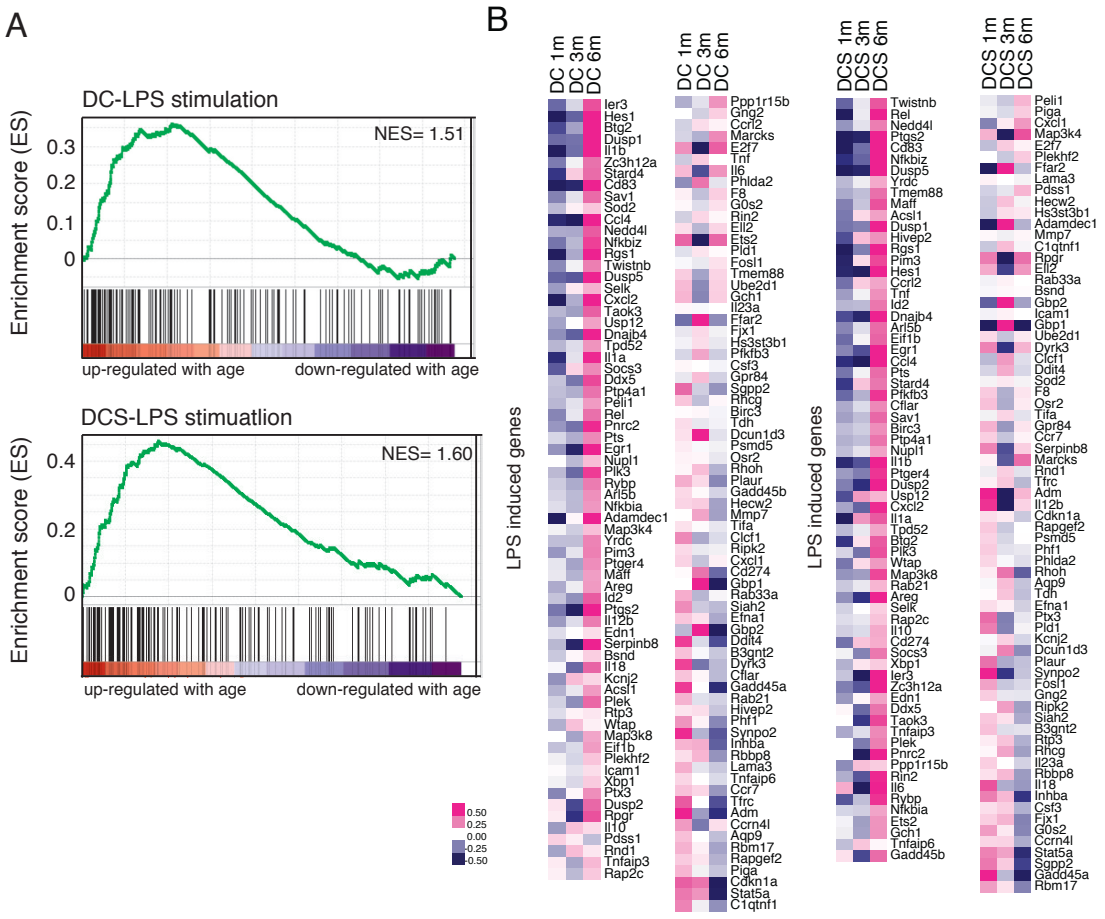

Figure 2.13 Increased expression of pro-inflammatory genes in aging DC and DCS subsets.

(A) GSEA analysis reveals a positive correlation between LPS stimulated genes and genes up-regulated with age in DC and DCS (NOM p-value=0.054, NES=1.51 for DC, NOM p-value=0.025, NES=1.6 for DCS). (B) The heat map displays the relative expression of all LPS induced genes that are positively correlated with aging in DC and DCS.

2.4.5 Diminished niche activity, declining TEC homeostasis, and a decrease in growth factors are associated with early thymic involution

We analyzed pathways and genes previously implicated in late thymic involution to determine if their expression was altered in stromal subsets during the early stages of thymic degeneration. *Dll4*, *Il7*, and *KitL,* which are all required for a functional thymocyte progenitor niche, were expressed at the highest levels by cTECs. Only *Dll4* expression diminished over 1 to 6 months (Figure 2.14A), suggesting a decline in Notch signaling contributes to early thymic involution.

Several studies have implicated decreased *Foxn1* expression as a major contributor to thymic involution (88, 96). *Foxn1* was not identified as an aging-associated DEG because it did not meet the <0.01 p-value criterion. However, *Foxn1* expression declined ~2 fold in both cTEC and mTEC^{lo} subsets from 1 to 6 months of age (Figure 2.14B), consistent with previous findings at later stages of involution (85, 88). Two recent studies associated late thymic involution with altered expression of Wnt pathway genes (88, 92). Consistent with these studies, *Wnt3a* and *Wnt4* were downregulated in early thymic involution, specifically in cTEC and mTEC^{lo} cells, while *Wnt10a* was upregulated in the mTEC^{lo} subset (Figure 2.14B). Consistent with Griffith et al., *Wnt5b* was slightly upregulated by 6 months; however, this increase occurred in fibroblasts. Taken together, some Wnt family members and *Foxn1* are deregulated early in thymic involution, suggesting that TEC homeostasis is impaired, consistent with decreased TEC proliferation and E2F3 activity described above.

Inflammatory cytokines are upregulated in aging human thyme (125). Similiarly, *Lif, Il6,* and *Osm* were upregulated in murine thymic dendritic cell subsets over 1 to 6 months (Figure 2.15A). Furthermore, *Tnf*, *Il1a* and *Il1b* were upregulated by DCS. Interestingly, the activating receptor *Il1r1* was expressed by all TECs and fibroblasts, while the IL1 antagonists *Il1rn* and *Il1r2* were expressed by mTECs, suggesting IL1 likely impinges preferentially on cTECs and fibroblasts. We also note a trend of increased *Csf1* expression by $mTEC^{lo}$ over 1 to 6 months, which can drive dendritic cell differentiation (126).

Sex steroids and growth factors can modulate thymic size (81). For example, castration transiently increases thymic size and output (91, 92). Androgen receptor, *Ar* is expressed predominantly on cTEC, but is not upregulated over 1 to 6 months (Figure 2.15B). Administration of growth hormone and KGF also induce growth of involuted thymi (81). Expression of the growth hormone receptor *Ghr* was not altered over 1 to 6 months in TECs (Figure 2.15B); however, it was decreased with age in fibroblasts, which expressed the highest levels of *Ghr* at 1 month. The expression of *Fgfr2*/*Kgfr* on cTEC and $mTEC^{lo}$ cells did not decline over 1 to 6 months. However, expression of the ligand, *Fgf7*/*Kgf* diminished in both $mTEC^{hi}$ cells and fibroblasts between 3 to 6 months (Figure 2.15B). Taken together, our data suggest that reduced growth factor signaling during early involution could affect both TECs and fibroblasts.

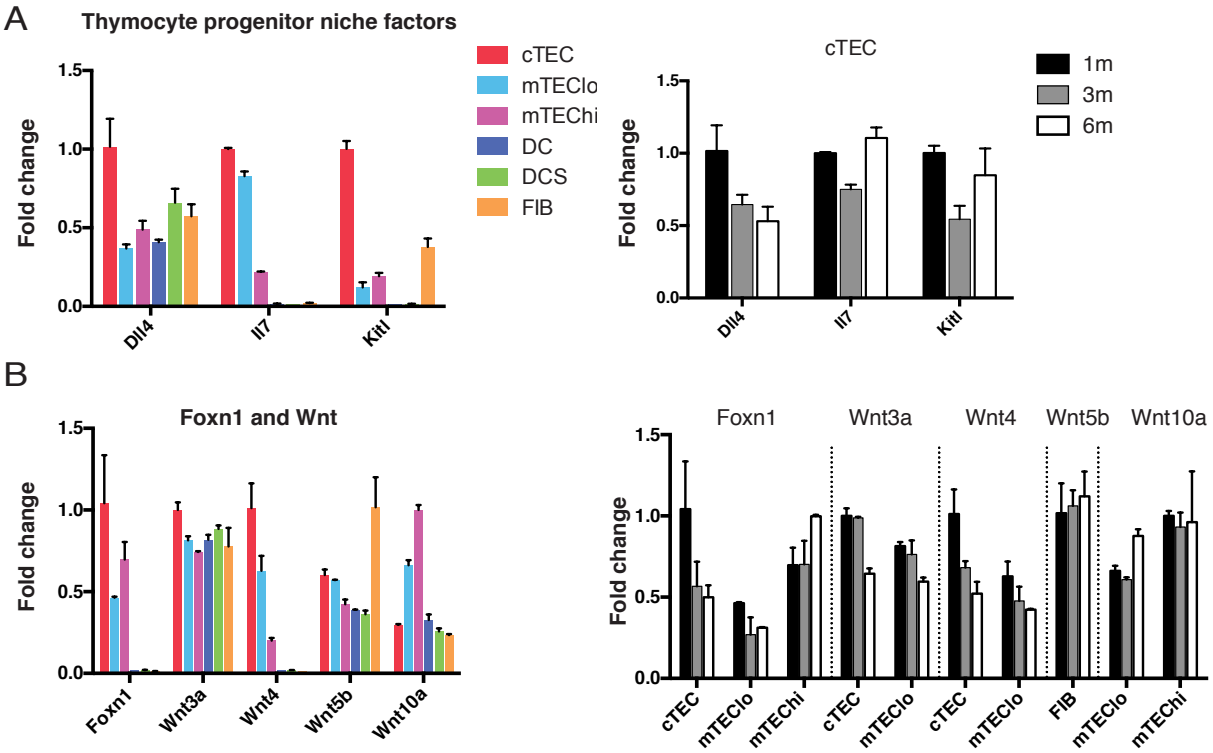

Figure 2.14 Thymocyte niche factors and TEC homeostasis implicated in late thymic involution are deregulated in thymic stroma by 3 to 6 months

Graphs display the relative expression levels of genes involved in (A) thymocyte progenitor niche activity, and (B) TEC homeostasis in the thymus. For all graphs, expression values are normalized to the subset expressing the highest level of each gene at 1 month of age. The color graphs on the left display expression levels of genes of interest for each stromal subset at 1 month. The grayscale graphs on the right display expression levels of the same genes from 1 to 6 months for the indicated thymic stromal subsets. Graphs depict the mean plus or minus range of expression values.

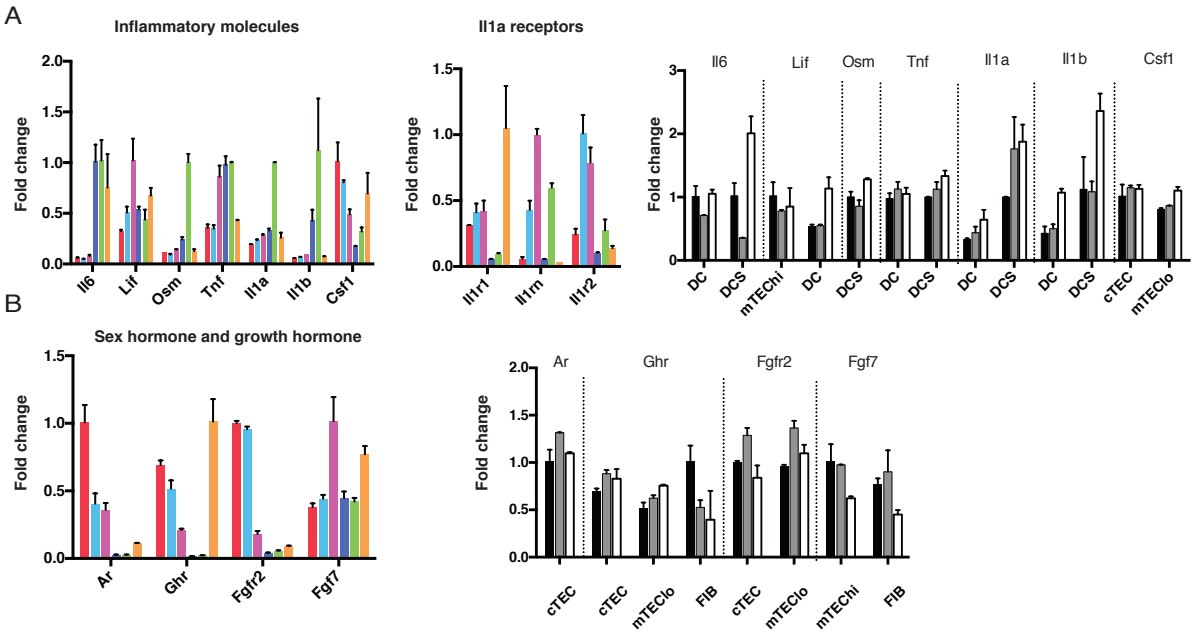

Figure 2.15 Inflammation and hormone implicated in late thymic involution are deregulated in thymic stroma by 3 to 6 months

Graphs display the relative expression levels of genes involved in (A) inflammation, and (B) sex steroid and growth hormone signaling in the thymus. For all graphs, expression values are normalized to the subset expressing the highest level of each gene at 1 month of age. The color graphs on the left display expression levels of genes of interest for each stromal subset at 1 month. The grayscale graphs on the right display expression levels of the same genes from 1 to 6 months for the indicated thymic stromal subsets. Graphs depict the mean plus or minus range of expression values

2.4.6 A searchable web-based platform containing thymocyte and thymic stromal cell gene expression data

To make our thymic stromal expression data easily accessible, we have uploaded the datasets to the web-based platform Gene Expression Commons (GExC), where we have generated an online model containing both thymic stromal microarray datasets and our previously published thymocyte datasets (106) (https://gexc.stanford.edu/model/475). Users can readily query expression of genes of interest (GOI) in thymocyte or thymic stromal subsets (Figure 2.16A). One of the most powerful features of this platform is that data are normalized against a common reference of ~12,000 diverse datasets; thus, gene expression values can be compared against the full dynamic range of expression values for each probe set (106). In addition to normalized signal intensity values, "gene expression activity values" are provided on GExC. After using a step function to determine the threshold of expression for each probe set, each intensity value above and below this cutoff was assigned a percentile rank, reflecting the distribution of values in the common reference, as seen in the histograms (Figure 2.16C-D). For example, if a 30% "gene expression activity" value is obtained, the subset queried expresses the gene at a level above the first 30% of the common reference datasets over the threshold, and below the remaining 70%. This enables users to determine how robustly a gene is expressed relative to the range of expression values across diverse tissues. A second key advantage is the ability to readily search for expression patterns of interest, such as genes uniquely expressed in cTEC (Figure 2.16B). Finally, the combination of thymic stromal data with our previously published thymocyte data (106), will enable users to search for partner

genes, such as receptors and ligands, that may contribute to thymocyte: stromal cell crosstalk. For example, the chemokine receptor Cxcr4 is expressed in cortical double negative (DN) and double positive (DP) thymocytes, as well as in thymic dendritic cells and fibroblasts, while its ligand Cxcl12 is highly expressed by cTECs (Figure 2.16C). This in silico model should greatly facilitate discovery of molecular mediators of thymocyte: stromal cell crosstalk, thymic stromal function, and altered gene expression in stromal cells during early thymic involution.

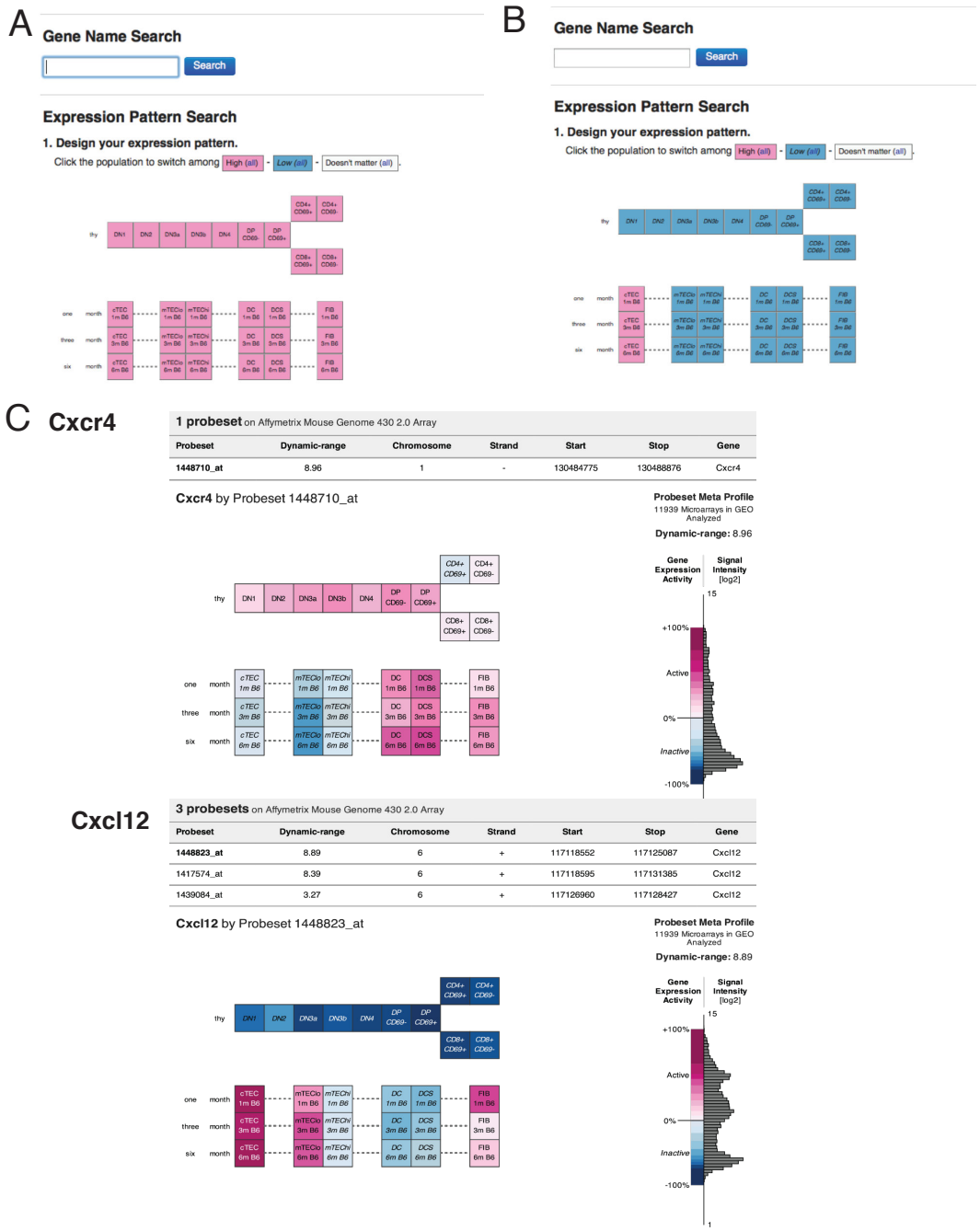

Figure 2.16 continued next page

Figure 2.16 GExC platform for exploring expression data from thymocytes and thymic stromal subsets.

(A) The "Complete thymocyte: stromal interaction" model in GExC (https://gexc.stanford.edu/model/475). Eleven thymocyte subsets (at 1 month of age) and six thymic stromal subsets (at 1, 3, or 6 months of age) are represented as boxes, with colors representing the average expression level of data from biological replicates (n=3 and n=2 replicates for thymocyte and stromal subsets, respectively). (B) In this example of the pattern search feature on GExC, high expression in cTECs relative to all other subsets will be queried. (C) The database is useful for querying ligand-receptor pairs involved in thymocyte: stromal cell crosstalk. For example, the chemokine *Cxcr4* is expressed by cortical thymocytes, as well as dendritic cells, while the ligand *Cxcl12*, is expressed at high levels by cTEC. The dynamic range of each probeset is displayed as a histogram, enabling users to ascertain expression levels relative to the range of values in publically available biological space (>12,000 diverse datasets are represented).

2.5 DISCUSSION

We present global gene expression data from six thymic stromal subsets over the course of early thymic involution (1, 3, and 6 months of age) on a web-based platform as a resource for the scientific community (https://gexc.stanford.edu/model/475). Unsupervised clustering reveals the datasets are highly consistent (Figure 2.2), and qRT-PCR analyses on independently sorted samples validate the microarray expression data (Figure 2.3A). Nonetheless, there are several potential caveats to consider when querying the GExC database. First, thymic fibroblasts were sorted based on the absence of markers on hematopoietic cells, erythrocytes and endothelial cells, enhancing the possibility for contamination with other cell types. Nevertheless, strong transcription of adhesion molecules, ECM components, and platelet-derived growth factor receptors reveal this population is highly enriched in mesenchymal cells. Second, the sorted populations may be heterogeneous. The transcriptional profile of rare TEC progenitors included in cTEC or $mTEC^{lo}$ subsets would be entangled in the larger population. As additional TEC subsets are identified, it will be important to compare their transcriptional profiles against the parental TEC population. Third, when viewing gene expression activity values in GExC, it is important to remember that gene expression activity values are scaled relative to the large common reference. This can cause a visual flattening of expression changes; for example, because Foxn1 is uniquely expressed in TECs, the ~2 fold decrease in expression over 1 to 6 months in cTEC and $mTEC^{lo}$ cells (Figure 2.14B) is not as visually striking as the high expression in TECs relative to all other cell types. Also, gene expression activity

values can be saturated (seen as 100%), as in the case of Psmb11/b5t in cTEC, obscuring the 20-50-fold increase in expression relative to other TEC subsets. In both cases above, it is important to compare the normalized signal intensity values, provided for download or on the "list" tab of GExC, to assess relative changes in expression with age or between subsets, respectively.

Surprisingly, our analyses revealed a significant association of mTEC^{hi} DEGs with the 'defense response' GO term. mTEC^{hi} is the most distal thymic stromal population by PCA analysis (Figure 2.2B), and its distinct transcriptional profile could result from expression of diverse TRAs. TRA expression is largely driven by Aire (44), and 38% of genes uniquely expressed in mTEC^{hi} overlapped with Aire-regulated genes (Figure 2.5A). However, not all Aire-regulated genes are TRAs (48), and the remaining 62% of mTEC^{hi} DEGs may serve a function beyond elimination of autoreactive thymocytes. The GO term category 'defense response', includes genes such as defensins and cytokines (Figure 2.5C), which are critical for early innate immune responses against pathogens. Some of these genes (Defb8, Defb3) are expressed at high levels in mTEC^{hi} relative to canonical TRAs (Crp, Gad67) (not shown), which tend to be expressed at low levels (43, 52). Therefore, we speculate that these 'defense response' genes may serve a functional role in mTEC^{hi} biology, perhaps to protect the thymus against infection.

Thymic involution results in diminished T cell output, leading to decreased immune function with age (81, 96). Both CD4^{+} and CD8^{+} T cells generated in aged mice have impaired effector functions (5, 89). These deficiencies can be attributed in part to the impact of an aged thymic environment, as fully functional T cells were generated when

bone marrow precursors from aged mice were transferred into young, but not old recipients (90). Therefore, it is important to understand the cellular and molecular drivers of thymic involution, with the ultimate goal of restoring functional T cells to aged individuals or patients following cytoablative therapies or infections.

Unbiased analyses of aging-associated transcriptional changes during early thymic involution revealed that cell cycle related genes and E2F3 transcriptional targets were significantly down-regulated in the $mTEC^{lo}$ and cTEC subsets (Figure 2.11-2.12). This is consistent with the reduced proportion and number of cycling TECs with age (82), and the finding that overexpression of cyclinD1 or inactivation of Rb family members prevents thymic involution (94, 95). Our data add the novel perspective that E2F3 target genes, many of which are required for cell cycle progression, are down-regulated in both cTEC and $mTEC^{lo}$ subsets by 6 months of age, suggesting that diminished cell cycle progression in TECs is an early hallmark of thymic involution. A recent study revealed that Foxn1 is an E2F3 target gene (94). Thus, diminished E2F3 activity could directly reduce Foxn1 levels, consistent with the reduction in Foxn1 expression in TECs by 6 months of age (Figure 2.14B). Foxn1 is a critical regulator of thymic involution, as diminished Foxn1 expression results in premature involution (86), while enforced re-expression in aged TECs increases TEC cellularity and function and thymocyte output (88). However, maintenance of Foxn1 expression in TECs was insufficient to prevent thymic involution (87), suggesting modulation of other E2F3 targets and pathways contribute to involution. Foxn1 has also been implicated in regulating genes associated with cell cycle, such as Ccnd1 (88); thus, there is likely a complex feedback mechanism driving both diminished cell cycle

progression and Foxn1 levels. Expression of e2f3 itself is not significantly altered in cTEC and mTEC^{lo} from 1 to 6 months (not shown), suggesting that E2F3 activity is modulated over the course of thymic involution. Identifying initial drivers of reduced E2F3 function will likely reveal critical regulators of thymic involution.

Diminished expression of Wnt pathway genes has also been implicated in age-associated TEC degeneration (88, 92). In agreement with these studies, we find that Wnt3a is diminished ~1.5 fold in cTEC and mTEC^{lo} at 6 months, while Wnt4 is decreased ~2 fold in cTEC (Figure 2.14B). As Wnt4 can induce Foxn1 expression (127) and Wnt3a is implicated in epithelial proliferation (128), diminished expression could contribute to impaired TEC homeostasis. Furthermore, the subtle increase in expression of Wnt5b by fibroblasts, which may drive adipogenesis (129), suggests thymic mesenchymal cells could promote the age-associated increase in adipose tissue early in involution. We did not find evidence for altered expression of other Wnt family members (not shown), suggesting that deregulation of some Wnts (88, 92) may occur late in the involution process.

Reduced potency of the thymocyte progenitor niche may also impair thymopoiesis during involution. IL-7, Dll4, and Kitl, expressed by TECs, are all critical for promoting survival and differentiation of early thymocyte progenitors (100). Of these niche factors, only expression of Dll4 was diminished in cTECs by 6 months of age (Figure 2.14A), suggesting the thymic niche may have a reduced capacity to stimulate Notch signaling, thus impairing thymopoiesis in early involution. IL-7 levels are reduced in late thymic involution (85); however, the lack of transcriptional downregulation over 6 months

suggests that diminished IL-7 may be due to reduced cTEC numbers in the involuted thymus.

Signaling via sex steroids and growth hormones has also been implicated in thymic involution (81). Our data do not reveal altered expression levels of Ar in TECs over 1 to 6 months (Figure 2.15B) or in estrogen or progesterone receptors (not shown). Taken together with the findings that sex steroid ablation induces only transient and partial regeneration of the thymus (92) and that sex steroids diminish with age, while the thymus continues to involute (96), our data do not suggest that sex steroids play a significant role in early thymic involution. However, it is possible that altered sensitivity to signaling by sex steroid hormones in aging TECs could promote involution. Our data suggest that altered growth factor signaling could contribute to early thymic involution because Ghr and Fgf7/Kgf expression was decreased in fibroblasts by 6 months (Figure 2.15B). Because both TECs and fibroblasts express Ghr, thymic rebound induced by growth hormone (130) may be due to signaling in both stromal subsets. Reduced expression of Fgf7/Kgf by aging fibroblasts may diminish signaling through FGFR2 on cTEC and mTEC^{lo} cells, contributing to TEC atrophy. Consistent with this notion, treatment with KGF causes transient thymic regeneration (104).

Unbiased analyses of our data revealed an increasingly proinflammatory signature of DC and DCS with age (Figure 2.13). A previous study demonstrated that expression of Osm, Lif, Scf, and Il6 increased in aged human thymi, and administration of these cytokines promoted thymic atrophy in mice (125). Our analyses add further insight that Osm, Lif and Il6 are upregulated by thymic dendritic cells early in the course of involution,

though we found no evidence for increased Scf, either due to species or temporal differences. We also identified additional genes associated with inflammation that are upregulated by thymic dendritic cells by 6 months of age (Figure 2.13). Il1a and Il1b are strikingly upregulated by thymic dendritic cells, whereas activating, but not inhibitory Il-1 receptors are expressed on cTEC and fibroblasts (Figure 2.15A). IL-1 administration promotes thymic atrophy(97), and Nlrp3 deficient mice, which cannot generate active IL-1, preferentially maintain the cTEC compartment with age (131). Taken together, these data suggest that IL-1 produced by thymic dendritic cells is likely a potent mediator of early thymic involution, signaling to both cTEC and thymic fibroblasts. Interestingly, Csf1, which can promote dendritic cell differentiation, is upregulated in $mTEC^{lo}$ at 6 months (Figure 2.15A). Thus, a feedback loop may exist in which aging TECs promote differentiation of dendritic cells, whose inflammatory cytokines in turn promote TEC degeneration. Further elucidation of the mechanisms driving DCs to adopt a pro-inflammatory signature and causing TECs to reduce E2F3 activity and cycling will be key to understanding the etiology of age associated thymic involution.

Chapter 3: EBI2 contributes to thymocyte central tolerance by promoting thymocyte medullary accumulation and rapid motility

The contents of the chapter are modified from Sanghee Ki, Jessica N. Lancaster, Zicheng Hu, and Lauren I.R. Ehrlich. EBI2 contributes to thymocyte central tolerance by promoting thymocyte medullary accumulation and rapid motility[3,4]

3.1 Abstract

A key function of the thymus is to avert autoimmunity by ensuring that autoreactive thymocytes are either deleted or disabled. Maturing thymocytes enter the thymic medulla, where they encounter a wide range of self-antigens presented by APCs. Those thymocytes that are strongly self-reactive either undergo negative selection or diversion into the regulatory T cell lineage. Although the majority of the proteome is expressed in the medulla, many self-antigens are expressed by only a minor fraction of medullary APCs; thus, thymocytes must efficiently enter the medulla and scan numerous APCs for complete self-tolerance induction. Chemokine receptors promote lymphocyte migration, organization within tissue microenvironments, and interactions with APCs in the thymus and other lymphoid organs. The chemokine receptor EBI2 governs localization of T cells,

[3] Acknowledgement: We thank Jason Cyster for provision of *Ebi2*$^{-/-}$ mice and for helpful suggestions, Hilary Selden for technical assistance, Ellen Richie for helpful suggestions, and the staff of the UT Austin animal facility for assistance with mice.

[4] Authorship contributions: SK performed most of experiments with advice from LE, and wrote the manuscript with LE. SK and JL performed slice deletion and 2photon imaging experiments. ZH generated qRT-PCR data of EBI2.

B cells, and dendritic cells (DCs) during immune responses in secondary lymphoid organs. However, the role of EBI2 in thymocyte development has not been elucidated. Here, we demonstrate that EBI2 is expressed by murine $CD4^+$ single positive (CD4SP) thymocytes and thymic DCs. Although EBI2 deficiency did not impact thymocyte cellularity or subset distribution, the TCR repertoire was altered in *Ebi2*$^{-/-}$ mice. Furthermore, negative selection of OT-II TCR transgenic thymocytes in response to an endogenous antigen was impaired due to thymocyte-intrinsic EBI2 deficiency, as opposed to deficiency in the DC compartment. Two-photon imaging revealed that EBI2 deficiency resulted in slower migration and impaired medullary accumulation of CD4SP thymocytes. These data identify a role for EBI2 in promoting efficient central tolerance.

3.2 INTRODUCTION

The thymus provides an environment that is conducive for differentiation of T cells that are self-MHC restricted and self-tolerant. During the early stages of T cell differentiation, thymocytes migrate throughout the cortex, where they commit to the T cell lineage and rearrange gene segments encoding TCRα and TCRβ chains. Thymocytes then undergo positive selection via interactions with cortical thymic epithelial cells (cTECs), enabling survival of only those cells expressing self-MHC restricted TCRs (30, 98). Following positive selection, thymocytes migrate into the medulla, where they undergo the final stages of maturation before emigrating to join the cohort of naïve T cells in secondary lymphoid organs.

The thymic medulla is a specialized microenvironment in which thymocyte tolerance against numerous self-antigens is induced. There are two major classes of medullary APCs responsible for self-tolerance induction, medullary TECs (mTECs) and DCs. $mTEC^{hi}$ cells, a subset of mTECs that express high levels of MHC-II and CD80, have a unique role in self-tolerance induction because they express the chromatin modulator *Aire*. AIRE promotes low-level, stochastic expression of a large number of tissue-restricted antigens (TRAs), genes otherwise expressed only in a small number of differentiated tissues, such as the retina or pancreas (45). Interestingly, $mTEC^{hi}$ cells collectively express about 90% of the proteome, representing the majority of proteins T cells will encounter throughout the body; however only a small percentage of $mTEC^{hi}$ cells express any given TRA (50, 51, 132). DCs also play an essential role in presenting self-antigens to medullary thymocytes for tolerance induction. In addition to presenting peptides from their own proteome, DCs acquire antigens from $mTEC^{hi}$ cells for presentation (9, 64). Furthermore, thymic $Sirp\alpha^{+}$ DCs and plasmacytoid DCs (pDC) present peptides from proteins in peripheral tissues or the circulation (9). Therefore, in order to screen the complete range of diverse but sparse TRAs in the medulla, thymocytes must efficiently enter the medulla and scan numerous APCs.

Chemokine receptors influence central tolerance by promoting thymocyte medullary entry, motility, and interactions with APCs. After undergoing positive selection, $CD4^{+}CD8^{+}$ double-positive (DP) thymocytes up-regulate CCR4, which is required for their efficient medullary entry and interactions with DCs. Thus, CCR4 deficiency results in impaired central tolerance (10). Subsequently, $CD4^{+}$ single positive (CD4SP) cells and

CD8SP cells express CCR7, which is critical for their accumulation within the medulla and rapid motility (74, 133). CCR7 deficiency also results in impaired central tolerance (74, 75, 134-136). In addition to these two chemokine receptors, our analysis of expression profiling data from thymocytes and thymic stromal cells identified other candidate chemokine: chemokine receptor pairs that could promote medullary accumulation (137). Furthermore, *Ccr4*$^{-/-}$*Ccr7*$^{-/-}$ SP cells are capable of entering the medulla (77), albeit inefficiently, but pertussis toxin completely inhibits SP medullary entry (74), indicating that other chemokine receptors contribute to medullary accumulation of SP cells, and thus central tolerance induction.

EBI2 (Epstein-Barr virus induced molecule 2) is a chemokine receptor expressed by several lymphocyte subsets that promotes chemotaxis in response to 7α25-OHC, a lipid metabolite of cholesterol (138-141). EBI2 regulates the localization of B cells within follicles during primary immune responses (142-144). In the absence of EBI2, B cells localize prematurely to the center of follicles, resulting in impaired generation of plasmablasts and GC B cells, and reduced early antibody production (138, 142). EBI2 also induces localization and homeostasis of CD4^{+} DC in splenic bridging channels, enabling them to efficiently acquire and present particulate antigens during primary immune responses (145). In addition, EBI2 guides activated CD4^{+} T cells towards follicles, promoting differentiation of Tfh cells through interactions with specialized DCs in the outer T cell zone (146). Interestingly, genome-wide studies have implicated single nucleotide polymorphisms near the *EBI2* locus in autoimmune diseases, such as Type 1 diabetes (147), indicating that mislocalization of lymphocytes impacts autoimmune

susceptibility as well as pathogen-driven immune responses. The contribution of EBI2 to thymocyte differentiation has not been established.

In this study, we have identified a role for EBI2 in thymocyte migration and negative selection. We demonstrate that EBI2 promotes chemotaxis of mature CD4SP cells and alters the TCR repertoire. EBI2 contributes to negative selection of OT-II TCR transgenic thymocytes in response to an endogenous auto-antigen, and shifts the balance in favor of negative selection as opposed to Treg generation in the presence of high-affinity auto-antigens. The impact of EBI2 on negative selection is thymocyte-intrinsic, and not due to activity in the thymic DC compartment. In addition, using two-photon microscopy to track the migration of CD4SP thymocytes on live thymic slices, we show that EBI2 promotes rapid motility of CD4SP cells and contributes to their medullary accumulation. Together, our findings provide evidence that EBI2 is required for full motility of medullary CD4SP thymocytes and contributes to efficient negative selection.

3.3 Experimental Procedures

Mice

C57BL/6J (CD45.2), B6.SJL-Ptprc^{a} Pepc^{b} (CD45.1), B6.Cg-Tg(TcraTcrb)425Cbn/J (OT-II), C57BL/6-Tg(Ins2-TFRC/OVA)296Wehi/WehiJ (RIP-mOVA) mice were purchased from The Jackson Laboratory. *Ebi2*$^{-/-}$ and pCX-EGFP(148) strains were generously provided by Jason Cyster (UCSF) and Irving L. Weissman (Stanford University, Stanford, CA), respectively. CD45.1/CD45.2, CD45.1 OT-II, and *Ebi2*$^{-/-}$ OT-II strains were bred in-house. All strains were bred and maintained under specific pathogen–free

conditions at the University of Texas at Austin animal facility. Mouse maintenance and experimental procedures were performed with approval from the University of Texas at Austin's Institutional Animal Care and Use Committee.

Antibodies and flow cytometry

All antibodies were obtained from eBioscience or Biolegend unless otherwise indicated: anti-CD8 (53-6.7), -CD69 (H1.2F3), -CD3 (145-2C11), -CD4(RM4-5), -CD25 (PC61.5), -CD45.1 (A20), -CD45.2 (104), -Vα2 (B20.1), -Vβ5 (MR9-4), -CD11c (N418), -Ter119 (TER-119), -B220 (RA3-6B2), -Gr-1 (RB6-8C5), -CD11c (M1/70), -NK1.1 (PK136), -cKit (2B8), -CD31 (390), -Sirpα (P84), -I-A/I-E (M5/114.15.2), -CD80 (16-10A1), -CD45 (30-F11;BD), -Ly51 (6C3), -EpCAM (G8.8), -PDCA1 (eBio917), -Aire (5H12). Anti-Streptavidin Qdot®-605 (Life Technologies) was used as a secondary reagent to detect biotinylated primary antibodies.

Antibodies used for immunofluorescent stains are listed below: anti-Pancytokeratin-FITC (C-11; Sigma-Aldrich), -keratin5 (rabbit polyclonal antibody; Covance), -CD4-APC (FM4-5; eBiosicence), -CD8-Alexa Fluor 488(53-6.7; eBioscience), CD11c-biotin (N418; BioLegend), Donkey anti-rabbit IgG DyLight 488, (Jackson ImmunoResearch Laboratory), Donkey anti-rabbit IgG DyLight 594 (Jackson ImmunoResearch Laboratory), Streptavidin Alexa 647 (Life Technologies).

For flow cytometry, single-cell suspensions of thymocytes were obtained by manual dissociation and filtration through a 40-μM cell strainer (Thermo Fisher Scientific).

$3x10^6$~10^7 thymocytes were stained with fluorochrome-conjugated or biotinylated antibodies for 20 min in the dark at 4°C in FACS wash (FW; PBS+ 2% bovine calf serum [BCS]; GemCell). Biotinylated antibodies were detected with Streptavidin Qdot 605 (Life Technologies). 1 μg/ml Propidium iodide (PI; Enzo) was added to identify dead cells, and the suspension was analyzed with a LSR Fortessa flow cytometer (BD). FlowJo ver.9.9 (Tree Star) was used for data analysis.

qRT-PCR

Single cell suspensions of thymocytes were obtained by mechanically dissociating C57BL/6J thymi, and thymocyte subsets were sorted as described previously (10). Single cell suspensions of thymic stromal cells were obtained by enzymatically dissociating C57BL/6J thymi with Collagenase D and Collagenase/Dispase (Roche) as previously described (107, 137) (see Figure 3.1 for gating strategies). Thymic stromal cells were immuno-stained with antibodies against MHCII, Epcam, CD45, CD80, UEA, Ly51, Ter-119, CD11c, CD31, Sirpα, B220 to sort TEC and DC subsets. Gating schemes were applied as described previously (137). Briefly, all TECs were gated as $CD45^-$ $MHCII^+$ $Epcam^+$ cells, and then subdivided into $mTEC^{hi}$ ($UEA\text{-}1^+$ $CD80^{hi}$ $MHCII^{hi}$), $mTEC^{lo}$ ($UEA\text{-}1^+$ $CD80^{lo}$ $MHCII^{lo}$) and cTEC ($UEA\text{-}1^-$ $MHCII^+$ $Ly51^+$) subsets. DCs were first gated as $MHCII^+Epcam^-$ $CD11c^+$ cells, and further divided by Sirpα expression. Thymocyte, TEC, and DC subsets were sorted to >95% purity using a FACSAria II (BD), and the cells were resuspended in TRIzol (Life Technologies), from which RNA was

extracted according to the manufactuer's protocol. cDNA was generated using SuperScript® III First-Strand Synthesis SuperMix (Life Technologies). qRT-PCR was performed as described previously (10).

Chemotaxis assays

For DC chemotaxis assays, thymi were enzymatically digested with Liberase, as previously described, with modifications (Roche)(149). Briefly, 3 sequential incubations in 4%Liberase+0.02%DNaseI were carried out for 12minutes at 37C, and released cells were collected in FW + 0.5mM EDTA after each incubation. Cells were immunostained with anti-CD11c-biotin (N418) for 30min on ice, followed by Streptavidin-MicroBeads (MACS; Miltenyi Biotec) for 20min on ice. MACS columns (25LS columns; Miltenyibiotec) were used to positively enrich $CD11c^+$ cells according to manufacturer's specifications. 3-7x10^4 DCs were aliquoted into the top chamber of a 5.0 μm pore 24 well chemotaxis plate, (Costar) in RPMI media (RPMI-1640 medium [Gibco] supplemented with 10% FBS[Hyclone]). 7α25-OHC (Sigma) was added to the bottom of each chamber at indicated concentrations, and plates were incubated at 37°C for 2 hours. Cells that had migrated into the bottom chamber were analyzed by flow cytometry after immunostaining with anti-: CD11c- eFluor®450, PDCA1-PE, Sirpα-APC, MHCII-PE/Cy7, B220-APC/Cy7. The chemotactic index was calculated as the ratio of the number of cells in the bottom chamber at a given concentration of ligand versus the number of cells in wells without ligand.

For thymocyte chemotaxis assays, $3x10^5$ thymocytes were placed in the upper well of a chemotaxis chamber and the indicated concentrations of 7α25-OHC were added in RPMI in the bottom wells. After 2 hours, cells in the bottom chamber were analyzed by flow cytometry with the following antibodies anti-: CD4-APC, CD8-eFluor®450, CD3-PE/Cy7, CD69-Qdot® 605, CD25-Alexa® Fluor700.

Immunofluorescence

Ebi2$^{+/+}$ and *Ebi2*$^{-/-}$ thymi from mice at 1 month of age were embedded in Tissue-Tek OCT compound (Sakura) and snap frozen. 6-9 μm cryosections were prepared on a Microm HM550 Cryostat (ThermoFisher) and stored at -80°C. Cryosections were fixed in 100% acetone at -20°C for 15min and washed 2X in PBS + 0.1% Tween 20. Immunostaining was carried out for 1hr at 4°C with indicated primary antibodies against the following: Keratin5 (rabbit polyclonal), PanCK (C11)-FITC, CD4-APC, CD8-FITC, and CD11c-biotin. TheTSA Signal Amplification kit was used (Perkin Elmer) to boost the CD11c signal. Incubation with the following secondary antibodies for 1hr at 4°C was used for detection: Donkey-anti-rabbit IgG DyLight 594. Images were acquired on a DMi8 (Leica) epifluorescent microscope, using HC PLAPO 10x/0.4DRY (NA=0.4) and HC PLAPO 20x/0.7 (NA=0.7) DRY objectives and LasX (Leica) software.

Bone marrow chimeras

For mixed bone marrow chimeras, donor *Ebi2*$^{+/+}$ CD45.1 and *Ebi2*$^{-/-}$ CD45.2 bone marrow (BM) cells were depleted of mature lineages by incubating for 30min on ice with

the following antibodies (BioXCell): CD3, CD4, CD8, Mac1, Gr-1, Ter1, NK1.1, B220, followed by incubation for 10min at room temperature with sheep anti-rat IgG Dynabeads® (Invitrogen), and magnetic depletion. *Ebi2*$^{+/+}$ and *Ebi2*$^{-/-}$ lineage-depleted BM cells were mixed at 1:1 ratio, and injected i.v. into lethally irradiated (900 rad in 2 split doses) CD45.1/45.2 congenic recipients. Thymic chimerism was assessed by flow cytometry 6 weeks after transplantation. For, OT-II chimeras, the same procedure was followed, but donor bone marrow came from *Ebi2*$^{+/+}$ OT-II mice or from *Ebi2*$^{+/+}$ OT-II, and recipients were either irradiated RIP-mOVA^{+} or RIP-mOVA^{-} mice, as indicated.

In vitro viability assay

10^6 thymocytes from *Ebi2*$^{+/+}$ CD45.1 and *Ebi2*$^{-/-}$ CD45.2 mice were incubated at 37°C in 5% CO_2 for 24 hours in the absence or presence of 7α,25-OHC at the indicated concentrations in 96 well plates in 200µl of complete RPMI (RPMI-1640 medium [Gibco] supplemented with 10% FBS [Hyclone], 1x GlutaMAX [2mM L-alanyl-L-glutamine], 1x Penicillin [100U/ml]- Streptomycin [100µg/ml]-Glutamine [300µg/ml; Gibco], 1mM Sodium Pyruvate, 1x MEM NEAA, and 50µM 2-mercaptoethanol [all from Gibco]). After 24hrs, cells were collected and stained with anti-CD8, CD69, CD45.1, CD25, CD3, CD4, and AnnexinV-PE (eBiosicence), and resuspended in FW + 1 µg/ml PI (Enzo). Viability was assessed flow cytometric analysis.

Two-photon imaging

Thymocytes were obtained from *Ebi2*$^{+/+}$ and *Ebi2*$^{-/-}$ mice, and CD4SP thymocytes were enriched by magnetic depletion after incubation with the following purified antibodies, as for lineage depletion of BM: CD8, Gr-1, Ter119, B220, CD25, CD11b, and purity was assessed by flow cytometry as >85%. 1x10^6 *Ebi2*$^{+/+}$ and *Ebi2*$^{-/-}$ CD4SP cells were stained with Indo-1AM (Sigma) and CMTPX red (Life Technologies), respectively, for 30min at 37°C, according to manufacturers' instructions. Cells were washed and destained in complete RPMI for 30min at 37°C. *Ebi2*$^{+/+}$ and *Ebi2*$^{-/-}$ stained cells were mixed at 1:1 ratio, and resuspended in complete RPMI. 3-4 week old pCX-EGFP thymi were embedded in low-melt agarose (Lonza) and vibratome sectioned, with a VT1000S Vibratome (Leica), as previously described (74). After incubation for 1-2 h at 37°C 5% CO_2, images of thymic slices were acquired every 15 s, through a depth of 40 μm, at 5-μm intervals using an Ultima IV microscope with a 20x objective, NA 1.0, and PraireView software (Prairie). The sample was illuminated with two MaiTai lasers one tuned to 740 nm, and the other to 900 nm, to excite Indo and EGFP/CMTPX, respectively. Emitted light was passed through 480/40, 535/50, and 607/45 bandpass filters (Chroma) for detection of Indo1, EGFP, and CMTPX fluorescence, respectively. Cell tracking and analysis was carried out using Imaris v.8 (Bitplane): average cellular velocity was calculated as path length divided by time; straightness was calculated as total displacement divided by path length.

Slice deletion

Thymocytes were obtained from CD45.1 *Ebi2*$^{+/+}$ OT-II, CD45.2 *Ebi2*$^{-/-}$ OT-II and CD45.1 (loading control) mice and mixed at a 1:1:1 ratio. Mixed cells were stained with CMF2HC cell tracker blue (Life Technologies), according to the manufacturer's protocol. $3x10^6$ cells were incubated on top of each *Ebi2*$^{+/+}$ or *Ebi2*$^{-/-}$ thymic slice, prepared as described fore two-photon microscopy. Slices were incubated for 24hours at 37°C, 5% CO_2 in complete RPMI on 0.4-μm cell culture inserts (Millipore) in 35mm dishes with the indicated concentrations of Ovalbumin$_{323-339}$ peptide (OVAp). Slices were then manually dissociated, and cells were immunostained for flow cytometric analysis.

To compare indicated cell populations, we first normalized cell numbers to the number of CD45.1 cells of the comparable population that entered each slice to account for differences in slice entry. These numbers were then normalized to either the number of cells of the same population input onto the slice or in slices without OVAp, as indicated. The percentage of responding cells= (100- the percentage of surviving cells) + (the percentage of CD4SP cells upregulating CD25). The percentage of surviving cells was calculated as the number of CD4SP cells (normalized for slice entry) at a given concentration of OVAp divided by the number of CD4SP cells in the 0nM OVA slices, times 100. The percentage of CD4SP cells upregulating CD25 for a given concentration of OVAp was calculated as the number of $CD4^+CD25^+$ cells (normalized for slice entry) divided by the number of these cells in slices without OVAp, times 100. Propagate R package v 1.0-4 was used to calculate standard variations.

For some slice deletion experiments, WT OT-II and CD45.1 thymocytes were mixed at 1:1 ratio, stained with CMF2HC cell tracker blue (Life Technologies), and incubated on either *Ebi2*$^{+/+}$ and *Ebi2*$^{-/-}$ thymic slices, prior to analysis as above.

Statistical analyses

Cortical and medullary regions were quantified from immunofluorescent stains using the K-means clustering plug-in in FIJI (150). The number of clusters were set to three to distinguish background, cortex, and medulla, followed by analysis of particles in each cluster. Two-way ANOVA was used to assess significance of differences in thymocyte subset cellularity due to the *Ebi2* genotype and/or the RIP-mOVA transgene. Paired t-tests were used to compare medullary/cortical densities of *Ebi2*$^{+/+}$ and *Ebi2*$^{-/-}$ CD4SP cells from 2-photon imaging data because cells of both genotypes were analyzed together in each dataset. Unpaired T-tests were used in remaining analyses. All statistical analysis was done using Prism6 (Graphpad). P-values are marked with asterisks (*); * p-value<0.05, ** p-value<0.01, *** p-value<0.001, **** p-value<0.0001

3.4 RESULTS

3.4.1 Expression and function of EBI2, implicate a contribution to CD4SP thymocyte differentiation

To identify candidate GPCR/ ligand pairs that could affect migration of post-positive selection thymocytes in the medulla, we analyzed our transcriptional profiling database of

thymocyte and thymic stromal cell subsets (137). EBI2 emerged as a candidate because it was expressed after positive selection in DP and CD4 SP thymocytes. Additionally, *Ch25h*, which encodes an enzyme required for generation of the EBI2 ligand 7α25-OHC (144), was highly expressed by $mTEC^{lo}$ cells (data not shown). qRT-PCR analysis of *Ebi2* and *Ch25h* in FACS sorted thymocyte and thymic stromal subsets (Figure 3.1), respectively, confirmed these expression patterns (Figure 3.1).

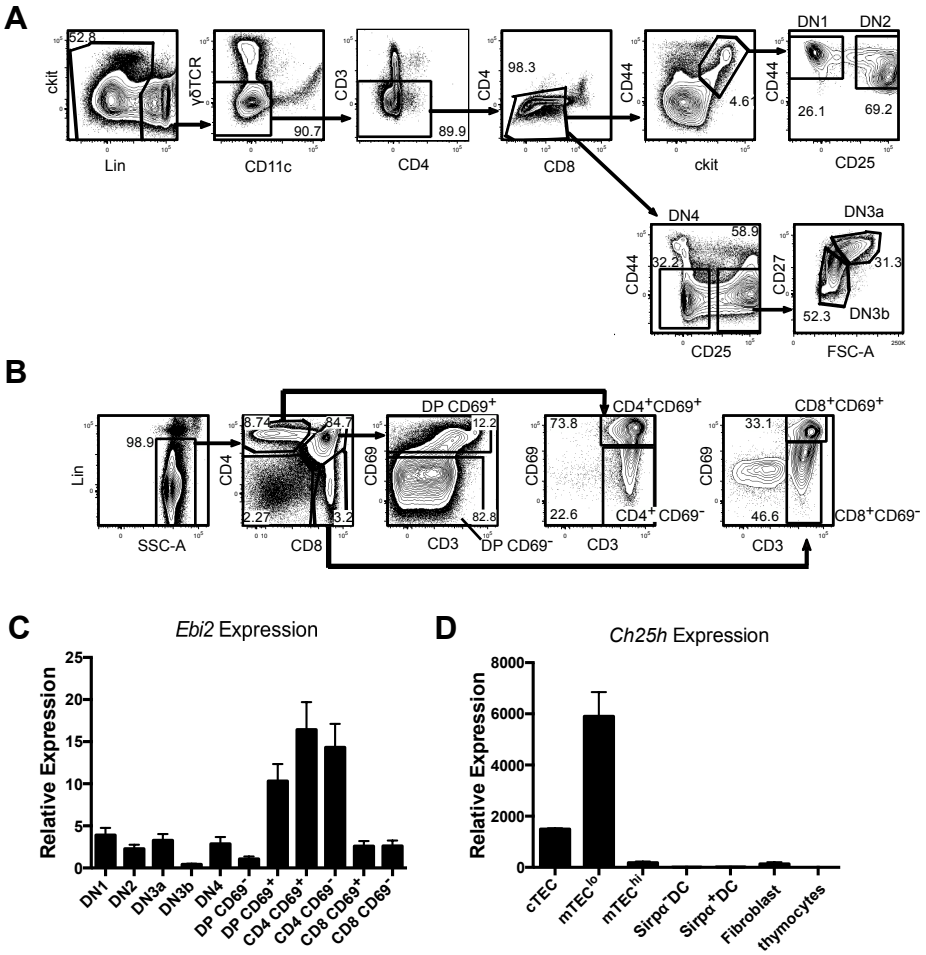

Figure 3.1 Gating schemes for thymocytes and expression patterns of *Ebi2* and, *Ch25h*.

(A) DN population (B) CD4SP and CD8SP gating schemes for FACS sorted thymocyte (C) *Ebi2* and (D) *Ch25h* mRNA expression levels were quantified by qRT-PCR in FACS sorted thymocyte and thymic stromal subsets. Expression was normalized to (C) DP $CD69^-$ levels and (D) thymocyte levels. Data are representative of 2 independent experiments, with technical triplicates for each subset. All graphs depict means±SEM.

Next, we analyzed GFP expression in thymocytes from *Ebi2*$^{+/+}$, *EBI2*$^{+/GFP}$ (*Ebi2*$^{+/-}$) and *EBI2*$^{GFP/GFP}$ (*Ebi2*$^{-/-}$) mice, in which the *Ebi2* open reading frame has been replaced with EGFP (143). GFP was first detectable at the immature CD4^{+} CD69^{+} stage, with the highest expression in mature CD4^{+} CD69^{-} cells, indicating that EBI2 protein is not produced until positively selected thymocytes are committed to the CD4SP lineage. CD4^{+}CD25^{+} thymocytes, which include Treg precursors (Tregp) and Treg cells, also expressed GFP (Figure 3.2). In addition, CD4^{+} T cells in the spleen and lymph nodes displayed robust GFP expression (Figure 3.2A, and 3.2B).

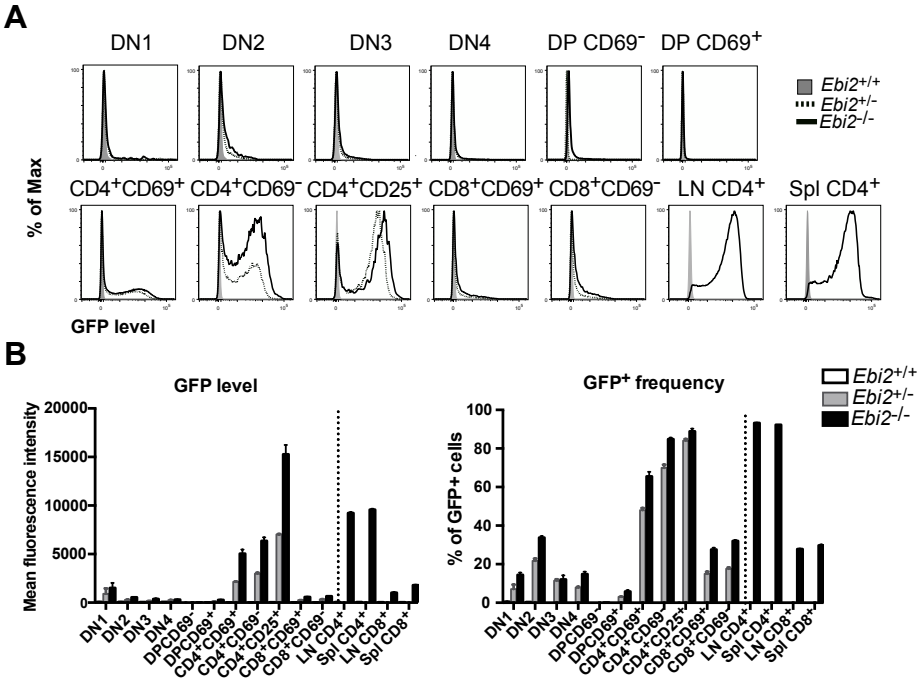

Figure 3.2 Expression patterns of *Ebi2* and, *Ch25h*, implicates *Ebi2* in post-positive selection CD4SP thymocytes.

(A) Representative flow cytometry plots showing GFP levels expressed by the indicated thymocyte subsets, and by lymph node and splenic $CD4^+$ T cells (LN $CD4^+$ and Spl $CD4^+$, respectively) from *Ebi2*-GFP knock-in mice of the indicated genotypes. (B) Quantification of the Mean Fluorescence Intensity (MFI) of GFP (left graph) and the percent of GFP^+ cells (right graph) for the indicated thymocyte subsets from *Ebi2*-GFP knock-in mice of the indicated genotypes, from data as in C. ($Ebi2^{+/+}$ n=9, $Ebi2^{+/-}$ n=5, $Ebi2^{-/-}$ n=9). All graphs depict means±SEM.

Because EBI2 signaling in response to 7α,25-OHC induces chemotaxis of B cells and $CD4^+$ T cells (139), we tested whether EBI2 promoted chemotaxis of CD4SP thymocytes. Indeed, 7α,25-OHC induced chemotaxis of CD4SP thymocytes in an *Ebi2*-dependent manner *in vitro* (Figure 3.3A). Notably, *Ebi2*$^{+/-}$ thymocytes did not undergo efficient chemotaxis in response to 7α,25-OHC, indicating a haploinsufficiency phenotype. EBI2 also promoted chemotaxis of $CD4^+CD25^+$ Treg and Tregp in response to 7α,25-OHC (Figure 3.3B). Consistent with the GFP expression data (Figure 3.3B), DP $CD69^+$cells did not undergo chemotaxis, and mature $CD69^-$ CD4SP cells were more responsive than immature CD4SP cells, suggesting increasing expression of functional EBI2 protein during CD4SP maturation (Figure 3.3B). These data demonstrate that EBI2 induces chemotaxis of post-positive selection CD4SP thymocytes, while the enzyme producing the EBI2 ligand 7α,25-OHC is made by mTECs, suggesting that EBI2 contributes to CD4SP migration and medullary accumulation.

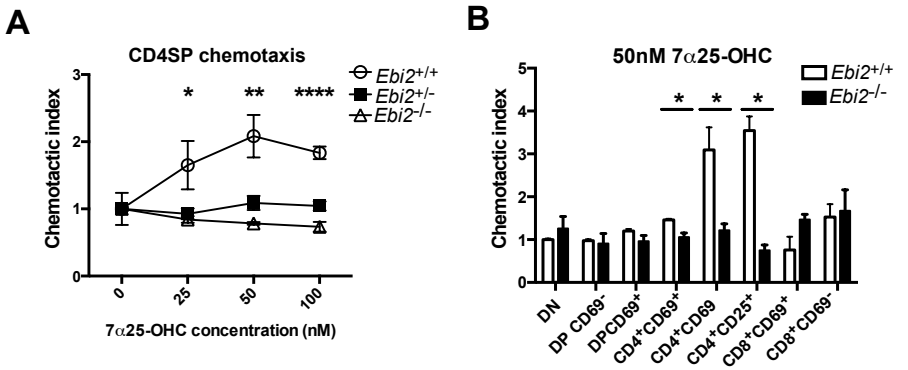

Figure 3.3 Chemotactic activity implicate *Ebi2* in migration of post-positive selection CD4SP thymocytes..

(A) Quantification of the chemotactic index of CD4SP cells of the indicated genotypes migrating in response to the indicated concentrations of 7α,25-OHC. (B) Chemotactic index of $Ebi2^{+/+}$ and $Ebi2^{-/-}$ thymocyte subsets responding to 50nM of 7α,25-OHC. Data in E and F are representative of 5 independent experiments, with triplicates per experiment. All graphs depict means±SEM

3.4.2 Normal thymocyte cellularity and subset composition in EBI2-deficient mice and competitive bone marrow chimeras

To determine whether EBI2 was required for thymocyte differentiation, we analyzed thymocyte subsets from *Ebi2*$^{-/-}$ mice by flow cytometry. We did not detect significant differences in thymocyte cellularity or subset distribution in *Ebi2*$^{-/-}$ versus *Ebi2*$^{+/+}$ thymi from mice 4-6 weeks of age (Figure 3.4A, 3.4B). Because signals from post-positive selection thymocytes that migrate efficiently into the medulla are required for proper differentiation of the mTEC compartment (73, 100), we determined whether cortical-medullary architecture was perturbed in *Ebi2*$^{-/-}$ mice. Quantification of cortical and medullary regions from cryosections immunostained to identify cTEC and mTEC did not show evidence of disrupted thymic architecture (Figure 3.4C, 3.4D). Furthermore, immunostaining did not reveal disruption of the cortical localization of DP cells or medullary localization of CD4SP or CD8SP cells (Figure 3.4E). Thus, EBI2 is not required for entry of SP cells into the medulla or thymic organization.

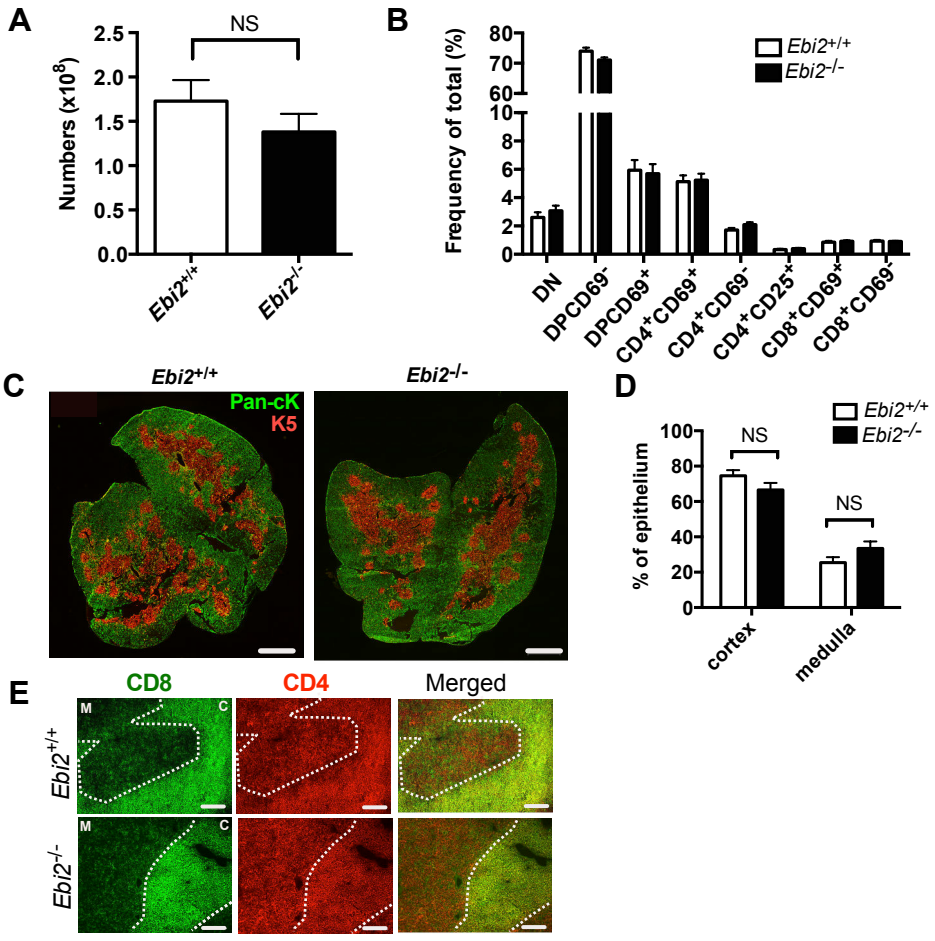

Figure 3.4 Thymocyte cellularity and subset composition is normal in EBI2-deficient mice

(A-B) Quantification of total thymocyte cellularity (A) and frequency of thymocyte subsets (B) in *Ebi2*$^{+/+}$ and *Ebi2*$^{-/-}$ mice (n=8 for each genotype). (C) Representative *Ebi2*$^{+/+}$ and *Ebi2*$^{-/-}$ thymic cryosections immunostained for Keratin5 (red), marking medullary regions, and Pan-cytokeratin (Pan-cK; green), marking cortical regions. Representative of 3 thymi each. Scale bar=1mm. (D) The percentage of cortical and medullary epithelium in *Ebi2*$^{+/+}$ and *Ebi2*$^{-/-}$ thymi, as determined by k-mean clustering analysis of images as in C (n=3 for each genotype). (E) Representative images of *Ebi2*$^{+/+}$ and *Ebi2*$^{-/-}$ thymic cryosections immunostained to detect CD4 (red) and CD8 (green). The white dashed line demarcates medullary (M) and cortical (C) (scale bar=100µm) (n=3). All graphs depict means±SEM.

To determine whether a defect in thymocyte differentiation would be revealed if *Ebi2*$^{-/-}$ thymocytes were placed in a competitive setting with wild-type thymocytes, we analyzed mixed bone marrow chimeras. Bone marrow cells from congenically marked *Ebi2*$^{+/+}$ (CD45.1) and *Ebi2*$^{-/-}$ (CD45.2) mice were lineage depleted, mixed at a 1:1 ratio, and injected intravenously into lethally irradiated congenic (CD45.1/CD45.2) recipient mice (Figure 3.5A). *Ebi2*$^{-/-}$ cells did not contribute differentially to thymocyte subsets relative to *Ebi2*$^{+/+}$ cells (Figure 3.5B). Thus, EBI2-deficient bone marrow cells have a comparable capacity to reconstitute the thymus and undergo T cell development under competitive conditions.

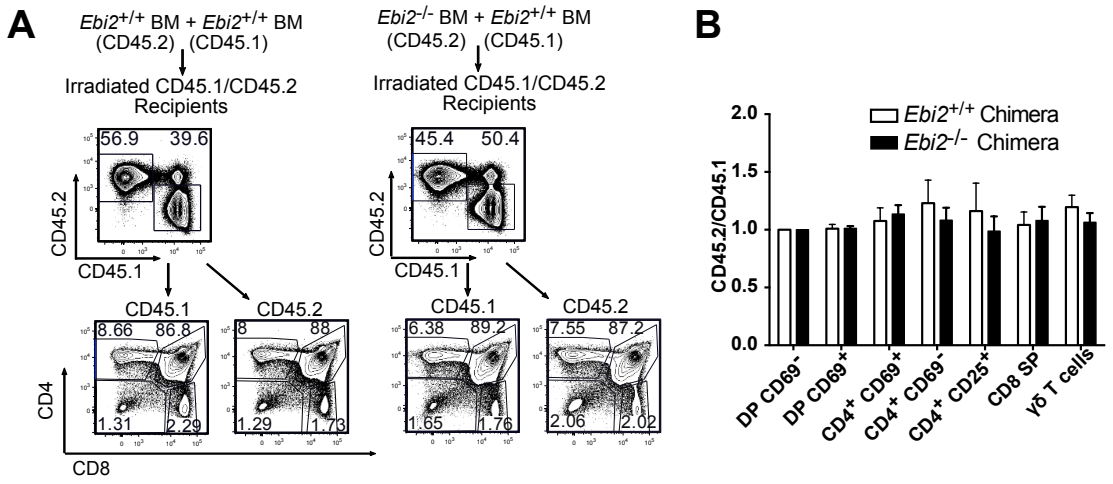

Figure 3.5 Thymocyte subset composition is normal in competitive bone marrow chimeras.

(A) Experimental schematic of competitive bone marrow chimeras and representative flow cytometric plots used for analysis. (B) Quantification of the ratio of CD45.2 to CD45.1 positive cells within thymocyte subsets in the indicated bone marrow chimera recipients. Ratios are normalized to the pre-positive selection DP CD69$^-$ subset (*Ebi2*$^{+/+}$ n=10, *Ebi2*$^{-/-}$ n=12). All graphs depict means±SEM

3.4.3 EBI2 deficiency results in impaired negative selection and enhanced Treg generation of OT-II CD4SP cells in response to self- antigens in vivo

If EBI2 were partially reduncant with other chemokine receptors that promote efficient medullary entry and/or scanning of thymic APCs, then *Ebi2*$^{-/-}$ thymocytes might not display overt perturbations in thymocyte differentiation, but might still have subtle defects in negative selection. To address this possibility, we first analyzed negative selection of monoclonal OT-II TCR CD4SP cells. We and others previously found that the OT-II TCR induces weak negative selection to an endogenous auto-antigen in C57BL/6 mice, and strong negative selection to a high affinity cognate antigen, allowing us to query two different levels of self-recognition (10, 64). The Vα2^{+} Vβ5^{+} OT-II TCR recognizes OVAp in the context of I-A^{b} (151). RIP-mOVA transgenic mice express a transmembrane form of Ovalbumin under control of the rat insulin promoter, such that mTECs express OVA in an AIRE-dependent fashion (152). In RIP-mOVA^{+} mice, OT-II thymocytes undergo negative selection due to encounter of their cognate antigen in the medulla (64).

We transplanted *Ebi2*$^{-/-}$ versus *Ebi2*$^{+/+}$ OT-II TCR transgenic bone marrow into lethally irradiated RIP-mOVA^{-} or RIP-mOVA^{+} mice, and thymic chimerism was analyzed after 6 weeks (Figure 3.6A). Flow cytometric analysis of recipient thymi revealed no differences in cellularity of post-positive selection DP CD69^{+} OT-II cells (Figure 3.6B), as expected since EBI2 does not show activity in thymocytes until the CD4SP stage (Figure 3.2C). *Ebi2*$^{+/+}$ OT-II CD4SP cells underwent negative selection, as expected, in RIP-mOVA^{+} recipients. *Ebi2*$^{-/-}$ OT-II CD4SP cells also underwent efficient

negative selection in response to the RIP-mOVA transgene. However, a striking increase in cellularity of *Ebi2*$^{-/-}$ versus *Ebi2*$^{+/+}$ OT-II CD4SP thymocytes was observed in RIP-mOVA^{-} recipients (Figure 3.6B). These data indicate that EBI2 is not required for negative selection of CD4SP cells in response to the high-affinity OVA antigen, but is required for negative selection in response to a weakly deleting endogenous C57BL/6J self-antigen. Two-way ANOVA analysis confirmed that the RIP-mOVA transgene resulted in significant deletion of CD4SP OT-II cells, while *Ebi2* deficiency resulted in a significant increase in the number of CD4SP OT-II cells (Figure 3.6B). Furthermore, *Ebi2*$^{-/-}$ thymocytes generated more CD4^{+}CD25^{+} Treg and Tregp cells (Figure 3.6B). Together, these results indicate that EBI2 promotes negative selection of CD4SP thymocytes to weak self-antigens, and inhibits Treg generation.

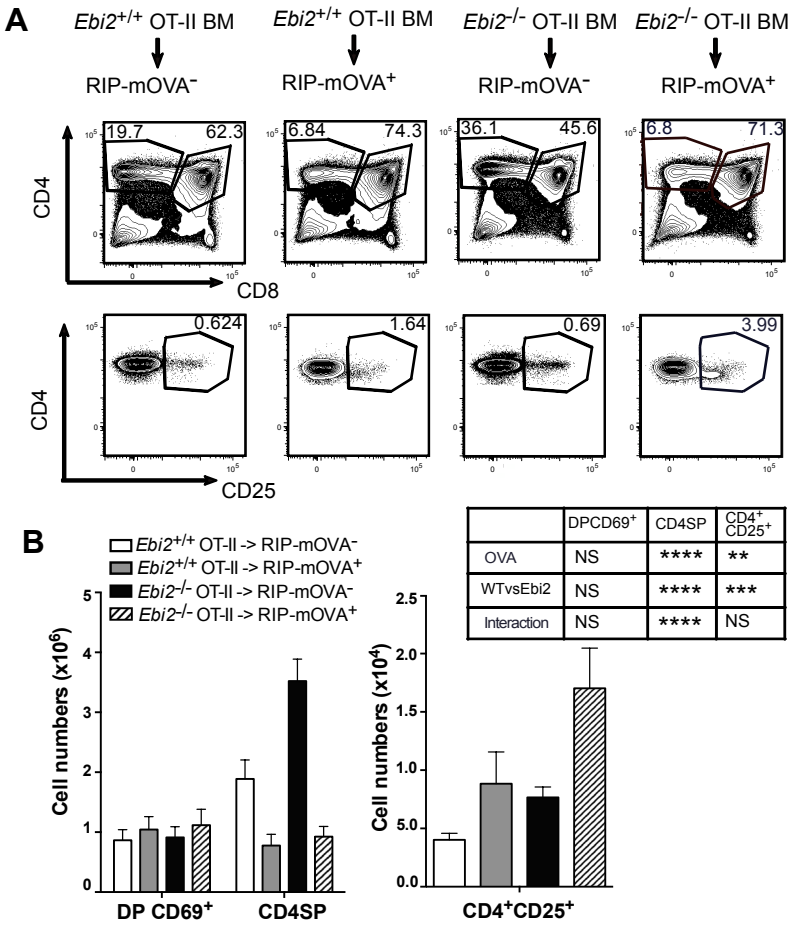

Figure 3.6 EBI2 is required for negative selection of OT-II thymocytes responding to an endogenous antigen, and restrains Treg generation

(A) Schematic of bone marrow chimeras generated by transplantation of *Ebi2*$^{+/+}$ or *Ebi2*$^{-/-}$ OT-II bone marrow into lethally irradiated RIP-mOVA^{-} or RIP-mOVA^{+} recipients. Thymic chimerism was analyzed 6 weeks after transplantation, and representative flow cytometric plots are shown. (B) Quantification of thymocyte subsets in the indicated chimeras. (n=10 *Ebi2*$^{+/+}$ OT-II-> RIP-mOVA^{-}; n=8 *Ebi2*$^{+/+}$ OT-II-> RIP-mOVA^{+}; n=15 *Ebi2*$^{-/-}$ OT-II-> RIP-mOVA^{-}; n=13 *Ebi2*$^{-/-}$ OT-II-> RIP-mOVA^{-}). The table shows the results of the two-way ANOVA to analyze significance of differences in cellularity of each subset due to the presence of OVA, genotype of *Ebi2*, or interaction of these factors. All graphs depict means±SEM.

We considered alternate mechanisms by which EBI2 deficiency could result in increased CD4SP OT-II thymocytes in wild-type mice. First, EBI2 signaling could inhibit proliferation of CD4SP OT-II cells. However, EBI2 deficiency did not result in an increase in the frequency of proliferating CD4SP OT-II thymocytes in any of the above chimeras (Figure 3.7A). Alternatively, EBI2 deficiency could enhance survival of CD4SP thymocytes in an antigen-independent manner, resulting in an accumulation of CD4SP cells. To test this possibility, we incubated *Ebi2*$^{-/-}$ versus *Ebi2*$^{+/+}$ thymocytes in the presence or absence of 7α,25-OHC overnight, and quantified the resultant viability of CD4SP thymocyte subsets. EBI2 deficiency did not confer increased survival on CD4SP thymocyte subsets (Figure 3.7B). The increase in CD4SP cells could also be due to impaired thymocyte egress, but this is unlikely because the proportion of CD4^{+} CD69^{-} cells does not increase in *Ebi2*$^{-/-}$ thymi, as would be expected if mature CD4SP cells were retained (Figure 3.4B) Thus, we conclude that the increase in CD4SP cellularity in wild-type recipients transplanted with *Ebi2*$^{-/-}$ OT-II bone marrow is not due to EBI2-mediated changes in proliferation or antigen-independent apoptosis of CD4SP thymocytes, and is most consistent with a defect in negative selection.

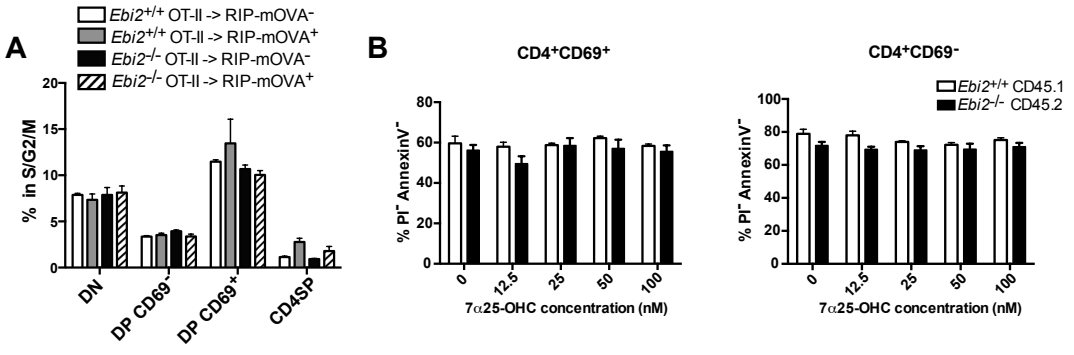

Figure 3.7 Proliferation and survivability is normal in EBI2-deficient CD4SP.

(A) The percentage of each thymocyte subset in the chimeras generated in Figure3.6 that are in cell cycle, as determined by flow cytometric analysis of DNA content. (B) *Ebi2*$^{-/-}$ and *Ebi2*$^{+/+}$ thymocytes were incubated for 24 hours *in vitro* in the presence or absence of 7α,25-OHC. The percentage of viable cells (AnnexinV^{-}PI^{-}) was quantified by flow cytometry. Data are representative of 3 experiments. All graphs depict means±SEM

3.4.4 EBI2 deficiency results in an altered TCR repertoire

If negative selection were truly impaired by EBI2 deficiency, then the TCR repertoire of CD4SP cells should be altered in *Ebi2*$^{-/-}$ mice. To test this, we analyzed TCRVβ gene usage in thymocytes subsets of *Ebi2*$^{+/+}$, *Ebi2*$^{+/-}$, and *Ebi2*$^{-/-}$ mice. We noticed a consistent trend of increased TCR Vβ5+ usage in CD4SP and CD4+CD25+populations in *Ebi2*$^{-/-}$ mice (p-value <0.05 by t-test analysis); however, the difference wasn't significant after multiple comparisons corrections (Figure 3.8A). Given that Vβ5 is used by the OT-II TCR, which underwent impaired negative selection to a weak self-antigen, we more rigorously evaluated whether EBI2 deficiency altered Vβ5 usage in CD4SP thymocytes. Evaluation of additional *Ebi2*$^{+/+}$ and *Ebi2*$^{-/-}$ thymocytes revealed that Vβ5 usage increased slightly, but significantly, in *Ebi2*$^{-/-}$ CD4SP cells (Figure 3.8B). Thus, EBI2 deficiency subtly alters the TCR repertoire of CD4SP cells. Previous studies suggest that an endogenous super-antigen deletes Vβ5^{+} CD4SP cells on the C57BL/6J background (151). Therefore, EBI2 deficiency in CD4SP cells may impair negative selection against endogenous super-antigens, in keeping with the increased cellularity of Vβ5^{+} OT-II *Ebi2*$^{-/-}$ CD4SP cells in C57BL/6J recipients (Figure 3.6B).

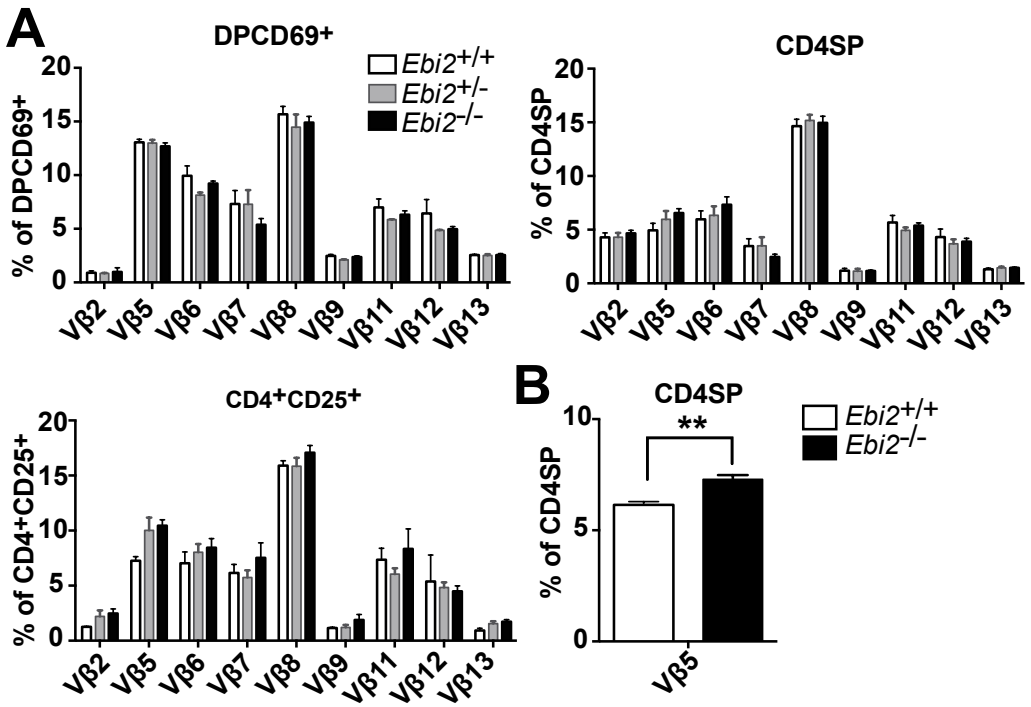

Figure 3.8 EBI2 deficiency alters the TCR repertoire of CD4SP thymocytes.

(A) Thymocytes of the indicated subsets and *Ebi2* genotypes were analyzed by flow cytometry to determine the frequency of CD4SP cells that expressed different TCRVβ segments. Using a t-Test, the p-value for Vβ5 was <0.05, but significance was lost after Holm-Sidak multiple comparison correction. ($Ebi2^{+/+}$ n=6, $Ebi2^{+/-}$ n=9, $Ebi2^{-/-}$ n=12). (B) The frequency of $Ebi2^{+/+}$ and $Ebi2^{-/-}$ CD4SP cells that express TCR Vβ5 was assessed in additional mice ($Ebi2^{+/+}$ n=5, $Ebi2^{-/-}$ n=5). All graphs depict means±SEM.

3.4.5 Impaired negative selection and enhanced Treg generation of *Ebi2*$^{-/-}$ OT-II CD4SP cells in response to self- antigens on wild-type thymic slices

Our data indicate that EBI2 deficiency impairs negative selection of CD4SP cells responding to a weak self-antigen, while promoting differentiation of $CD4^{+}CD25^{+}$ Tregp and Treg cells, even in the presence of a high affinity self-antigen (Figure 3.6B). To determine if EBI2 deficiency results in comparable phenotypes under conditions where *Ebi2*$^{+/+}$ and *Ebi2*$^{-/-}$ OT-II thymocytes compete for negatively selecting ligands in a wild-type thymic environment, we analyzed negative selection and Treg generation in wild-type live thymic slices (74, 153). An equivalent number of CD45.1 *Ebi2*$^{+/+}$ OT-II thymocytes, CD45.2 *Ebi2*$^{-/-}$ OT-II thymocytes, and CD45.1 thymocytes (which served as a slice loading control) were mixed together, labeled with a blue cell-tracker dye, and incubated on live thymic slices in the presence of OVAp, at concentrations ranging from 0nM to 10uM. After 24 hours, thymocyte subsets derived from each OT-II population were analyzed by flow cytometry to assess whether negative selection and/or upregulation of CD25 had occurred (Figure 3.9A).

Ebi2$^{+/+}$ OT-II CD4SP $CD25^{-}$ cellularity diminished following incubation on slices for 24 hours in the absence of OVAp, indicating that negative selection of OT-II thymocytes to an endogenous self-antigen can be detected on thymic slices. Notably, *Ebi2*$^{-/-}$ OT-II CD4SP thymocytes were not deleted in response to the endogenous self-antigen, resulting in a significant increase in their cellularity relative to EBI2 sufficient OT-II CD4SP cells (Figure 3.9B, left panel). Both *Ebi2*$^{+/+}$ OT-II and *Ebi2*$^{-/-}$ OT-II

$CD4^+CD25^-$ cells diminished in number, as they underwent negative selection in response to increasing concentrations of OVAp. In fact, when OT-II $CD4^+CD25^-$ cellularity was normalized to slices without OVAp, such that relative deletion in response to increasing OVAp could be directly compared, *Ebi2*$^{-/-}$ OT-II $CD4^+CD25^-$ cells underwent deletion as efficiently as *Ebi2*$^{+/+}$ OT-II cells (Figure 3.9B, middle panel). This result is consistent with efficient negative selection of *Ebi2*$^{-/-}$ OT-II $CD4^+CD25^-$ cells in RIP-mOVA bone marrow chimeras (Figure 3.6B), and further indicates that EBI2 is not required for negative selection to a high-avidity antigen, but only to a weakly deleting self-antigen.

In the presence of OVAp, *Ebi2*$^{-/-}$ CD4SP OT-II thymocytes generated significantly more $CD4^+CD25^+$ Tregp and Treg than *Ebi2*$^{+/+}$ CD4 OT-II cells (Figure 3.9B, right panel). This suggests that EBI2 modulates the decision to undergo negative selection versus Treg generation in the presence of high-affinity antigens. To further evaluate this possibility, we quantified the CD4SP cells that underwent deletion plus those that upregulated CD25, to evaluate the percentage of CD4SP that responded to each concentration of OVAp. EBI2 deficiency did not alter the frequency of CD4SP cells that responded to OVAp at any concentration (Figure 3.9C, left panel). We next calculated the percentage of CD4SP that survived deletion and the percentage that became $CD25^+$ cells (Figure 3.9C, middle and right panels, respectively). We observed a small, but significant increase in survival of EBI2 deficient OT-II CD4SP thymocytes at 10μM OVAp (Figure 3.9C, middle panel). We also observed a consistent, though non-statistically significant, trend towards increased generation of $CD4^+$ $CD25^+$ Treg and Tregp from *Ebi2*$^{-/-}$ OT-II thymocytes (Figure 3.9C, right panel). This loss of significance for the difference in

$CD4^+CD25^+$ cells when normalized to 0nM slices results from the high variability and very small numbers of Treg in OT-II thymocytes in the absence of OVAp, Taken together, these data support the conclusion that EBI2 is required for efficient negative selection to weak self-antigens, and promotes negative selection over Treg generation in the presence of high-affinity antigens.

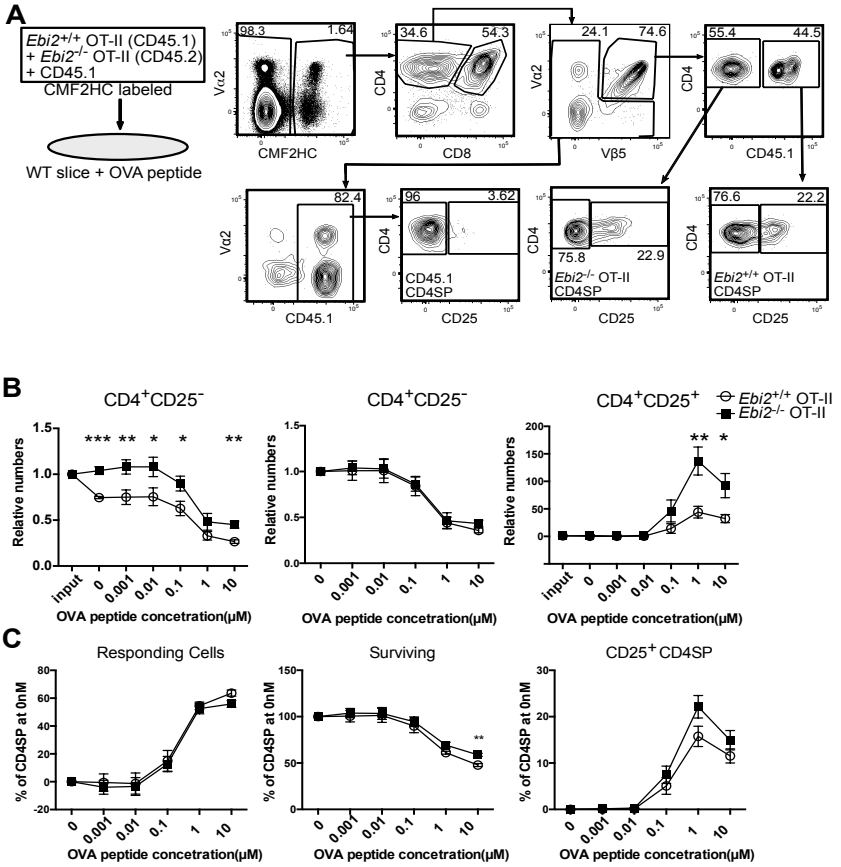

Figure 3.9 EBI2 promotes negative selection of OT-II CD4SP thymocytes responding to an endogenous self-antigen and restrains Tregp generation in thymic slices in the presence of OVAp.

(A) Schematic of slice deletion experiments to assess negative selection and CD25 upregulation by *Ebi2*$^{+/+}$ and *Ebi2*$^{-/-}$ OT-II thymocytes in the presence or absence of OVAp. The gating schematic used to analyze slice deletion experiments is depicted. (B) The relative number of OT-II cells of the indicated subsets and genotypes in slices incubated with increasing concentrations of OVAp. Cell numbers were normalized for slice entry using the CD45.1 control, and then to the number of the corresponding subset input onto the slices (left and right panels) or to the number of the same subset present in slices without OVAp (middle panel). Data are representative of 3 independent experiments, using triplicate slices per condition. (C) Quantification of the percent of OT-II CD4SP that responded to the indicated concentrations of OVAp by undergoing either deletion or upregulation of CD25 (left panel), that survived (middle), or that upregulated CD25 (right). Percentages were calculated relative to the number of CD4SP cells in slices with 0nM OVAp. All graphs depict means±SEM.

3.4.6 EBI2 expressed by thymic DCs is dispensable for intrathymic DC localization and negative selection of CD4SP cells

We found that EBI2 is also expressed by thymic DCs (Figure 3.10A-B). Thus, the increased cellularity of *Ebi2*$^{-/-}$ OT-II CD4SP cells in RIP-mOVA^{-} recipients (Figure 3.6) could EBI2 deficiency in the thymocyte and/or DC compartments. While slice deletion experiments using *Ebi2*$^{-/-}$ versus *Ebi2*$^{+/+}$ OT-II CD4SP thymocytes undergoing negative selection on wild-type thymic slices (Figure 3.9) clearly revealed a T cell-intrinsic role for EBI2 in negative selection and Treg generation, we also evaluated the contribution of EBI2 in thymic DCs. EBI2 is known to regulate localization and survival of DCs in splenic bridging channels (145, 154), and could affect thymic DCs in a similar manner. While EBI2 was expressed by all three thymic DC subsets, Sirpα^{+}DC, Sirpα^{-}DC, and plasmacytoid DC (Figure 3.10B), Sirpα^{+} DC expressed the highest levels and were the only subset to undergo EBI2-dependent chemotaxis (Figure 3.10C). Because Sirpα^{+}DCs migrate into the thymus from the periphery, EBI2 could promote their thymic recruitment. To test this, we evaluated cellularity of DC subsets in *Ebi2*$^{-/-}$ thymi. We did not observe significant differences in the total cellularity or subset distribution of thymic DCs in *Ebi2*$^{-/-}$ mice (Figure 3.10D).

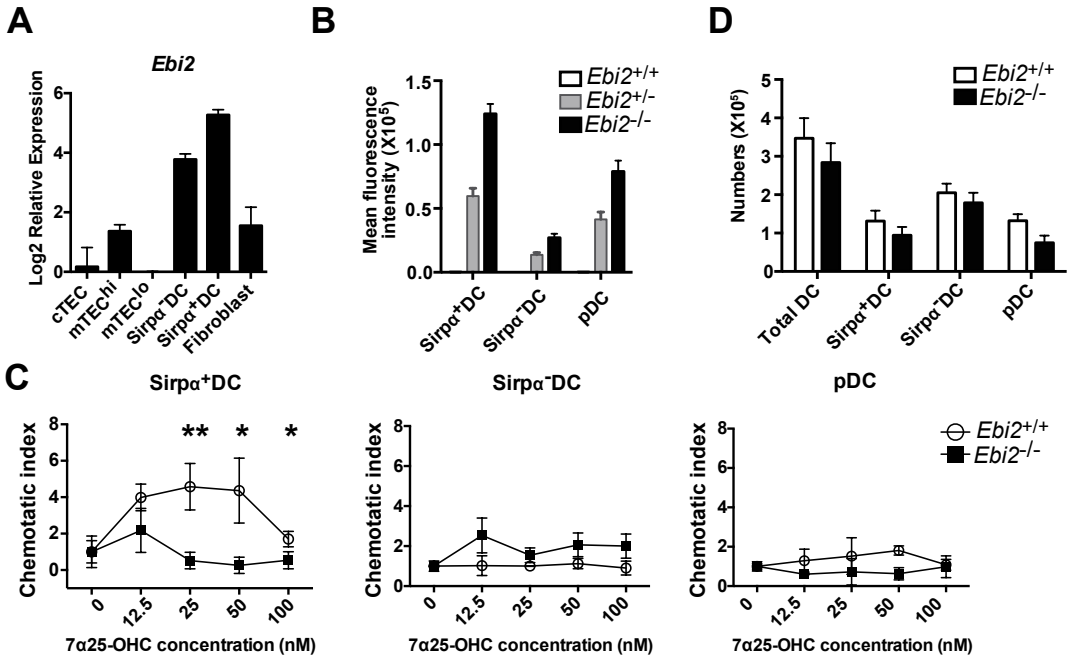

Figure 3.10 EBI2 deficiency in thymic DCs does not impair DC cellularity.

(A) Relative *Ebi2* mRNA levels in the indicated thymic stromal cell subsets from our previously reported gene expression profiling data (137). (B) Quantification of the MFI of GFP expression in thymic DC subsets from EBI2-EGFP knock-in mice of the indicated genotypes. ($Ebi2^{+/+}$ n=4, $Ebi2^{+/-}$ n=6, $Ebi2^{-/-}$ n=9) (C) Quantification of the chemotactic index of $Ebi2^{+/+}$ and $Ebi2^{-/-}$ DCs migrating towards the indicated concentrations of 7α,25-OHC in transwell chemotaxis assays. Data are representative of 3 independent experiments. (D) The number of thymic DCs of the indicated subsets in $Ebi2^{+/+}$ and $Ebi2^{-/-}$ mice. ($Ebi2^{+/+}$ n=8, $Ebi2^{-/-}$ n=9) All graphs depict means±SEM

Furthermore, immunofluorescent analyses revealed that *Ebi2*$^{-/-}$ DCs are properly localized within the medulla (Figure 3.11). Thus, we were unable to detect a significant role for EBI2 in promoting thymic recruitment or medullary localization of DCs.

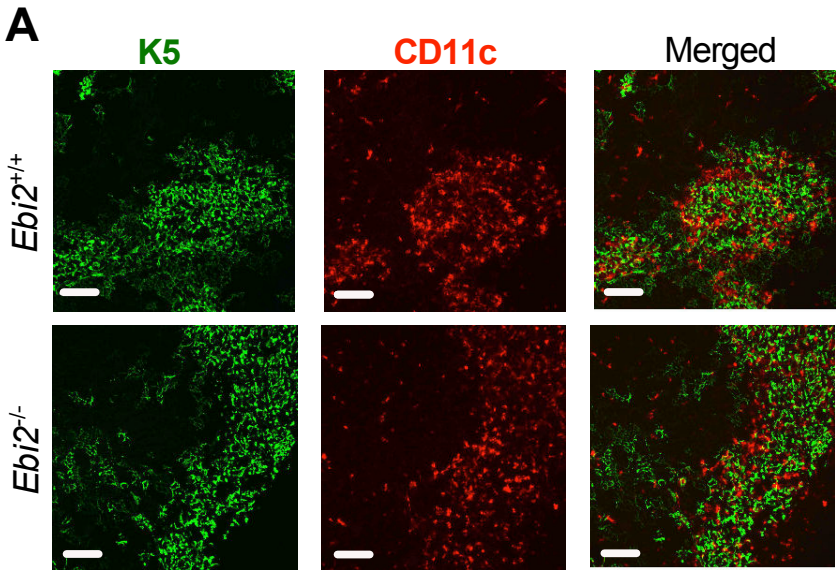

Figure 3.11 EBI2 deficiency in thymic DCs does not impair intrathymic localization.

(A) Representative *Ebi2*$^{+/+}$ and *Ebi2*$^{-/-}$ thymic cryosections immunostained for Keratin5 (green), to highlight medullary regions, and CD11c (red) to identify DCs. Scale bar=100μm. Representative of sections from 3 mice of each genotype.

To directly assess whether EBI2 deficiency in DCs could impact negative selection, we analyzed deletion of *Ebi2*$^{+/+}$ OT-II CD4SP cells in *Ebi2*$^{+/+}$ or *Ebi2*$^{-/-}$ thymic slices in the presence of increasing concentrations of OVAp (Figure 3.12A). Previous studies demonstrated that exogenously administered antigens are most efficiently presented by thymic DCs, relative to other thymic stromal subsets (155). Thus, if EBI2 expression on DCs were required for efficient negative selection, we would expect that OT-II CD4SP cells would not undergo efficient negative selection on *Ebi2*$^{-/-}$ slices in response to OVAp. However, negative selection of OT-II CD4SP cells occurred equivalently on *Ebi2*$^{+/+}$ and *Ebi2*$^{-/-}$ thymic slices, and CD25 was upregulated comparably (Figure 3.12A, B). Thus, we find no evidence that EBI2 deficiency in the thymic DC compartment contributes to impaired negative selection of OT-II CD4SP cells to weak endogenous antigens or to CD4^{+}CD25^{+} generation in response to OVA. These findings further indicate that EBI2 expression in the thymocyte compartment is important for efficient negative selection and restrained Treg generation.

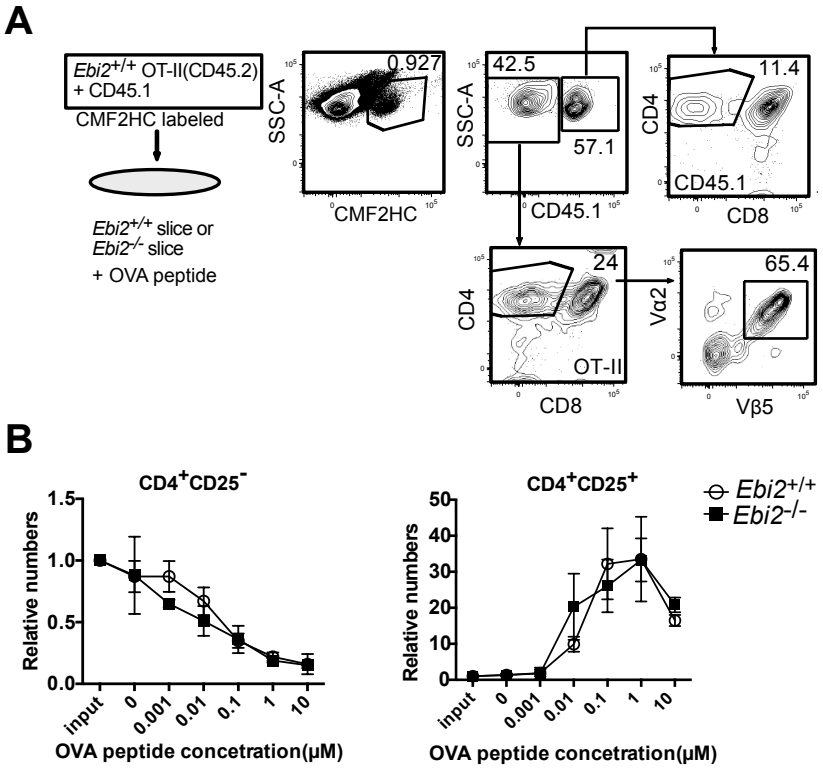

Figure 3.12 EBI2 deficiency in thymic DCs does not impair DC capacity to induce negative selection.

(A) Schematic of slice deletion experiments to assess negative selection and CD25 upregulation by *Ebi2*$^{+/+}$ OT-II thymocytes on *Ebi2*$^{+/+}$ versus *Ebi2*$^{-/-}$ thymic slices. The gating schematic used for analysis is also depicted (B) The relative number of $CD4^+CD25^-$ and $CD4^+CD25^+$ cells in slices incubated with the indicated concentrations of OVAp were calculated by normalization to input cell numbers, as in Figure 5B. All graphs depict means$\pm$SD. Representative of 3 experiments, using triplicate slices per condition.

3.4.7 EBI2 is required for rapid motility and efficient medullary accumulation of CD4SP thymocytes

EBI2 deficiency could impact negative selection by altering the capacity of CD4SP thymocytes to efficiently accumulate in the medulla and rapidly scan medullary APCs. To investigate this possibility, we used two-photon microscopy to image migration and localization of *Ebi2*$^{+/+}$ and *Ebi2*$^{-/-}$ CD4SP cells in the cortex and medulla of pCX-EGFP live thymic slices (10) (Figure 3.13A). CD4SP thymocytes accumulate at a 5-10 fold higher density in the thymic medulla relative to the cortex (74). EBI2 deficiency resulted in a subtle but significant reduction in the enrichment of CD4SP cells in the medulla (Figure 3.13B). Notably, *Ebi2*$^{-/-}$ CD4SP cells migrated at a significantly slower speed than *Ebi2*$^{+/+}$ CD4SP cells, although the straightness of their trajectories was not altered (Figure 3.13C, 3,13D). These results demonstrate that EBI2 deficiency impairs the capacity of CD4SP cells to migrate rapidly and to accumulate in the medulla, indicating that EBI2 contributes to the induction of negative selection by promoting efficient scanning of medullary APCs.

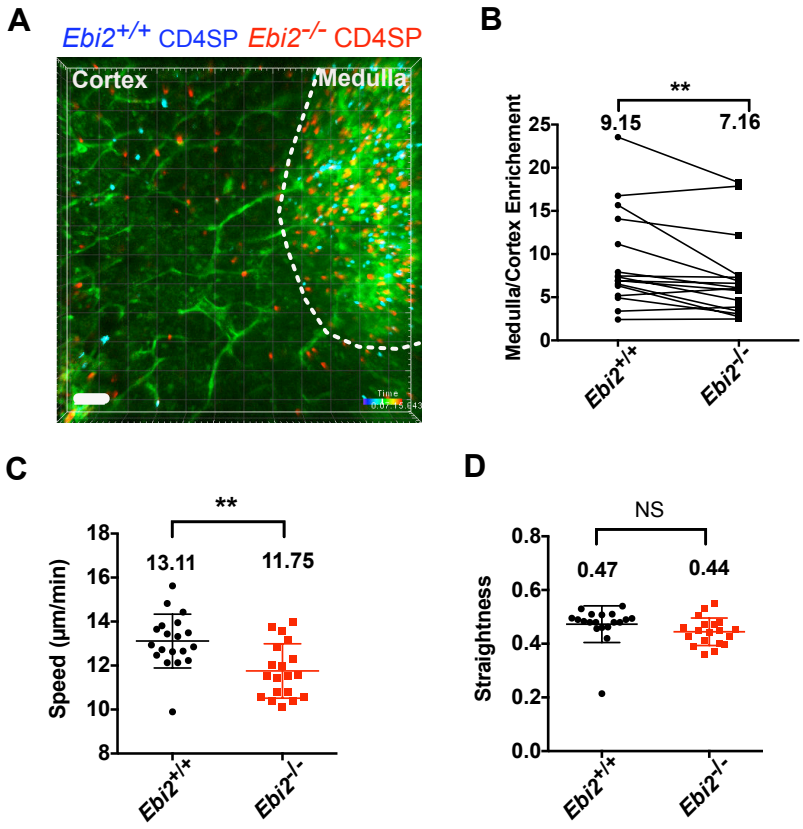

Figure 3.13 EBI2 contributes to accumulation within the medulla and promotes rapid motility of CD4SP cells.

(A) A maximum intensity projection of *Ebi2*$^{+/+}$ (blue) and *Ebi2*$^{-/-}$ (red) CD4SP thymocytes in live pCX-EGFP (green) thymic slices. The boundary between the cortex and medulla is indicated with a dashed line. Supplemental Video 1 shows the corresponding two-photon imaging data. Scale Bar= 50µm. (B) The density (cells/µm^2) of CD4SP cells in medullary versus cortical regions was quantified from images as in (A), and enrichment of CD4SP cells in the medulla was quantified as the ratio of medullary/cortical cell densities. Lines connect the paired analysis of *Ebi2*$^{+/+}$ and *Ebi2*$^{-/-}$ CD4SP medullary enrichment on a single slice. Data are compiled from 3 independent experiments, with 5-9 slices analyzed per experiment. (Paired T-test) (C) Velocity and (D) straightness of *Ebi2*$^{+/+}$ and *Ebi2*$^{-/-}$ CD4SP cells migrating on pCX-EGFP thymic slices were quantified after tracking cells from imaging data as in (A). Each dot represents the average velocity (C) or straightness (D) of 150-450 CD4SP cells imaged on a single thymic slice. Means±SD are depicted

3.5 DISCUSSION

To ensure complete central tolerance, positively selected thymocytes must efficiently enter the medulla and migrate rapidly to encounter numerous, but sparse self-peptide:MHC complexes displayed by mTECs and DCs. Here, we have identified a role for EBI2 in promoting central tolerance. We demonstrate that EBI2 deficiency results in impaired negative selection in response to a weakly negatively selecting ligand, and modulates the outcome of encounter with high affinity self-antigens in favor of Treg generation over negative selection. Although thymocyte cellularity and subset distribution are normal in *Ebi2*$^{-/-}$ mice, the TCR repertoire is altered, consistent with a role for EBI2 in thymocyte selection. Two-photon imaging revealed a mechanism by which EBI2 could affect negative selection: EBI2 promotes rapid motility and medullary accumulation of CD4SP cells, likely increasing the number of APCs encountered during medullary residence.

In order to promote medullary accumulation, the EBI2 ligand 7α,25-OHC should be produced in the medulla. The synthesis of 7α,25-OHC requires the enzymes CH25H and CYP7B1 (139, 141). We find that CH25H is expressed preferentially by mTEC^{lo} cells, and our expression profiling data indicate that CYP7B1 is also expressed by TECs (not shown)(137). Furthermore, a previous study detected functional EBI2 ligands in the mouse thymus (156). Taken together, these findings indicate that a gradient of 7α,25-OHC likely emanates from the thymic medulla. Consistent with this possibility, our two-

photon imaging data reveal that EBI2 deficiency impairs the accumulation of CD4SP cells within the thymic medulla.

Upon entering the medulla, thymocytes promote maturation of mTEC cells via signaling through TNFR superfamily members, such as RANKL and CD40L (39, 40, 42, 100). Thus, the medullary compartment is small and disorganized in *Ccr7*$^{-/-}$ mice, likely due to the impaired capacity of CD4SP cells to interact with mTECs (73, 74, 134). We examined whether medullary accumulation of *Ebi2*$^{-/-}$ CD4SP could also impair mTEC differentiation. We did not find any defects in cortical/medullary organization in *Ebi2*$^{-/-}$ thymi, nor in upregulation of Aire in mTECs (data not shown). Thus, although EBI2 contributes to medullary accumulation of CD4SP cells, it is dispensable for mTEC maturation, likely due to partial redundancies with other chemokine receptors. The increase in expression of EBI2 with CD4SP maturation suggests EBI2 would not affect entry of early post-positive selection CD4SP cells. These cells should undergo normal medullary accumulation due to signals from the chemokine receptor CCR4 (10), and could thus promote normal mTEC maturation.

The chemokine receptors XCR1 and CCR2 have been implicated in DC localization in the thymus (71, 72). Because EBI2 was expressed by thymic DCs and induced their chemotaxis, we suspected EBI2 could promote thymic DC recruitment or medullary localization. However, *Ebi2*$^{-/-}$ DCs localized properly to the medulla, and were present at normal frequencies and numbers. In addition, EBI2-deficient DCs induced normal negative selection and Treg generation when presenting high-affinity negatively selecting peptides. Nonetheless, more subtle effects of EBI2 on thymic DCs could impact negative

selection. For example, mTECs transfer self-antigens to DCs for presentation to thymocytes (67). If EBI2 promotes proximity between DCs and mTECs, EBI2 deficiency could impair acquisition of antigens from mTECs, and thus alter the repertoire of peptides presented by thymic DCs

Our results indicate that EBI2 cooperates with CCR4 and CCR7 to promote CD4SP medullary accumulation and central tolerance (10, 73-75, 134). CCR4 is expressed by early post-positive selection DP and CD4SP thymocytes, while CCR7 is expressed by more mature $CD4^+$ $CD69^+$and $CD4^+$ $CD69^-$ cells. Our expression and chemotaxis data suggest that EBI2 has the biggest impact on the more mature $CCR7^+$ CD4SP cells. Like CCR7, EBI2 also promotes rapid motility of CD4SP thymocytes, while CCR4 does not (10, 74). Interestingly, EBI2 deficiency resulted in, a 10% reduction in CD4SP speed. Given that CD4SP cells have a limited medullary residence time on the order of ~5 days (79), this reduction in velocity would diminish the chance that a cell will encounter any given medullary antigen. Because CCR7 and EBI2 have overlapping roles in CD4SP motility and localization, it would be interesting to determine if double deficiency for CCR7 and EBI2 more severely impacts thymocyte differentiation.

Chemokine receptors can contribute to TCR activation, but our data do not support this activity for EBI2. *Ebi2*$^{-/-}$ OT-II thymocytes undergo normal negative selection in the context of the RIP-mOVA transgene. Furthermore a previous study showed that *Ebi2*$^{-/-}$ T cells upregulate activation markers (CD69) comparably after TCR stimulation (146). These findings support our conclusion that EBI2 impacts negative selection and Treg generation by promoting rapid motility and medullary accumulation of

CD4SP cells. However, it is not entirely clear why *Ebi2*$^{-/-}$ CD4SP cells are preferentially diverted to a CD4^{+}CD25^{+} Treg fate, even in the presence of high-affinity self-antigens (both *in vivo* and in thymic slices). CCR7 and CCR4 can directly promote interactions between CD4^{+} T cells or thymocytes and APCs (10, 157). EBI2 could promote interactions with APCs that induce strong TCR signals favoring negative selection over Treg generation. Alternatively, the slower speed of *Ebi2*$^{-/-}$ CD4SP cells could reduce serial engagement with APCs that would elevate TCR signaling beyond the threshold needed to induce negative selection, as opposed to Treg generation. Another possibility is that the slower velocity could result in accumulation of more soluble signals, such as common gamma cytokines like IL-2, within the local microenvironment of an APC that promote Treg generation.

Previous study showed that EBI2 is required to guides activated CD4^{+} T cells towards follicles and the interaction with DCs in the outer T cell zone promotes differentiation of Tfh cells (146). This result could be related to our finding of decreased speed in *Ebi2*$^{-/-}$ thymocytes. It is possible that mislocalization of *Ebi2*$^{-/-}$ CD4^{+} T cells in secondary lymphoid organ is caused by the reduction of migration speed. Also, the fact that EBI2 deficiency causes CD4^{+} T cells mislocalization in secondary lymphoid organs correlates with our finding of less accumulation of *Ebi2*$^{-/-}$ CD4^{+} SP in medulla region in the thymus. Also, this slow migration speed may retain cells in a distinct area which could reduce efficient interaction with other cells.

Single nucleotide polymorphisms near the *Ebi2* locus have been associated with autoimmune disorders, including Type-1 diabetes, a T cell mediated disease (147). Thus,

although we have not observed overt autoimmunity in *Ebi2*$^{-/-}$ mice, EBI2 deficiency could contribute to central tolerance defects with autoimmune consequences in some cases. Interestingly we observed gene dosage effects of *Ebi2* in chemotaxis assays. It is possible that the downstream signaling that are induced by EBI2 is dependent on gene dosage and requires certain amount of signal intensity. This is reminiscent of the gene dosage effect of CCR4 on autoantibody production (10). Thus, it is possible that individuals who are haploinsufficient for chemokine receptors impacting thymocyte medullary entry could be more susceptible to autoimmunity. The effect of EBI2 deficiency on negative selection of OT-II cells in response to a weakly deleting endogenous antigen in C57BL/6J mice was significant, resulting in an almost 1.7-fold increase in CD4SP cells. Importantly, recent studies suggest that self-antigens near the threshold of negative selection for a given TCR are the most likely to result in export of T cells that can induce autoimmunity (158). Thus, subtle defects in negative selection driven by impaired chemokine receptor expression could contribute to autoimmunity. Because EBI2 plays multiple roles in distinct lymphoid subsets during an immune response, resolving the contribution of its impact on central tolerance versus peripheral lymphocyte responses is important. It will be informative to determine whether EBI2 is essential for negative selection of T cells that can otherwise induce autoimmunity. Altogether, our studies demonstrate that EBI2 contributes to the generation of central tolerance by promoting efficient thymocyte migration, medullary entry, and negative selection.

Chapter 4: The role of GPR146 in thymocyte development[5]

4.1 INTRODUCTION

Thymocytes are hematopoietic progenitor cells that develop into T cells, which are vital to defense against foreign antigens. Thymocyte progenitors migrate from bone marrow to the thymus where they develop and are specifically programmed to become mature T cells (6). In order to establish the self-tolerance of maturing T cells, the thymus has a specialized microenvironment in the medulla. Thymocytes normally interact with antigen presenting cells in the medulla to avert auto-reactive thymocytes, but if T cells do not enter the medulla, autoimmune disease will arise. Therefore, it is important to elucidate which molecules induce thymocyte medullary entry, thereby preventing autoimmune disorders.

Previous studies have shown that GPCRs, and particularly chemokine receptors are important for guiding positively selected thymocytes into the medulla, where they encounter the antigen presenting cells that induce central tolerance (159). For example, it is well documented that the chemokine receptor CCR7, which is highly expressed in single positive thymocytes, is critical for the accumulation of SP cells within the medulla and their negative selection. The CCR7 ligands CCL19 and CCL21 are highly expressed by

[5] Authorship contributions: Sanghee Ki performed most of experiments, with advice from Lauren Ehrlich. Sanghee Ki performed southern blot, with help from Qiang Li and advice from Steven Vokes. Zicheng Hu generated qRT-PCR data of GPR146. UT mouse core facility generated chimera mice.

mTECs, resulting in a chemokine gradient, attracting SP cells towards the medulla (159). CCR7-deficient CD4SP have decreased medullary enrichment and deficient negative selection, resulting in autoimmune disease in *Ccr7*$^{-/-}$ mice. However, Pertussis Toxin (PTX), which inhibits GPCR signals, completely abolishes medullary entry of SP thymocytes, while CCR7 only reduces the accumulation of SP cells in the medulla, suggesting that other GPCRs are involved in governing medullary entry and negative selection (74).

GPR146 is a member of the Rhodopsin family of GPCRs. It was identified by using the Hidden Markov Model to search the human genomic data set to find new GPCRs (160). Human GPR146 blast results showed that GPR146 has a 23% homology in amino acid sequence with CCR7, which is essential for thymocyte migration and development. Interestingly, GPR146 shows an expression pattern similar to that of CCR7, based on our microarray expression profiling data (137). GPR146 was regarded as an orphan receptor until 2013 when Yosten *et al* demonstrated that c-peptide, an intermediate product in the transition from proinsulin to insulin, was a ligand for GPR146 (161). They showed that GPR146 co-localized with c-peptide on the membrane of KATOIII cells and was essential for c-Fos expression in response to c-peptide-induced signaling. A previous study showed that human CD4SP cells migrated toward c-peptide *in vitro,* further suggesting that GPR146 could promote chemotaxis of thymocytes (162). However, the role of GPR146 in thymocyte development remains largely unknown.

In this study, we generated *Gpr146*$^{-/-}$ mice using a GPR146 targeting vector from the KOMP repository to explore the role of GPR146 in the thymocyte differentiation and

selection. Initial studies indicate that *Gpr146*$^{-/-}$ mice do not have altered thymocyte cellularity or subset composition, and the organization of cortical and medullary regions are intact. However, in competitive bone marrow chimeras *Gpr146*$^{-/-}$ CD4SP and CD8SP out-competed wild type cells, suggesting GPR146 may impact the survival, proliferation or selection of post positive-selection thymocytes. In this chapter, I describe the generation and initial characterization of *Gpr146*$^{-/-}$ mice.

4.2 Experimental Procedures

Mice

C57BL/6J (CD45.2), B6.SJL-Ptprca Pepcb (CD45.1) mice were purchased from The Jackson Laboratory. CD45.1/CD45.2 were bred in-house. GPR146 chimeric mice were generated by electroporation of V6.5, 129;C57BL hybrid ES cells with a GPR146-targeting allele. The ES cells used for injection were. Five generation of backcrossing resulted in a 98.375% C57BL/6j background.

Vector preparation and ES cell transfections

A GPR146 targeting vector (GPR146-tm1aKOMP Mbp) was purchased from the KOMP repository. The vector was in DH10 E.coli and amplified by culturing in Lysogeny broth (LB) media. Maxiprep (Qiagen) was performed following the manufacturers protocol. 50ug of targeting vector was linearized by digesting with AsisI enzyme (NEB).

The digest was confirmed by gel analysis. Linearized vector was inserted into ES cells by electroporation which is performed by the UT mice core facility.

Southern blot for screening

After electroporation, we obtained duplicate plates from the mice core facility. Approximately 300 ES cells transfected with the targeting vector in a 96-well plate were lysed with lysis buffer [10nM Tris-HCL pH8.0, 10nM EDTA pH8.0, 10nM NaCl, 1mg/ml proteinase K (freshly added)]. The plate was incubated overnight at 65°C followed by an incubation with DNA precipitation solution [100% EtOH, 75mM NaCl] for 30min at room tempterature (RT). The precipitate was recovered by careful removal of the supernatant and air-drying. The dried precipitate was digested with 10-15U of DraI (5' probe and Neo probe) and AvrII (3' probe) enzyme at 37°C overnight in what volume of 25μl. Digested DNA was loaded on gels followed by transfer to a membrane (Biodyne or Hybond N+) overnight. DNA on the membrane was detected using 32P labeled probes. Primers that were used for making the probes are listed are below:

5'probe forward primer: 5'- GGACAGCGTCCACTGCTTAC-3'

5'probe reverse primer: 5'- TCGGGCAAGAACAGAACGACAC-3'

3'probe forward primer: 5'-GTTAGAAGACTTCCTCTGCCCTCAGTTGGCTAGGG-ACAGGACC-3'

3'probe reverse primer: 5'- AAGCAGGGAGTGGTGGTCAG-3'

Generation of BM chimeras

Gpr146$^{+/+}$ (CD45.1) and*Gpr146*$^{-/-}$ (CD45.2) bone marrow cells were obtained from two long bones. Thymocytes were incubated with CD3, CD4, CD8, Mac1, Gr1, Ter-119, NK1.1, and B220 antibodies for 30min at 4°C to deplete mature hematopoietic lineages. After washing with FACS wash buffer (FW; PBS+ 2% bovine calf serum [BCS]; GemCell), anti-Rat IgG Magnetic Beads (Invitrogen) were incubated with the cells (beads and cell ratio = 1:4) for 10 minutes at RT and then washed 2 times in FW. Cells were then magnetically depleted, and the flow-through lineage depleted cells were collected. *Gpr146*$^{+/+}$ and *Gpr146*$^{-/-}$ BM donor cells were mixed at 1:1 ratio and injected intraorbitally into recipient CD 45.1/45.2 congenic mice. Six weeks after injection, thymi were analyzed by LSR Fortessa flow cytometer (BD)

qRT-PCR

Thymi from *Gpr146*$^{+/+}$ or *Gpr146*$^{-/-}$ mice were stained with antibodies against CD8, CD69, Lin (B220, Gr-1, Ter119, NK1.1, Mac1, CD11c, γδTCR), CD3, and CD4 to distinguish thymocyte subsets. Immunostained cells were sorted on a FACSAria II (BD) and $5x10^4$ ~ $1x10^5$ cells were subjected directly to Trizol to extract RNA. cDNA was synthesized using SuperScript® III First-Strand Synthesis SuperMix (Life Technologies). qRT-PCR using SyBr (Applied Biosystems) was carried out with the following primers:

-GPR146 forward primer for qRT PCR : 5'-GGGGTCCCTGTGAGCTTAG-3'

-GPR146 Reverse primer for qRT PCR : 5'- CCATGTTCACGAAGTACACGTC-3'

Antibodies

All antibodies were obtained from eBioscience or Biolegend unless otherwise indicated: anti-CD8 (53-6.7), -CD69 (H1.2F3), -CD3 (145-2C11), -CD4(RM4-5), -CD25 (PC61.5), -CD45.1 (A20), -CD45.2 (104), -CD11c (N418), -Ter119 (TER-119), -B220 (RA3-6B2), -Gr-1 (RB6-8C5), -CD11c (M1/70), -NK1.1 (PK136), -cKit (2B8), -CD31 (390), -Sirpα (P84), -I-A/I-E (M5/114.15.2), -CD80 (16-10A1), -CD45 (30-F11;BD), -Ly51 (6C3), -EpCAM (G8.8). Anti-Streptavidin Qdot®-605 (Life Technologies) was used as a secondary reagent to detect biotinylated primary antibodies.

Antibodies used for immunofluorescent stains are listed below: anti-Pancytokeratin-FITC (C-11; Sigma-Aldrich), -keratin5 (rabbit polyclonal antibody; Covance), Donkey anti-rabbit IgG DyLight 594 (Jackson ImmunoResearch Laboratory).

Immunofluorescence staining

Thymi from one month old *Gpr146*$^{+/+}$ and *Gpr146*$^{-/-}$ mice were harvested and snap frozen in OCT (manufacturer). 6-9 μm sections were obtained using a Microm HM550 Cryostat (ThermoFisher) and stored at -80°C. Cryosections were fixed in 100% acetone at -20°C for 15min and washed 2X in PBS + 0.1% Tween 20. Immunostaining was carried out for 1hr at 4°C with indicated primary antibodies against the following: Keratin5 (rabbit polyclonal), PanCK (C11)-FITC. Images of stained sections were observed using an Eclipse 80i microscope using 10X objective (Nikon).

4.3 RESULTS

4.3.1 Generation and confirmation of GPR146 deficient mice

By analyzing our expression profiling dataset (137), we identified Gpr146 as a GPCR protein that could be involved in medullary accumulation of post positive selected thymoctyes. *Gpr146* transcripts are expressed in post-positive selection DP cells and levels are sustained in CD4SP and CD8SP. Given that GPR146 has been implicated in chemotaxis of human CD4SP (162), we hypothesized that GPR146 is involved in the migration of SP cells into the medulla, and would thus affect central tolerance. We performed qRT-PCR to confirm the expression pattern of *Gpr146*, and found that it is first expressed in positively selected DP cells and further upregulated in both CD4SP and CD8SP thymocytes. Additionally, we found that the DN1 population (c-Kit^{+}, CD44^{+}, CD25^{-}) expresses detectable levels of GRP146 (Figure 4.1), indicating that it may also regulate early progenitors.

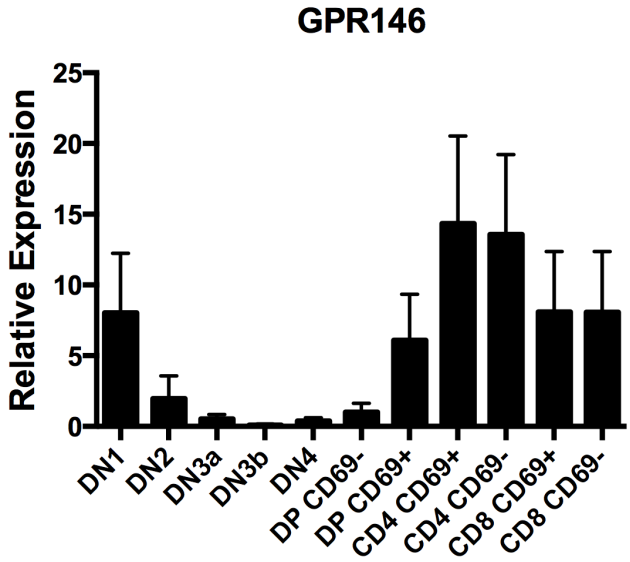

Figure 4.1 Expression of *Gpr146* transcripts in thymocyte subsets

Gpr146 transcript levels were quantified by qRT-PCR on cDNA from FACS purified thymocyte subsets from C57BL/6J mice. *Gpr146* is up-regulated in positively selected DP (DP CD69+) and expression remains in both CD4 and CD8 SP cells. Relative expression is calculated by normalizing to DN3b subsets. Representative of 2 independent experiments. Means±SEM.

To test the role of GPR146 in T cell development and selection, we generated GPR146 deficient mice. A GRP146 "knock-out first" targeting vector was obtained from the UCDAVIS KOMP repository (Knockout mouse project). GPR146 has 2 exons, one in a non-coding and a second (Exon2) encoding GPR146. In the targeting vector, Exon 2 is flanked by loxP sites, and is preceded by a FRT-LacZ-neomycin-FRT fragment. Because of the polyadenylation signal after LacZ, mice homozygous for the "knockout first" allele express lacZ instead of GPR146, allowing us to generate a constitutive GPR146 knockout. (Figure 4.2) (163).

In order to generate thymus-specific GPR146-deficient mice, we can cross GPR146 knockout mice with ROSA26Flpo mice. ROSA26Flpo mice express the Flpo gene in the broadly expressed ROSA26 locus and show efficient deletion of sequences flanked by FRT sites (164). This will eliminate lacZ and neo genes, leaving only exon2 flanked by loxP sites. This GPR146^{fl} allele will enable us to delete exon2, which contains the entire coding sequence of GPR146, in a tissue specific manner. Then GPR146$^{fl/fl}$ mice can be bred with Lck-cre mice, which express the recombinase Cre under control of the T cell specific Lck promoter, inducing deletion at DN stage of T development (165).

The vector was introduced into V6.5, 129:C57BL/6J hybrid ES cells by electroporation. ES cell colonies were screened by Southern blot for proper homologous recombination with the vector sequence, and a number of colonies containing a correctly targeted allele were identified. These were confirmed by probing with 5', 3', and Neomycin gene (Neo) probes (Figure 4.3).

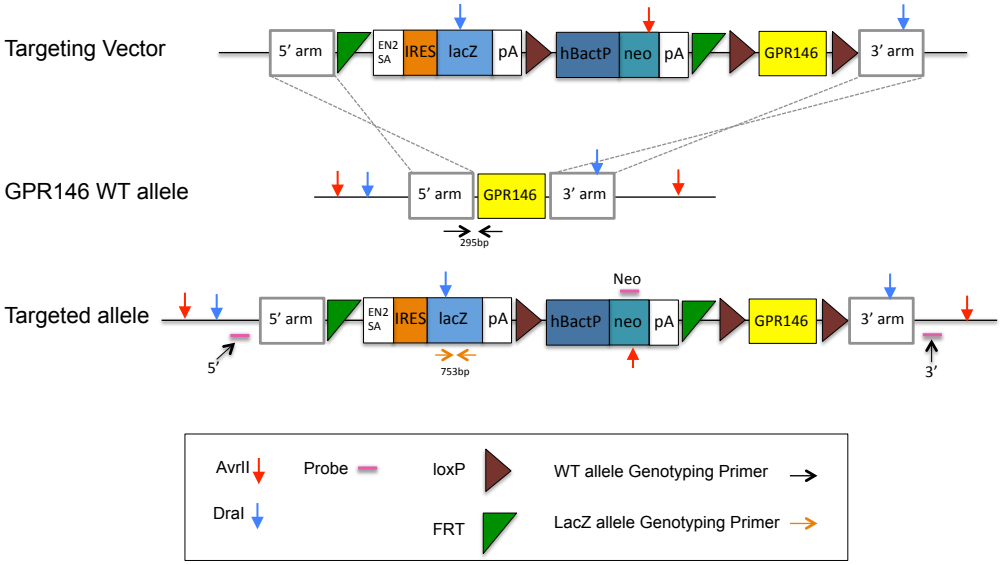

Figure 4.2 GRP146 targeting strategy

In the targeting vector, Exon 2 is flanked by loxP sites and the inserted lacZ and Neo genes are flanked by FRT sites. Enzyme sites used for southern blots are indicated by red and blue arrows. Neo, 5' and 3'arm probes for southern blots are indicated by the pink bars.

Three of the ES cell colonies were injected into C57BL/6J blastocysts, and implanted in pseudo-pregnant females. Fifteen chimeras out of a possible 29 were obtained and five of these (one from E5, two each from E8 and D10) were bred with B6 female mice. The germ line transmission efficiency in male pups from chimera breeding was almost 100%. We are now maintaining two founders (E8 and D10), backcrossing them

onto a C57BL/6J background for five generations to obtain a 98.365% C57BL/6J congenic strain.

By taking advantage of the GPR 146 "knockout first" allele, we could determine the protein level of LacZ in the GPR146 locus as an indication of which thymocyte subsets would express GPR146 protein. Figure 4.3B shows the MFI of lacZ in *Gpr146*$^{+/+}$ and *Gpr146*$^{+/-}$ mice. Consistent with our qRT-PCR data, we observed that GPR146 is highly expressed in CD4SP and CD8SP. However, DP CD69^{+} expression was lower than expected, which can be explained by the time delay between RNA transcript and protein generation. In our final strain of backcrossed mice which is either from E8 or D10, we also confirmed that mRNA expression of *Gpr146* was eliminated in thymocytes by qRT-PCR. Sorted thymocytes from *Gpr146*$^{+/+}$ mice showed high expression of GPR146 in CD4 and CD8SP cells, and we confirmed GPR146 was abolished in our knockout mice. (Figure 4.3C).

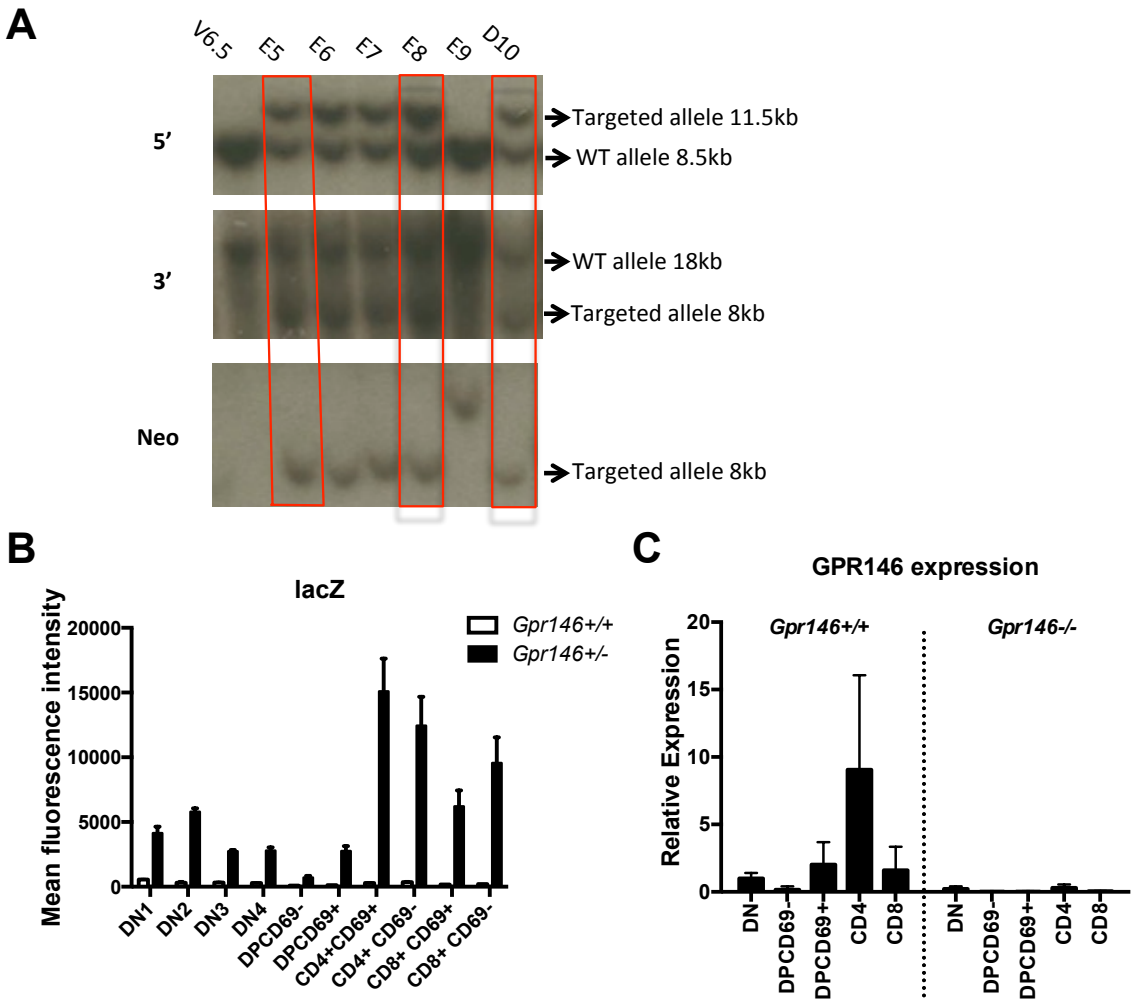

Figure 4.3 Confirmation of GPR146$^{-/-}$ ES cells and resultant mice

(A) Southern blot for screening GPR146 targeted ES cell lines. We confirmed proper insertion of the targeting vector using 5', 3', and neomycin probes. V6.5 are negative control ES cells, and E5, E6, E7, E8, and D10 were targeted ES cell lines, and E9 was a negative result. E8 and D10 which were used to generate GPR146$^{-/-}$ chimera mice are indicated by red rectangles. (B) Mean Fluorescence Intensity of lacZ in *Gpr146*$^{+/+}$ and *Gpr146*$^{+/-}$ thymocyte subsets. (n=3) (C) qRT-PCR of sorted thymocyte subsets from *Gpr146*$^{+/+}$ and *Gpr146*$^{+/-}$ mice. Data are representative of two independent experiments.

4.3.2 *Gpr146*$^{-/-}$ mice do not show gross defects in thymocyte cellularity or subset composition

To determine if deletion of GPR146 impacts thymocyte development, we compared the cellularity and composition of thymocyte subsets in *Gpr146*$^{+/+}$ and *Gpr146*$^{-/-}$ mice by flow cytometry. The cellularity of thymus, spleen, and lymph nodes were comparable between *Gpr146*$^{+/+}$ and *Gpr146*$^{-/-}$ mice (Figure 4.4). There was also no differential subset distribution between *Gpr146*$^{+/+}$ and *Gpr146*$^{-/-}$ thymocytes.

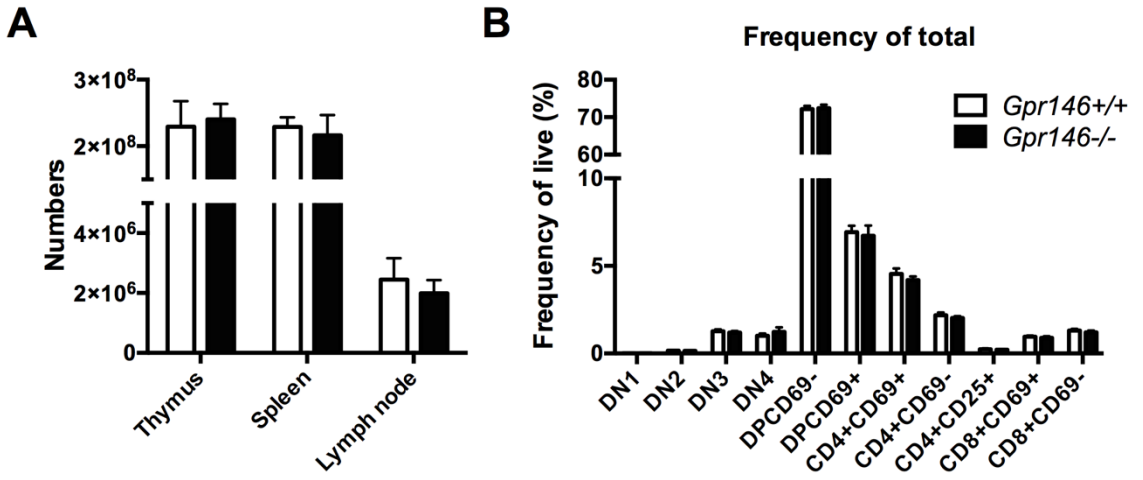

Figure 4.4 Comparison of cellularity and thymocyte composition between *Gpr146*$^{+/+}$ and *Gpr146*$^{-/-}$ mice

(A) Comparison of the cellularity of thymus, spleen, and lymph nodes from *Gpr146*$^{+/+}$ and *Gpr146*$^{-/-}$ mice 4 to 6 weeks of age. Means±SEM (n=6) (B) Comparison of thymocyte subset composition from mice of the indicated genotypes. Means±SEM (n=6)

Previous studies indicated that the signal from positively selected thymocytes is essential for establishing proper medulla development (39) Additionally, CCR7 deficient mice accumulated fewer single positive thymocytes in medullary regions and developed small and disorganized medullas (166). Therefore, we investigated whether *Gpr146*$^{-/-}$ mice had disorganized medullary architecture. Initial analyses of immunofluorescence images of thymic cryosections immunostained to reveal cTEC (PanCytokeratin) and mTEC (Keratin5) markers suggest that *Gpr146*$^{-/-}$ thymi might have larger medullary regions than *Gpr146*$^{+/+}$mice. However, a greater number of wild type images will be needed to determine if this apparent difference is significant (Figure 4.5A). Quantification of cortical and medullary regions by K-mean clustering did not reveal significant differences between *Gpr146*$^{+/+}$ and *Gpr146*$^{-/-}$ with this limited dataset (Figure 4.5B).

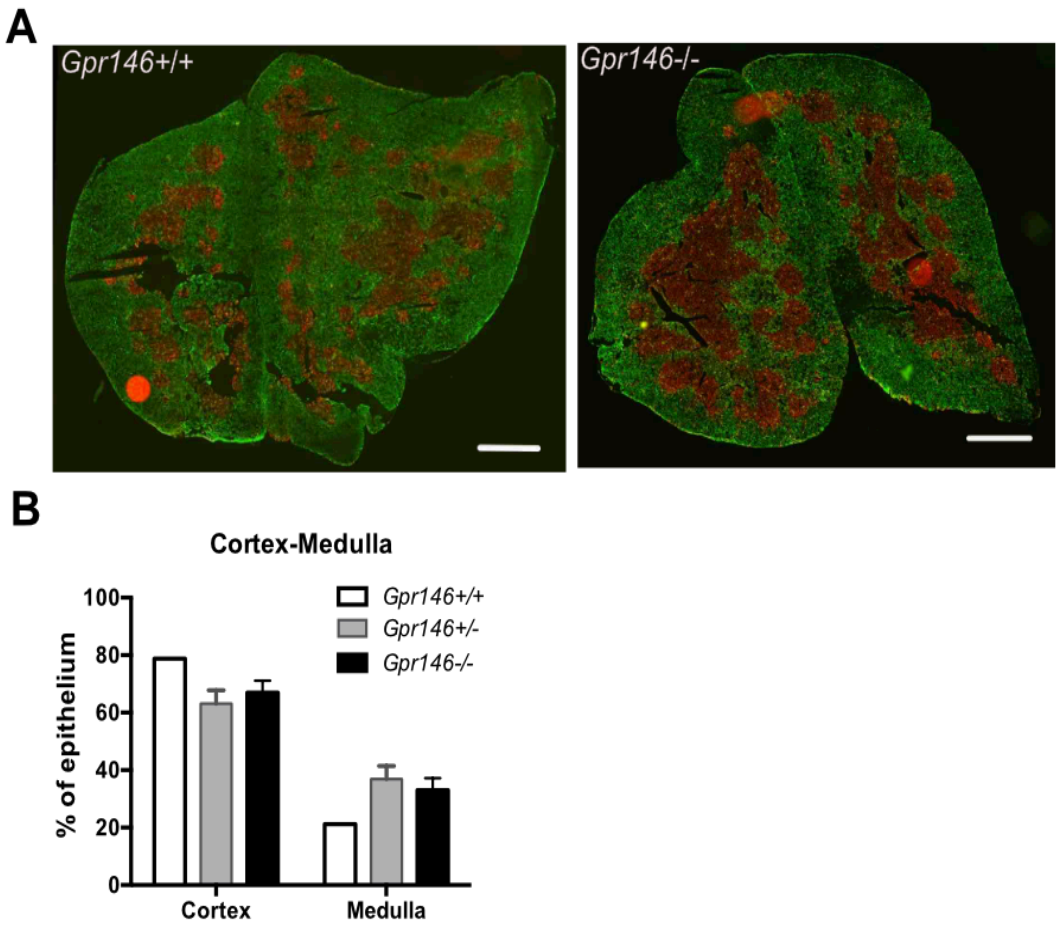

Figure 4.5 *Gpr146*$^{-/-}$ thymus do not show a subtle defect in cortical/medullary organization.

(A) Representative image of immunostained thymic cryosections from *Gpr146*$^{+/+}$ and *Gpr146*$^{-/-}$ mice (one month old). PanCytokeratin (green) reveals cortical regions while K5 (red) demarcates the medulla. Scale bar=1000μM (B) Quantification of medulla and cortex regions by K-mean clustering from images as in A. Means$\pm$SEM (*Gpr146*$^{+/+}$ n=1, *Gpr146*$^{+/-}$ n=2, *Gpr146*$^{-/-}$ n=4) NS.

4.3.3 Competitive bone marrow chimeras reveal a role for GPR146 in thymocyte differentiation

To determine whether the contribution of GPR146 to thymocyte development would be more pronounced in a competitive situation, we analyzed thymocyte development in mixed bone marrow (BM) chimeras, in which GPR146 deficient thymocytes competed with wild type cells in a wild-type thymic environment. BM cells were harvested from congenically marked *Gpr146*$^{+/+}$ (CD45.1) and *Gpr146*$^{-/-}$ (CD45.2) mice, depleted of mature lineages, and mixed at 1:1 ratio. This donor mixture was injected into congenically marked (CD45.1/CD45.2), lethally irradiated recipient mice, and thymic chimerism was analyzed six weeks after transplantation. Interestingly, we found that the *Gpr146*$^{-/-}$ (CD45.2) thymocytes contributed preferentially to the CD4 and CD8 SP compartments, in which GPR146 is normally highly expressed (Figure 4.6A). These results suggest many possible roles of GPR146. Deficiency of GPR146 may cause less effective negative selection, which would increase the number of CD4SP and CD8SP thymocytes. Also, deficiency of GPR146 may induce increased proliferation, decreased apoptosis, and increased retention of CD8SP and CD4SP thymocytes in the thymus. The increase in the contribution of *Gpr146*$^{-/-}$ cells was not observed in the spleen (Figure 4.6B).

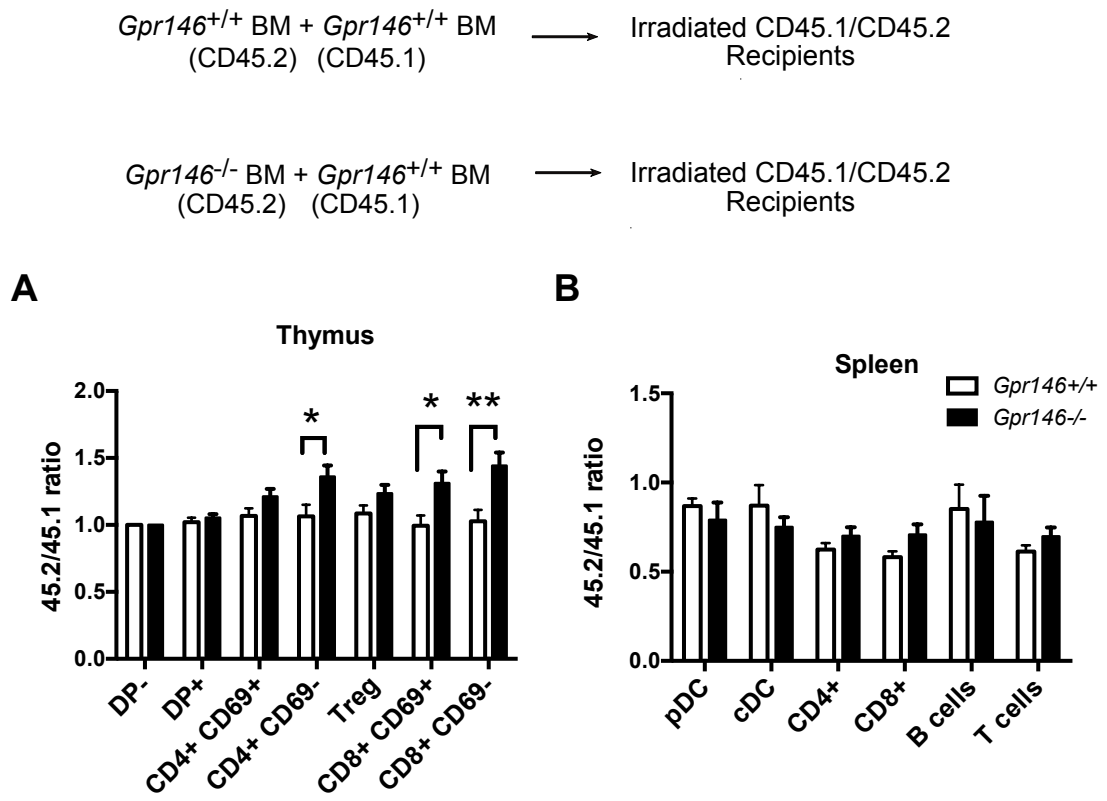

Figure 4.6 BM chimeras reveal an elevated contribution of *Gpr146*$^{-/-}$ in CD4SP and CD8SP

(A) Graph showing ratio of CD45.2(*Gpr146*$^{-/-}$) to CD45.1(*Gpr146*$^{+/+}$) in chimeric thymus. Means±SEM (*Gpr146*$^{+/+}$ n=8, *GPR146*$^{-/-}$ n=9). *, p-value <0.05, **, p-value <0.01 (B) Graph showing ratio of CD45.2(*Gpr146*$^{-/-}$) to CD45.1(*Gpr146*$^{+/+}$) in chimeric spleen. Means±SEM (*Gpr146*$^{+/+}$ n=5, *GPR146*$^{-/-}$ n=6).NS.

4.4 DISCUSSION

In this study, *Gpr146*$^{-/-}$ mice were generated to investigate the role of GPR146 in thymocyte development. Based on expression profiling data, we found that the expression pattern of GPR146 was similar to that of CCR7 in that they are both upregulated in maturing SP thymocytes. Together with previous studies indicating that GPR146 is a chemokine receptor and the homology between CCR7 and GPR146, this expression pattern suggests GPR146 could contribute to SP thymocyte medullary entry and negative selection. Although *Gpr146*$^{-/-}$ mice showed no gross defects in thymocyte cellularity and subset composition, *Gpr146*$^{-/-}$ thymocytes contributed preferentially to CD4SP and CD8SP compartments when competing against wild-type thymocytes. These findings indicate that GPR146 impacts SP thymocyte differentiation, potentially affecting negative selection and migration of SP cells.

Deficiency of a chemokine receptor in thymocytes could affect thymocyte development in many ways. First, it has been shown that the crosstalk between thymic epithelial cells and developing thymocytes is critical for maturation and maintenance of both compartments. Therefore, disrupting GPR146 may interfere with development of the thymic stroma. For example, mice deficient for *Ccr7* have altered thymic architecture, with small medullary regions dispersed throughout thymus and extending to the subcapsule (167). This could be due to a decreased ability of *Ccr7*$^{-/-}$ T cells to localize to the medulla and provide the RANKL signals responsible for regulating proliferation and maturation of mTECs (136). Secondly, GPCR deficiency could impair thymocyte development in a cell-intrinsic manner by altering TCR signaling (136, 168), migration (74, 134), localization

(167), and interaction with APCs (10). Thus, GPCRs, and chemokine receptors in particular, can contribute to maintenance of proper thymic structure as well as thymocyte development. Based on our analysis of *Gpr146*$^{-/-}$ thymocytes, we conclude that deficiency of GPR146 does not induce changes in total thymocyte cellularity and subset composition. However, it appears that deficiency of GPR146 increases thymocyte compartments in our BM chimera experiment. (Figure 4.6) Future studies will further elucidate how GPR146 affects thymocyte development.

Given that GPR146 is highly expressed in positively-selected SP cells which accumulate in the medulla and are subject to negative selection, GPR146 may contribute to these processes. SP cells in the thymus move faster and with straighter trajectories than DN or DP cells. Moreover, movement of SP cells in the medulla is slightly faster than migration in the cortex, consistent with their need to scan rare TRAs presented on mTECs in the medulla (74). CCR7 deficiency abrogates chemotaxis of CD4 SP cells towards the medulla and reduces their velocity relative to WT cells. However, CCR7 deficiency does not prevent medullary entry of SP cells, though *Ccr7*$^{-/-}$ CD4 SP cells accumulate less efficiently in the medulla. This indicates that CCR7 contributes to CD4 SP chemokinesis, chemotaxis towards the medulla, and accumulation within the medulla, but CCR7 is not required for medullary entry (74). Furthermore, a previous study showed that *Ccr7*$^{-/-}$ thymocytes had an impaired cell-intrinsic response for TCR-mediated signaling required for negative selection (136). Thus, it is possible that other GPCRs such as GPR146 could also directly contribute to TCR-mediated signaling, migration, medullary entry, and negative selection processes.

C-peptide is an intermediate product generated during the cleavage of pro-insulin to form the mature form of insulin (169). C-peptide is present in the blood stream of type2 diabetes patients. Previous studies have shown that C-peptide has the chemotactic capacity to recruit human CD4SP *in vitro*, which in turn is involved in pertussis toxin sensitive G protein signaling. Additionally, in Type 2 diabetic patients, it has been shown that c-peptide and $CD4^+$ T cells colocalize in early arteriosclerotic lesions (162). However, a receptor that is involved in c-peptide signaling was not identified until Yosten et al showed that c-peptide is the ligand for GPR146 (161). $mTEC^{hi}$ expresses insulin as TSA. Therefore, it is possible that c-peptide generated by insulin expressing mTEC cells could induce chemotaxis of CD4SP and CD8SP towards the thymic medulla. Future studies using two-photon microscopy to analyze migration of *Gpr146*$^{-/-}$ thymocytes will address this possibility.

It has been shown that if insulin is deficient in a thymic specific manner, mice develop autoimmune diabetes (170), and the working model is that this is due solely to impaired negative selection against insulin itself. This paper reveals that thymic specific deletion of insulin is sufficient to induce insulin specific autoimmune disease. There is also a possibility that chemotaxis of CD4SP induced by c-peptide is impaired in this model. Determining whether *Gpr146*$^{-/-}$ mice are subject to autoimmune disease will be critical in determining the role of GPR146 in thymocyte differentiation and selection.

Chapter 5: Summary and Future Directions

In this dissertation, I addressed three different aspects of thymocyte development. In Chapter 2, I identified molecular signatures in TECs and DCs in early thymic involution. In Chapter 3, I identified a role for EBI2 in promoting rapid motility of SP cells and efficient negative selection. In Chapter 4, I described the generation and initial characterization of thymocyte development in *Gpr146*$^{-/-}$ mice.

Understanding the gene expression changes of thymic stromal cells during aging

In Chapter 2, we analyzed global transcription profiles of purified thymic stromal cells to reveal the molecular players contributing to thymic atrophy associated with aging. By analyzing changes in gene expression levels, we found a prominent decrease in E2F3 target gene levels and expression of cell-cycle related genes in mTEC^{lo} and cTEC populations. E2F3 is a master transcription factor that controls cell cycle progression. Interestingly, E2F3 mRNA levels were unchanged, suggesting that other factors involved in regulating E2F3 activity were involved. Previous studies demonstrated that RB family mutant TECs showed an E2F3 mediated increase of Foxn1 expression, which prevents thymic involution (94). Therefore, further studies of molecular mechanisms underlying Rb family genes and E2F3 are needed.

While our studies suggest a key role for diminished E2F3 activity in thymic atrophy, the mechanism by which these transcriptional targets impact TEC function is

currently not known. A decrease in E2F3 target genes may directly lead to thymic atrophy through reduction of the turn-over rate of all TEC subsets. Alternatively, a rare TEC subset with stem cell or transit amplifying properties could be particularly affected by the loss of E2F3 Interestingly, a recent study showed that bipotent adult thymic epithelial cells that retain stem/progenitor activities reside within mTEC^{lo} integrin-α6^{hi} Sca-1^{hi} subsets (171). Further studies are needed to reveal molecular and cellular mechanisms by which E2F3 activity impacts TEC cellularity during age associated thymic involution.

Moreover, we found that DC and DCS showed pro-inflammatory signals in aged mice, which also may contribute to thymic involution. We found that Il1a and Il1b were upregulated in DC and DCS at 6months. Interestingly, Il-1 activating receptors are present on cTEC and fibroblasts. Additional studies on Nlrp3-deficient mice, which are deficient for active IL-1, showed that cTEC compartments were preferentially sustained compared to other stromal subsets (131). Given that the administration of IL-1 induces thymic atrophy (97), this suggests that IL-1 plays a role in contributing to thymic involution.

Given that expression of the E2F3 transcription factor does not change with age, it will be intriguing to see if there are any other modulators that control E2F3 activity in mTEC^{lo} and cTEC. Also, it has been shown that E2F3 controls Foxn1, which is important for thymic epithelial cell development. Rb mutant mice have high activity of E2F3 and high expression of Foxn1, which results in sustained thymic growth and the prevention of involution with age (94). Another study showed that FOXN1 can also promote expression of cell cycle genes such as Ccnd1(88). Therefore, it will be important to investigate whether an increase in cell cycle activity alone downstream of E2F3 and FOXN1 activity prevents

the age-associated decline in TEC function, or whether other cell cycle pathways, along with E2F3 and FOXN1, prevent involution. These studies would reveal candidate pathways that could be targeted to restore or retain thymic function, and thus a diverse and self-tolerant T cell repertoire to promote functional immunity throughout the lifespan.

Elucidating the role of chemokine receptors in thymocyte interactions with stromal cells

In Chapter 3, we investigated the role of EBI2 in thymocyte development and selection. EBI2 has been shown to promote chemotaxis of multiple lymphocyte subsets, including B cells, DCs, and naïve T cells, and the endogenous EBI2 ligand, 7α25-OHC, has been identified (139, 141). We found that *Ebi2* is upregulated in post-positive thymocytes, and the enzyme CH25H, which is required to generate 7α25-OHC is expressed by $mTEC^{lo}$ cells. This suggests that EBI2 could promote migration of SP thymocytes toward medulla; however, further two-photon microscopy studies in which chemotaxis of SP cells is evaluated will be required to fully address this possibility. Consistent with a possible role for EBI2 in promoting chemotaxis of SP cells towards the medulla, we did identify a slight defect in medullary accumulation in EBI2-deficient SP cells. Strikingly, $Ebi2^{-/-}$ CD4SP migrated more slowly than wildtype thymocytes. In keeping with the idea that rapid SP motility would be important to scan APCs presenting self-peptides to induce negative selection, we found that $Ebi2^{-/-}$ OTII cell were impaired in their ability to undergo negative selection to an endogenous C57BL/6J self-antigen. Also,

Ebi2$^{-/-}$ OT-II cells preferentially diverted towards a regulatory T cell fate in the presence of the high-affinity OVA antigen. These studies demonstrate a previously unanticipated role for EBI2 in promoting thymocyte negative selection.

Our studies revealed that EBI2 did not affect negative selection in response to an abundant exogenous antigen or an endogenous high affinity antigen, but rather affected negative selection in response to weakly deleting endogenous antigens. We speculate that thymocytes have a greater chance of encountering sufficient self-peptide:MHC complexes to trigger negative selection if there are abundant self-antigens, as would be the case when OVAp was added to thymic slices, leading to imperceptible differences in negative selection in the absence of EBI2 in this system. However, in the case of rare or much lower affinity endogenous self-antigens, the 10% reduction in the migration speed of SP thymocytes caused by EBI2 deficiency could significantly reduce the likelihood of encountering enough self-peptide:MHC complexes to push the thymocyte over the threshold of TCR signaling required for negative selection. Furthermore, our data showed that in the presence of abundant high affinity antigens, cell fate decision to undergo negative selection versus Treg generation is modified by EBI2. Previous studies showed that CCR4, another chemokine receptor, promoted interactions between DCs and CCR4-expressing thymocytes (10). We speculate that EBI2 could directly contribute to interactions between CD4SP cells and mTEC^{lo} cells, which might contribute to mTEC differentiation, thus impacting thymocyte development. However, our current studies did not reveal a defect in mTEC differentiation. It is also possible that interactions between SP thymocytes and mTEC^{lo} cells have an unanticipated role in promoting negative selection.

It will be interesting to see if EBI2 has a direct effect on the interaction between thymocytes and mTECs.

Also, because EBI2 is not the only receptor contributing toward accumulation of CD4SP in the medulla, it will be important to distinguish the contribution of other chemokine receptors. For instance, CCR7 and CCR4 have prominent roles in thymocyte migration into the medulla and may mask effects of EBI2 deficiency. EBI2 has been shown to have large role in B cell and DC migration in secondary lymphoid organs (138, 142, 154, 172). EBI2 is also related to autoimmune disease such as type I diabetes and Multiple sclerosis (MS) (147, 173). Although we could not find evidence showing apparent autoimmunity in *Ebi2*$^{-/-}$ mice, autoimmune disease can be induced by EBI2 in various ways. It will be important to study whether EBI2 promotes autoimmunity at least in part through its effects on central tolerance in the thymus.

In Chapter 4, we identified GPR146 as a candidate GPCR that could contribute to thymocyte medullary entry and/or negative selection and generated GPR146 knockout first mice to evaluate the contribution of GPR146 to thymocyte development and selection. Not only is GPR146 up-regulated just after thymocytes enter the medulla, which is consistent with a role in medullary entry, but GPR146 also has homology with CCR7, a known chemokine receptor that drives medullary entry (174). Based on these findings, we hypothesized that GPR146 may contribute to thymocyte medullary entry and central tolerance. We generated GPR146 deficient mice and found that a higher proportion of $CD4^+CD69^-$, $CD8^+CD69^+$, and $CD8^+CD69^-$ thymocytes were derived from *Gpr146*$^{-/-}$ progenitors in thymi of mixed bone marrow chimeras. This indicates that

GPR146 may play a role in negative selection of CD4SP and CD8SP thymocytes. However, further studies are required to determine if GPR146 is required for efficient negative selection and if GPR146 is required for TCR signaling, migration, or interacton with APC. In the future, we will generate additional bone marrow chimeras to address the role of GPR146 in negative selection. We will generate *Gpr146*$^{-/-}$ OT-I and OT-II TCR transgenic mice. Given that OT-I and OT-II transgenic mice have a monoclonal TCR on all thymocytes and T cells with specificity for peptides of Ovalbumin displayed on MHC-I and MHCI-II molecules, respectively, we will examine the impact of GPR146 deficiency on negative selection in chimeras where OVA is expressed as a model TRA in mTEC^{hi} cells. Because CCR7 can induce medulla accumulation and negative selection, and because it would be expressed normally on GPR146 deficient T cells, we may not observe defects in negative selection. In this case, we would breed *Gpr146*$^{-/-}$; *Ccr7*$^{-/-}$mice and examine the impact on the polyclonal repertoire. Furthermore, by breeding the mice doubly deficient for the chemokine receptors to OT-I or OT-II mice, we could determine if the double knockout is more severely impaired in its capacity to undergo negative selection than either single knockout mouse.

C-peptide, which is generated during the conversion of pro-insulin to Insulin, is a candidate ligand for GPR146. It will be important to determine if GPR146^{+} thymocytes respond to c-peptide via chemotaxis or other cell signaling pathways. Insulin is expressed at low levels by mTEC^{hi} cells (52), which raises the question of whether c-peptide is abundant in the thymus and available to promote SP chemotaxis.

In the future, two-photon imaging experiments will test whether GPR146 is involved in medullary entry, the accumulation of SP cells, and other aspects of T cell motility that could impact the efficiency of negative selection. Furthermore, it will be important to evaluate the possibility that GPR146 activation could directly contribute to TCR-mediated signal transduction. Future studies are needed to elucidate the role of GPR146 in thymocyte development and selection and to uncover the mechanisms by which it affects these processes.

References

1. Ladi E, Yin X, Chtanova T, Robey EA (2006) Thymic microenvironments for T cell differentiation and selection. *Nat Immunol* 7(4):338–343.

2. Lind EF, Prockop SE, Porritt HE, Petrie HT (2001) Mapping precursor movement through the postnatal thymus reveals specific microenvironments supporting defined stages of early lymphoid development. *J Exp Med* 194(2):127–134.

3. Jenkinson EJ, Jenkinson WE, Rossi SW, Anderson G (2006) The thymus and T-cell commitment: the right niche for Notch? *Nat Rev Immunol* 6(7):551–555.

4. Moran AE, Hogquist KA (2012) T-cell receptor affinity in thymic development. *Immunology* 135(4):261–267.

5. Nikolich-Žugich J, Li G, Uhrlaub JL, Renkema KR, Smithey MJ (2012) Age-related changes in CD8 T cell homeostasis and immunity to infection. *Seminars in Immunology* 24(5):356–364.

6. Petrie HT, Zúñiga-Pflücker JC (2007) Zoned out: functional mapping of stromal signaling microenvironments in the thymus. *Annu Rev Immunol* 25:649–679.

7. Takahama Y (2006) Journey through the thymus: stromal guides for T-cell development and selection. *Nat Rev Immunol* 6(2):127–135.

8. Starr TK, Jameson SC, Hogquist KA (2003) Positive and negative selection of T cells. *Annu Rev Immunol* 21:139–176.

9. Klein L, Hinterberger M, Wirnsberger G, Kyewski B (2009) Antigen presentation in the thymus for positive selection and central tolerance induction. *Nat Rev Immunol* 9(12):833–844.

10. Hu Z, Lancaster JN, Sasiponganan C, Ehrlich LIR (2015) CCR4 promotes medullary entry and thymocyte-dendritic cell interactions required for central tolerance. *Journal of Experimental Medicine* 212(11):1947–1965.

11. Daley SR, Hu DY, Goodnow CC (2013) Helios marks strongly autoreactive CD4+ T cells in two major waves of thymic deletion distinguished by induction of PD-1 or NF-κB. *J Exp Med* 210(2):269–285.

12. Sawicka M, et al. (2014) From pre-DP, post-DP, SP4, and SP8 Thymocyte Cell Counts to a Dynamical Model of Cortical and Medullary Selection. *Front*

Immunol 5:19.

13. Stritesky GL, et al. (2013) Murine thymic selection quantified using a unique method to capture deleted T cells. *Proceedings of the National Academy of Sciences* 110(12):4679–4684.

14. Sakaguchi S, Yamaguchi T, Nomura T, Ono M (2008) Regulatory T cells and immune tolerance. *Cell* 133(5):775–787.

15. Boehmer von H (2005) Mechanisms of suppression by suppressor T cells. *Nat Immunol* 6(4):338–344.

16. Thornton AM, Shevach EM (1998) CD4+CD25+ immunoregulatory T cells suppress polyclonal T cell activation in vitro by inhibiting interleukin 2 production. *J Exp Med* 188(2):287–296.

17. Takahashi T, et al. (1998) Immunologic self-tolerance maintained by CD25+CD4+ naturally anergic and suppressive T cells: induction of autoimmune disease by breaking their anergic/suppressive state. *Int Immunol* 10(12):1969–1980.

18. Read S, Malmström V, Powrie F (2000) Cytotoxic T lymphocyte-associated antigen 4 plays an essential role in the function of CD25(+)CD4(+) regulatory cells that control intestinal inflammation. *J Exp Med* 192(2):295–302.

19. Maynard CL, et al. (2007) Regulatory T cells expressing interleukin 10 develop from Foxp3+ and Foxp3- precursor cells in the absence of interleukin 10. *Nat Immunol* 8(9):931–941.

20. Uhlig HH, et al. (2006) Characterization of Foxp3+CD4+CD25+ and IL-10-secreting CD4+CD25+ T cells during cure of colitis. *J Immunol* 177(9):5852–5860.

21. Gray DHD, Chidgey AP, Boyd RL (2002) Analysis of thymic stromal cell populations using flow cytometry. *Journal of Immunological Methods* 260(1-2):15–28.

22. Klug DB, et al. (1998) Interdependence of cortical thymic epithelial cell differentiation and T-lineage commitment. *Proceedings of the National Academy of Sciences of the United States of America* 95(20):11822–11827.

23. Hozumi K, et al. (2008) Delta-like 4 is indispensable in thymic environment specific for T cell development. *Journal of Experimental Medicine* 205(11):2507–2513.

24. Alves NL, et al. (2009) Characterization of the thymic IL-7 niche in vivo. *Proceedings of the National Academy of Sciences* 106(5):1512–1517.

25. Nitta T, Suzuki H (2016) Thymic stromal cell subsets for T cell development. *Cell Mol Life Sci* 73(5):1021–1037.

26. Schmitt TM, Zúñiga-Pflücker JC (2002) Induction of T cell development from hematopoietic progenitor cells by delta-like-1 in vitro. *Immunity* 17(6):749–756.

27. Maillard I, Fang T, Pear WS (2005) Regulation of lymphoid development, differentiation, and function by the Notch pathway. *Annu Rev Immunol* 23:945–974.

28. Harman BC, Jenkinson EJ, Anderson G (2003) Microenvironmental regulation of Notch signalling in T cell development. *Seminars in Immunology* 15(2):91–97.

29. Boudil A, et al. (2015) IL-7 coordinates proliferation, differentiation and Tcra recombination during thymocyte β-selection. *Nature Publishing Group* 16(4):397–405.

30. Klein L, Kyewski B, Allen PM, Hogquist KA (2014) Positive and negative selection of the T cell repertoire: what thymocytes see (and don't see). *Nat Rev Immunol* 14(6):377–391.

31. Murata S, et al. (2007) Regulation of CD8+ T cell development by thymus-specific proteasomes. *Science* 316(5829):1349–1353.

32. Nitta T, et al. (2010) Thymoproteasome shapes immunocompetent repertoire of CD8+ T cells. *Immunity* 32(1):29–40.

33. Sasaki K, et al. (2015) Thymoproteasomes produce unique peptide motifs for positive selection of CD8(+) T cells. *Nature Communications* 6:7484.

34. Xing Y, Jameson SC, Hogquist KA (2013) Thymoproteasome subunit- 5T generates peptide-MHC complexes specialized for positive selection. *Proceedings of the National Academy of Sciences* 110(17):6979–6984.

35. Gommeaux J, et al. (2009) Thymus-specific serine protease regulates positive selection of a subset of CD4+ thymocytes. *Eur J Immunol* 39(4):956–964.

36. Nakagawa T, et al. (1998) Cathepsin L: critical role in Ii degradation and CD4 T cell selection in the thymus. *Science* 280(5362):450–453.

37. Metzger TC, et al. (2013) Lineage tracing and cell ablation identify a post-Aire-expressing thymic epithelial cell population. *Cell Rep* 5(1):166–179.

38. Nishikawa Y, et al. (2014) Temporal lineage tracing of Aire-expressing cells reveals a requirement for Aire in their maturation program. *The Journal of Immunology* 192(6):2585–2592.

39. Hikosaka Y, et al. (2008) The cytokine RANKL produced by positively selected thymocytes fosters medullary thymic epithelial cells that express autoimmune regulator. *Immunity* 29(3):438–450.

40. Akiyama T, et al. (2008) The tumor necrosis factor family receptors RANK and CD40 cooperatively establish the thymic medullary microenvironment and self-tolerance. *Immunity* 29(3):423–437.

41. Boehm T, Scheu S, Pfeffer K, Bleul CC (2003) Thymic medullary epithelial cell differentiation, thymocyte emigration, and the control of autoimmunity require lympho-epithelial cross talk via LTbetaR. *J Exp Med* 198(5):757–769.

42. Irla M, et al. (2008) Autoantigen-specific interactions with CD4+ thymocytes control mature medullary thymic epithelial cell cellularity. *Immunity* 29(3):451–463.

43. Derbinski J, Schulte A, Kyewski B, Klein L (2001) Promiscuous gene expression in medullary thymic epithelial cells mirrors the peripheral self. *Nat Immunol* 2(11):1032–1039.

44. Anderson MS, et al. (2002) Projection of an immunological self shadow within the thymus by the aire protein. *Science* 298(5597):1395–1401.

45. Metzger TC, Anderson MS (2011) Control of central and peripheral tolerance by Aire. *Immunol Rev* 241(1):89–103.

46. Consortium F-GA (1997) An autoimmune disease, APECED, caused by mutations in a novel gene featuring two PHD-type zinc-finger domains. *Nat Genet* 17(4):399–403.

47. Nagamine K, et al. (1997) Positional cloning of the APECED gene. *Nat Genet* 17(4):393–398.

48. Derbinski J (2005) Promiscuous gene expression in thymic epithelial cells is regulated at multiple levels. *Journal of Experimental Medicine* 202(1):33–45.

49. St-Pierre C, Trofimov A, Brochu S, Lemieux S, Perreault C (2015) Differential Features of AIRE-Induced and AIRE-Independent Promiscuous Gene Expression in Thymic Epithelial Cells. *The Journal of Immunology* 195(2):498–506.

50. Sansom SN, et al. (2014) Population and single-cell genomics reveal the Aire

dependency, relief from Polycomb silencing, and distribution of self-antigen expression in thymic epithelia. *Genome Res* 24(12):1918–1931.

51. Brennecke P, et al. (2015) Single-cell transcriptome analysis reveals coordinated ectopic gene-expression patterns in medullary thymic epithelial cells. *Nature Publishing Group* 16(9):933–941.

52. Derbinski J, Pinto S, Rösch S, Hexel K, Kyewski B (2008) Promiscuous gene expression patterns in single medullary thymic epithelial cells argue for a stochastic mechanism. *Proc Natl Acad Sci USA* 105(2):657–662.

53. Wu L, Shortman K (2005) Heterogeneity of thymic dendritic cells. *Seminars in Immunology* 17(4):304–312.

54. Lahoud MH, et al. (2006) Signal regulatory protein molecules are differentially expressed by CD8- dendritic cells. *J Immunol* 177(1):372–382.

55. Ardavin C, Wu L, Li CL, Shortman K (1993) Thymic dendritic cells and T cells develop simultaneously in the thymus from a common precursor population. *Nature* 362(6422):761–763.

56. Saunders D, et al. (1996) Dendritic cell development in culture from thymic precursor cells in the absence of granulocyte/macrophage colony-stimulating factor. *J Exp Med* 184(6):2185–2196.

57. Bonasio R, et al. (2006) Clonal deletion of thymocytes by circulating dendritic cells homing to the thymus. *Nat Immunol* 7(10):1092–1100.

58. Hadeiba H, et al. (2012) Plasmacytoid dendritic cells transport peripheral antigens to the thymus to promote central tolerance. *Immunity* 36(3):438–450.

59. Donskoy E, Goldschneider I (2003) Two developmentally distinct populations of dendritic cells inhabit the adult mouse thymus: demonstration by differential importation of hematogenous precursors under steady state conditions. *J Immunol* 170(7):3514–3521.

60. Li J, Park J, Foss D, Goldschneider I (2009) Thymus-homing peripheral dendritic cells constitute two of the three major subsets of dendritic cells in the steady-state thymus. *Journal of Experimental Medicine* 206(3):607–622.

61. van Meerwijk JP, et al. (1997) Quantitative impact of thymic clonal deletion on the T cell repertoire. *J Exp Med* 185(3):377–383.

62. Hinterberger M, et al. (2010) Autonomous role of medullary thymic epithelial cells in central CD4(+) T cell tolerance. *Nature Publishing Group* 11(6):512–

519.

63. Ohnmacht C, et al. (2009) Constitutive ablation of dendritic cells breaks self-tolerance of CD4 T cells and results in spontaneous fatal autoimmunity. *Journal of Experimental Medicine* 206(3):549–559.

64. Hubert F-X, et al. (2011) Aire regulates the transfer of antigen from mTECs to dendritic cells for induction of thymic tolerance. *Blood* 118(9):2462–2472.

65. Proietto AI, et al. (2008) Dendritic cells in the thymus contribute to T-regulatory cell induction. *Proc Natl Acad Sci USA* 105(50):19869–19874.

66. Perry JSA, et al. (2014) Distinct contributions of Aire and antigen-presenting-cell subsets to the generation of self-tolerance in the thymus. *Immunity* 41(3):414–426.

67. Koble C, Kyewski B (2009) The thymic medulla: a unique microenvironment for intercellular self-antigen transfer. *The Journal of experimental medicine* 206(7):1505–1513.

68. Aschenbrenner K, et al. (2007) Selection of Foxp3+ regulatory T cells specific for self antigen expressed and presented by Aire+ medullary thymic epithelial cells. *Nat Immunol* 8(4):351–358.

69. Atibalentja DF, Byersdorfer CA, Unanue ER (2009) Thymus-blood protein interactions are highly effective in negative selection and regulatory T cell induction. *The Journal of Immunology* 183(12):7909–7918.

70. Atibalentja DF, Murphy KM, Unanue ER (2011) Functional redundancy between thymic CD8α+ and Sirpα+ conventional dendritic cells in presentation of blood-derived lysozyme by MHC class II proteins. *The Journal of Immunology* 186(3):1421–1431.

71. Baba T, Nakamoto Y, Mukaida N (2009) Crucial contribution of thymic Sirp alpha+ conventional dendritic cells to central tolerance against blood-borne antigens in a CCR2-dependent manner. *The Journal of Immunology* 183(5):3053–3063.

72. Lei Y, et al. (2011) Aire-dependent production of XCL1 mediates medullary accumulation of thymic dendritic cells and contributes to regulatory T cell development. *J Exp Med* 208(2):383–394.

73. Ueno T, et al. (2004) CCR7 signals are essential for cortex-medulla migration of developing thymocytes. *J Exp Med* 200(4):493–505.

74. Ehrlich LIR, Oh DY, Weissman IL, Lewis RS (2009) Differential contribution of chemotaxis and substrate restriction to segregation of immature and mature thymocytes. *Immunity* 31(6):986–998.

75. Kurobe H, et al. (2006) CCR7-dependent cortex-to-medulla migration of positively selected thymocytes is essential for establishing central tolerance. *Immunity* 24(2):165–177.

76. Ueda Y, et al. (2012) Mst1 regulates integrin-dependent thymocyte trafficking and antigen recognition in the thymus. *Nature Communications* 3:1098.

77. Cowan JE, et al. (2014) Differential requirement for CCR4 and CCR7 during the development of innate and adaptive αβT cells in the adult thymus. *The Journal of Immunology* 193(3):1204–1212.

78. Le Borgne M, et al. (2009) The impact of negative selection on thymocyte migration in the medulla. *Nat Immunol* 10(8):823–830.

79. McCaughtry TM, Wilken MS, Hogquist KA (2007) Thymic emigration revisited. *J Exp Med* 204(11):2513–2520.

80. Dowling MR, Hodgkin PD (2009) Why does the thymus involute? A selection-based hypothesis. *Trends Immunol* 30(7):295–300.

81. Lynch HE, et al. (2009) Thymic involution and immune reconstitution. *Trends Immunol* 30(7):366–373.

82. Gray DHD, et al. (2006) Developmental kinetics, turnover, and stimulatory capacity of thymic epithelial cells. *Blood* 108(12):3777–3785.

83. Corbeaux T, et al. (2010) Thymopoiesis in mice depends on a Foxn1-positive thymic epithelial cell lineage. *Proceedings of the National Academy of Sciences* 107(38):16613–16618.

84. Itoi M, Tsukamoto N, Amagai T (2007) Expression of Dll4 and CCL25 in Foxn1-negative epithelial cells in the post-natal thymus. *Int Immunol* 19(2):127–132.

85. Ortman CL, Dittmar KA, Witte PL, Le PT (2002) Molecular characterization of the mouse involuted thymus: aberrations in expression of transcription regulators in thymocyte and epithelial compartments. *Int Immunol* 14(7):813–822.

86. Chen L, Xiao S, Manley NR (2009) Foxn1 is required to maintain the postnatal thymic microenvironment in a dosage-sensitive manner. *Blood* 113(3):567–574.

87. Zook EC, et al. (2011) Overexpression of Foxn1 attenuates age-associated thymic involution and prevents the expansion of peripheral CD4 memory T cells. *Blood* 118(22):5723–5731.

88. Bredenkamp N, Nowell CS, Blackburn CC (2014) Regeneration of the aged thymus by a single transcription factor. *Development* 141(8):1627–1637.

89. Haynes L, Maue AC (2009) Effects of aging on T cell function. *Curr Opin Immunol* 21(4):414–417.

90. Eaton SM, Maue AC, Swain SL, Haynes L (2008) Bone marrow precursor cells from aged mice generate CD4 T cells that function well in primary and memory responses. *The Journal of Immunology* 181(7):4825–4831.

91. Sutherland JS, et al. (2005) Activation of Thymic Regeneration in Mice and Humans following Androgen Blockade. *The Journal of Immunology*.

92. Griffith AV, Fallahi M, Venables T, Petrie HT (2012) Persistent degenerative changes in thymic organ function revealed by an inducible model of organ regrowth. *Aging Cell* 11(1):169–177.

93. Kim M-J, Miller CM, Shadrach JL, Wagers AJ, Serwold T (2015) Young, proliferative thymic epithelial cells engraft and function in aging thymuses. *The Journal of Immunology* 194(10):4784–4795.

94. Garfin PM, et al. (2013) Inactivation of the RB family prevents thymus involution and promotes thymic function by direct control of Foxn1 expression. *J Exp Med* 210(6):1087–1097.

95. Robles AI, et al. (1996) Expression of cyclin D1 in epithelial tissues of transgenic mice results in epidermal hyperproliferation and severe thymic hyperplasia. *Proc Natl Acad Sci USA* 93(15):7634–7638.

96. Chinn IK, Blackburn CC, Manley NR, Sempowski GD (2012) Changes in primary lymphoid organs with aging. *Seminars in Immunology* 24(5):309–320.

97. Morrissey PJ, Charrier K, Alpert A, Bressler L (1988) In vivo administration of IL-1 induces thymic hypoplasia and increased levels of serum corticosterone. *J Immunol* 141(5):1456–1463.

98. Love PE, Bhandoola A (2011) Signal integration and crosstalk during thymocyte migration and emigration. *Nat Rev Immunol* 11(7):469–477.

99. Nitta T, Ohigashi I, Nakagawa Y, Takahama Y (2011) Cytokine crosstalk for thymic medulla formation. *Curr Opin Immunol* 23(2):190–197.

100. Anderson G, Takahama Y (2012) Thymic epithelial cells: working class heroes for T cell development and repertoire selection. *Trends Immunol* 33(6):256–263.

101. McCaughtry TM, Baldwin TA, Wilken MS, Hogquist KA (2008) Clonal deletion of thymocytes can occur in the cortex with no involvement of the medulla. *J Exp Med* 205(11):2575–2584.

102. Klein L, Hinterberger M, Rohrscheidt von J, Aichinger M (2011) Autonomous versus dendritic cell-dependent contributions of medullary thymic epithelial cells to central tolerance. *Trends Immunol* 32(5):188–193.

103. Berent-Maoz B, Montecino-Rodriguez E, Dorshkind K (2012) Genetic regulation of thymocyte progenitor aging. *Seminars in Immunology* 24(5):303–308.

104. Min D, et al. (2007) Sustained thymopoiesis and improvement in functional immunity induced by exogenous KGF administration in murine models of aging. *Blood* 109(6):2529–2537.

105. Griffith AV, et al. (2009) Spatial mapping of thymic stromal microenvironments reveals unique features influencing T lymphoid differentiation. *Immunity* 31(6):999–1009.

106. Seita J, et al. (2012) Gene Expression Commons: an open platform for absolute gene expression profiling. *PLoS ONE* 7(7):e40321.

107. Gray DHD, et al. (2008) Unbiased analysis, enrichment and purification of thymic stromal cells. *Journal of Immunological Methods* 329(1-2):56–66.

108. McCall MN, Bolstad BM, Irizarry RA (2010) Frozen robust multiarray analysis (fRMA). *Biostatistics* 11(2):242–253.

109. Smyth GK (2004) Linear models and empirical bayes methods for assessing differential expression in microarray experiments. *Stat Appl Genet Mol Biol* 3:Article3.

110. Gautier L, Cope L, Bolstad BM, Irizarry RA (2004) affy--analysis of Affymetrix GeneChip data at the probe level. *Bioinformatics* 20(3):307–315.

111. Huang DW, Sherman BT, Lempicki RA (2009) Systematic and integrative analysis of large gene lists using DAVID bioinformatics resources. *Nat Protoc* 4(1):44–57.

112. Subramanian A, et al. (2005) Gene set enrichment analysis: a knowledge-based approach for interpreting genome-wide expression profiles. *Proc Natl Acad Sci USA* 102(43):15545–15550.

113. Blackburn CC, et al. (1996) The nu gene acts cell-autonomously and is required for differentiation of thymic epithelial progenitors. *Proc Natl Acad Sci USA* 93(12):5742–5746.

114. Repass JF, et al. (2009) IL7-hCD25 and IL7-Cre BAC transgenic mouse lines: new tools for analysis of IL-7 expressing cells. *Genesis* 47(4):281–287.

115. Ribeiro AR, Rodrigues PM, Meireles C, Di Santo JP, Alves NL (2013) Thymocyte selection regulates the homeostasis of IL-7-expressing thymic cortical epithelial cells in vivo. *The Journal of Immunology* 191(3):1200–1209.

116. Plotkin J, Prockop SE, Lepique A, Petrie HT (2003) Critical role for CXCR4 signaling in progenitor localization and T cell differentiation in the postnatal thymus. *J Immunol* 171(9):4521–4527.

117. Wurbel M-A, et al. (2000) The chemokine TECK is expressed by thymic and intestinal epithelial cells and attracts double- and single-positive thymocytes expressing the TECK receptor CCR9. *Eur J Immunol* 30(1):262–271.

118. Hamazaki Y, et al. (2007) Medullary thymic epithelial cells expressing Aire represent a unique lineage derived from cells expressing claudin. *Nat Immunol* 8(3):304–311.

119. Foster K, et al. (2008) Contribution of neural crest-derived cells in the embryonic and adult thymus. *J Immunol* 180(5):3183–3189.

120. Yano M, et al. (2008) Aire controls the differentiation program of thymic epithelial cells in the medulla for the establishment of self-tolerance. *J Exp Med* 205(12):2827–2838.

121. Kong L-J, Chang JT, Bild AH, Nevins JR (2007) Compensation and specificity of function within the E2F family. *Oncogene* 26(3):321–327.

122. Humbert PO, et al. (2000) E2f3 is critical for normal cellular proliferation. *Genes Dev* 14(6):690–703.

123. Dower K, Ellis DK, Saraf K, Jelinsky SA, Lin L-L (2008) Innate immune responses to TREM-1 activation: overlap, divergence, and positive and negative cross-talk with bacterial lipopolysaccharide. *J Immunol* 180(5):3520–3534.

124. Chung HY, et al. (2009) Molecular inflammation: underpinnings of aging and age-related diseases. *Ageing Res Rev* 8(1):18–30.

125. Sempowski GD, et al. (2000) Leukemia Inhibitory Factor, Oncostatin M, IL-6, and Stem Cell Factor mRNA Expression in Human Thymus Increases with Age

and Is Associated with Thymic Atrophy. *The Journal of Immunology* 164(4):2180–2187.

126. Fancke B, Suter M, Hochrein H, O'Keeffe M (2008) M-CSF: a novel plasmacytoid and conventional dendritic cell poietin. *Blood* 111(1):150–159.

127. Balciunaite G, et al. (2002) Wnt glycoproteins regulate the expression of FoxN1, the gene defective in nude mice. *Nat Immunol* 3(11):1102–1108.

128. Liu X, et al. (2010) Sox17 modulates Wnt3A/ -catenin-mediated transcriptional activation of the Lef-1 promoter. *AJP: Lung Cellular and Molecular Physiology* 299(5):L694–L710.

129. van Tienen FHJ, Laeremans H, van der Kallen CJH, Smeets HJM (2009) Wnt5b stimulates adipogenesis by activating PPARgamma, and inhibiting the beta-catenin dependent Wnt signaling pathway together with Wnt5a. *Biochem Biophys Res Commun* 387(1):207–211.

130. Chen BJ, Cui X, Sempowski GD, Chao NJ (2003) Growth hormone accelerates immune recovery following allogeneic T-cell-depleted bone marrow transplantation in mice. *Exp Hematol* 31(10):953–958.

131. Youm Y-H, et al. (2012) The Nlrp3 inflammasome promotes age-related thymic demise and immunosenescence. *Cell Rep* 1(1):56–68.

132. Meredith M, Zemmour D, Mathis D, Benoist C (2015) Aire controls gene expression in the thymic epithelium with ordered stochasticity. *Nature Publishing Group* 16(9):942–949.

133. Ueno T, et al. (2004) CCR7 signals are essential for cortex-medulla migration of developing thymocytes. *J Exp Med* 200(4):493–505.

134. Nitta T, Nitta S, Lei Y, Lipp M, Takahama Y (2009) CCR7-mediated migration of developing thymocytes to the medulla is essential for negative selection to tissue-restricted antigens. *Proc Natl Acad Sci USA* 106(40):17129–17133.

135. Davalos-Misslitz ACM, et al. (2007) Generalized multi-organ autoimmunity in CCR7-deficient mice. *Eur J Immunol* 37(3):613–622.

136. Davalos-Misslitz ACM, Worbs T, Willenzon S, Bernhardt G, Förster R (2007) Impaired responsiveness to T-cell receptor stimulation and defective negative selection of thymocytes in CCR7-deficient mice. *Blood* 110(13):4351–4359.

137. Ki S, et al. (2014) Global transcriptional profiling reveals distinct functions of thymic stromal subsets and age-related changes during thymic involution. *Cell*

Rep 9(1):402–415.

138. Pereira JP, Kelly LM, Xu Y, Cyster JG (2009) EBI2 mediates B cell segregation between the outer and centre follicle. *Nature* 460(7259):1122–1126.

139. Liu C, et al. (2011) Oxysterols direct B-cell migration through EBI2. *Nature* 475(7357):519–523.

140. Birkenbach M, Josefsen K, Yalamanchili R, Lenoir G, Kieff E (1993) Epstein-Barr virus-induced genes: first lymphocyte-specific G protein-coupled peptide receptors. *J Virol* 67(4):2209–2220.

141. Hannedouche S, et al. (2011) Oxysterols direct immune cell migration via EBI2. *Nature* 475(7357):524–527.

142. Gatto D, Paus D, Basten A, Mackay CR, Brink R (2009) Guidance of B cells by the orphan G protein-coupled receptor EBI2 shapes humoral immune responses. *Immunity* 31(2):259–269.

143. Pereira JP, Kelly LM, Xu Y, Cyster JG (2009) EBI2 mediates B cell segregation between the outer and centre follicle. *Nature* 460(7259):1122–1126.

144. Cyster JG, Dang EV, Reboldi A, Yi T (2014) 25-Hydroxycholesterols in innate and adaptive immunity. *Nat Rev Immunol*. doi:10.1038/nri3755.

145. Gatto D, et al. (2013) The chemotactic receptor EBI2 regulates the homeostasis, localization and immunological function of splenic dendritic cells. *Nature Publishing Group* 14(5):446–453.

146. Li J, Lu E, Yi T, Cyster JG (2016) EBI2 augments Tfh cell fate by promoting interaction with IL-2-quenching dendritic cells. *Nature* 533(7601):110–114.

147. Wallace C, et al. (2012) Statistical colocalization of monocyte gene expression and genetic risk variants for type 1 diabetes. *Hum Mol Genet* 21(12):2815–2824.

148. Wright DE, et al. (2001) Cyclophosphamide/granulocyte colony-stimulating factor causes selective mobilization of bone marrow hematopoietic stem cells into the blood after M phase of the cell cycle. *Blood* 97(8):2278–2285.

149. Seach N, Wong K, Hammett M, Boyd RL, Chidgey AP (2012) Purified enzymes improve isolation and characterization of the adult thymic epithelium. *Journal of Immunological Methods* 385(1-2):23–34.

150. Schindelin J, et al. (2012) Fiji: an open-source platform for biological-image analysis. *Nat Methods* 9(7):676–682.

151. Barnden MJ, Allison J, Heath WR, Carbone FR (1998) Defective TCR expression in transgenic mice constructed using cDNA-based alpha- and beta-chain genes under the control of heterologous regulatory elements. *Immunology and Cell Biology* 76(1):34–40.

152. Kurts C, et al. (1996) Constitutive class I-restricted exogenous presentation of self antigens in vivo. *J Exp Med* 184(3):923–930.

153. Ross JO, Melichar HJ, Halkias J, Robey EA (2016) Studying T Cell Development in Thymic Slices. *Methods Mol Biol* 1323:131–140.

154. Yi T, Cyster JG (2013) EBI2-mediated bridging channel positioning supports splenic dendritic cell homeostasis and particulate antigen capture. *Elife* 2:e00757.

155. Klein L, Hinterberger M, Rohrscheidt von J, Aichinger M (2011) Autonomous versus dendritic cell-dependent contributions of medullary thymic epithelial cells to central tolerance. *Trends in immunology* 32(5):188–193.

156. Kelly LM, Pereira JP, Yi T, Xu Y, Cyster JG (2011) EBI2 Guides Serial Movements of Activated B Cells and Ligand Activity Is Detectable in Lymphoid and Nonlymphoid Tissues. *The Journal of Immunology* 187(6):3026–3032.

157. Friedman RS, Jacobelli J, Krummel MF (2006) Surface-bound chemokines capture and prime T cells for synapse formation. *Nat Immunol* 7(10):1101–1108.

158. Koehli S, Naeher D, Galati-Fournier V, Zehn D, Palmer E (2014) Optimal T-cell receptor affinity for inducing autoimmunity. *Proceedings of the National Academy of Sciences* 111(48):17248–17253.

159. Hu Z, Lancaster JN, Ehrlich LIR (2015) The Contribution of Chemokines and Migration to the Induction of Central Tolerance in the Thymus. *Front Immunol* 6:398.

160. Gloriam DEI, Schiöth HB, Fredriksson R (2005) Nine new human Rhodopsin family G-protein coupled receptors: identification, sequence characterisation and evolutionary relationship. *Biochimica et biophysica acta* 1722(3):235–246.

161. Yosten GLC, Kolar GR, Redlinger LJ, Samson WK (2013) Evidence for an interaction between proinsulin C-peptide and GPR146. *J Endocrinol* 218(2):B1–8.

162. Walcher D, et al. (2004) C-peptide induces chemotaxis of human CD4-positive cells: involvement of pertussis toxin-sensitive G-proteins and phosphoinositide 3-kinase. *Diabetes* 53(7):1664–1670.

163. Osterwalder M, et al. (2010) Dual RMCE for efficient re-engineering of mouse mutant alleles. *Nat Methods* 7(11):893–895.

164. Raymond CS, Soriano P (2010) ROSA26Flpo deleter mice promote efficient inversion of conditional gene traps in vivo. *genesis* 48(10):603–606.

165. Hennet T, Hagen FK, Tabak LA, Marth JD (1995) T-cell-specific deletion of a polypeptide N-acetylgalactosaminyl-transferase gene by site-directed recombination. *Proceedings of the National Academy of Sciences of the United States of America* 92(26):12070–12074.

166. Ueno T, et al. (2004) CCR7 signals are essential for cortex-medulla migration of developing thymocytes. *The Journal of experimental medicine* 200(4):493–505.

167. Misslitz A, et al. (2004) Thymic T cell development and progenitor localization depend on CCR7. *The Journal of experimental medicine* 200(4):481–491.

168. Hwang S, et al. (2012) Reduced TCR signaling potential impairs negative selection but does not result in autoimmune disease. *Journal of Experimental Medicine* 209(10):1781–1795.

169. Tager HS, Emdin SO, Clark JL, Steiner DF (1973) Studies on the conversion of proinsulin to insulin. II. Evidence for a chymotrypsin-like cleavage in the connecting peptide region of insulin precursors in the rat. *J Biol Chem* 248(10):3476–3482.

170. Fan Y, et al. (2009) Thymus-specific deletion of insulin induces autoimmune diabetes. *The EMBO Journal* 28(18):2812–2824.

171. Wong K, et al. (2014) Multilineage potential and self-renewal define an epithelial progenitor cell population in the adult thymus. *Cell Rep* 8(4):1198–1209.

172. Chiang EY, Johnston RJ, Grogan JL (2013) EBI2 is a negative regulator of type I interferons in plasmacytoid and myeloid dendritic cells. *PLoS ONE* 8(12):e83457.

173. Sun S, Liu C (2015) 7α, 25-dihydroxycholesterol-mediated activation of EBI2 in immune regulation and diseases. *Front Pharmacol* 6(e83457):60.

174. Gloriam DEI, Schiöth HB, Fredriksson R (2005) Nine new human Rhodopsin family G-protein coupled receptors: identification, sequence characterisation and evolutionary relationship. *Biochim Biophys Acta* 1722(3):235–246.

Vitae

Sanghee Ki attended Yale High School in Seoul, Korea. She graduated from Ewha Womans University in Seoul, Korea with a bachelor's degree in Life Sciences in 2007. She earned a Masters of Science in education, Biology Major from Seoul National University, Seoul Korea, in 2009. In the fall of 2010, she enrolled in the Institute for Cell and Molecular Biology at the University of Texas at Austin as a Ph.D. student.

Email: sangheeki@utexas.edu

This dissertation was typed by Sanghee Ki